UNIVERSITÀ DEGLI STUDI DI PADOVA

Dipartimento di Fisica e Astronomia "Galileo Galilei"

Master Degree in Physics

Final Dissertation

Pattern formation in ecosystem with resource competition

Thesis supervisors

Prof. Amos Maritan

Prof. Sandro Azaele

Candidate

Alice Doimo

Academic Year 2021/2022

Adesso avete capito: se io amo l'ordine, non è come per tanti altri il segno d'un carattere sottomesso a una disciplina interiore, a una repressione degli istinti. In me l'idea d'un mondo assolutamente regolare, simmetrico, metodico, s'associa a questo primo impeto e rigoglio della natura.

— Italo Calvino, "I cristalli" in *Ti con zero* (1967)

Abstract

In recent years, theoretical ecology has developed a growing interest in spatial models for population dynamics, led by the empirical evidence that spatial effects have a considerable influence on the distribution of species and on the structure of communities, affecting for instance their biodiversity levels. In such perspective, this work aims at providing a spatial extension of the MacArthur resource-consumer model - which describes the dynamical evolution of species and resource abundances - in order to account for the emergence of spatially heterogeneous steady-state patterns from a homogeneous equilibrium solution.
Following the approach adopted by Turing in his famous paper "The chemical basis of morphogenesis" (1952), a mechanism for pattern formation is investigated by adding some diffusion-like terms to the dynamical equations: the conditions for pattern initiation can then be analytically derived by studying the linearised system's instability to spatially dependent infinitesimal perturbations. Lastly, a numerical integration is performed to gain insight into the out of equilibrium behavior of the system in the nonlinear regime, thus determining the outcome of instability and the resulting patterns in the distribution of abundances.

Acknowledgements

I sincerely thank my supervisors, Professor Amos Maritan and Professor Sandro Azaele, for their constant guidance and for introducing me into the fascinating field of theoretical ecology. I am also grateful to Davide Zanchetta, Emanuele Pigani and Giorgio Nicoletti, who helped me during the course of this work.

Contents

Introduction and motivation

Spatial self-organization is a process in which large-scale ordered spatial patterns emerge from disordered initial conditions through local interactions. Recently, this phenomenon is raising growing interest among theoretical ecologists, due to its centrality for the understanding of ecological stability and diversity and its utility to predict the dynamics of natural systems in response to global environmental change.
Indeed, many examples of pattern formation in natural ecosystems have been discovered in the last years, revealing striking cross-system similarities. Such observations suggest to search for a unifying mechanism, able to explain the rising of regular patterns independently of the details of the system.

Ecological patterns are often observed in systems having little underlying heterogeneity, i.e. lacking strong environmental gradients. This is an evidence supporting the idea that the observed spatial structures probably form spontaneously, rather than being the result of preexisting environmental heterogeneity. However, the explanation of the origin of regular patterns in ecosystem is still a debated issue. The main alternative hypotheses include pre-determined regularity, related for instance to geophysical processes, or other mechanisms ascribable to noise, although growing evidence seems to favour self-organized structure formation.

Besides, spatial patterns are more commonly observed in habitats characterized by adverse environmental conditions, where the competition for resources is particularly strong: for example, in highly arid regions (see Fig. 0.1), where plants would become extinct if homogeneously distributed. The spontaneous spatial organization of vegetation can be seen in this context as a mechanism for survival [2, 3], fueled by competitive dynamics. Other examples include wetland ecosystems, savanna ecosystems, mussel beds, coral reefs, ribbon forests, inter-tidal mudflats and marsh tussocks (Fig. 0.2). From the ecological point of view, all these systems seem to share a common underlying mechanism: a scale-dependent feedback, similar to Turing's principle of *local activation with lateral inhibition* [4], which suits many diverse systems in different ways, depending on their distinctive details [1].

Much theoretical work has been developed around this topic, proving that spatially heterogeneous population distributions have a very positive impact on the ecosystem's functioning: several models

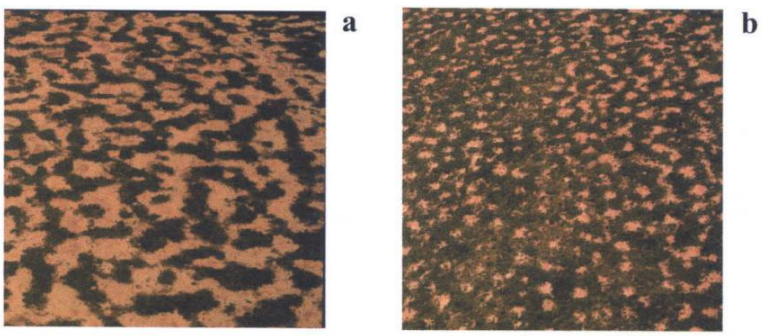

FIG. 0.1. Example of a natural ecosystem pattern from [2]. Aerial photographs from patterned vegetation in Niger: a) labyrinths with spots; b) gap pattern. Scale is 400 x 400 m.

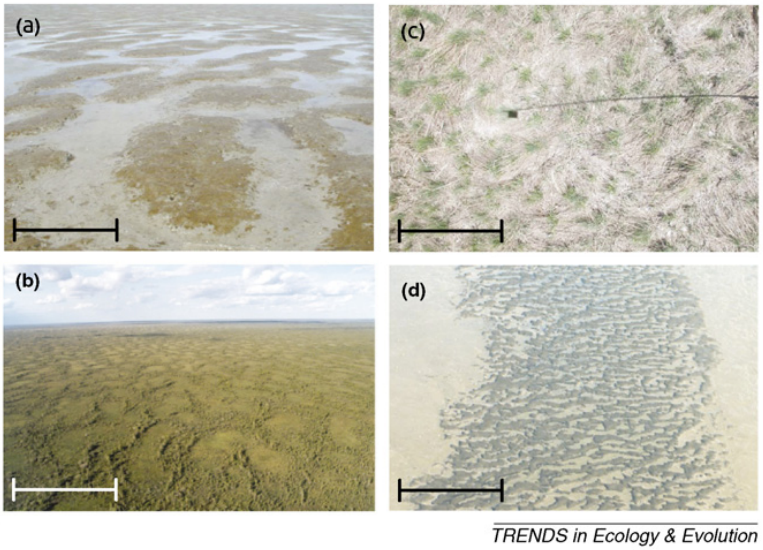

FIG. 0.2. Other examples of ecosystem patterns from [1]. a) Labyrinth pattern of marine benthic diatoms in the Netherlands (scale = $1m$); b) regular maze patterns of shrubs and trees in West Siberia (scale = $100m$); c) regular spaced tussocks of the sedge Carex stricta (scale = $2m$); d) patterned mussel bank in the Wadden Sea, the Netherlands (scale = $50m$).

predict that the systems displaying ordered patterns are more resilient to disturbances, thanks to their improved resource optimization, which also enhances productivity and diversity inside the ecological community.

This thesis aims at finding a physical model able to account for the spontaneous formation of spatially periodic patterns, based on an exploitative competition interaction dynamics.
The theoretical framework is represented by the MacArthur's consumer resource model, introduced in Chapter 1. Chapter 2 provides a brief outline of the theory and analytical methods used to study pattern formation, focusing in particular on the linear stability analysis and on the classification of the instabilities according to Hohenberg [5]. These methods are finally applied to the MacArthur's reaction dynamics in Chapter 3, by proposing a spatial extension of the model which accounts for the dispersal behavior of the populations. The conditions for the rising of a spatially heterogeneous pattern in the species abundances are then derived in terms of the system parameters. The possibility for an alternative perspective, based on non-local resource consumption, is outlined in Section 3.6. Finally, the resulting model is integrated and the numerical results are presented in Chapter 4.

Chapter 1

MacArthur's consumer-resource model

In this chapter I present the model which will be used as the theoretical foundation of this work: the resource-consumer model by Robert MacArthur.
I start by outlining the basic approach for ecosystem modeling in Section 1.1, and later introduce the most relevant equations used to describe the ecological communities based on exploitative competition: the competitive Lotka-Volterra's (Section 1.2) and the MacArthur's (Section 1.3), which have the advantage of overcoming the main limitations of the former. A remarkable result concerning resource-competing communities, the *competitive exclusion principle*, is briefly discussed, together with the main strategies proposed to solve its apparent irreconcilability with observations: in particular, the spontaneous formation of spatial structure will be the focus of this work. Hence, in Section 1.4 I give a brief overview on spatial models in theoretical ecology, which provides an introduction to the spatial extension of the MacArthur equations treated in Chapter 3.

1.1 Modeling interactions in an ecosystem

Ecosystems are extremely complex systems, made up of several species' populations that can interact with each other in multiple ways, as well as evolve and migrate to other territories. Populations themselves are characterized by a variety of parameters and ecological descriptors, such as distribution, number and spacing of individuals, age distributions, birth and death rates, immigration and emigration rates, rates of growth, etc.
When studying the dynamical evolution of a population, we are mainly interested in two characteristics: its distribution in space and its *abundance*, which is defined as the total number of individuals, or biomass, of a species in a specified area. The easiest way to achieve an analytical description is to coarse-grain the discrete population into a real, continuous field $n_i(\vec{x}, t)$ representing the population abundance of species i at time t in an infinitesimal area of the territory, as a function of a spatial variable $\vec{x}$, belonging to a plane.
If we want to adopt a physical approach, we must then define the interactions between the components of the ecosystem. In ecology, the variety of interactions observed in natural system are classified according to the positive, negative, or neutral impact that the interaction has over two interacting species [3] :

- Competition: $(-,-)$ the interaction has negative effect on both the interacting species;
- Mutualism: $(+,+)$ both the species benefit from the interaction;
- Predation/Parasitism: $(+,-)$ one species benefits from the interaction, while the other is harmed;
- Commensalism: $(+,0)$ one species is advantaged and the other is not influenced by the interaction;
- Amensalism: $(-,0)$ one species is is penalized and the other is not influenced by the interaction;
- Neutralism: $(0,0)$ the two species have no effect on each other.

If the impact is negative, it means that energy is expended or injury incurred, leading to a decrease

in the population. A positive impact favors instead the growth of the population. Moreover, beyond inter-specific interactions above described, one should also consider what intra-specific effects may be present in an ecosystem, which will be formally represented as auto-interaction terms.

1.1.1 Resource competition

Amongst the many possible interactions between species forming an ecosystem, we will focus on exploitative competition, i.e. competition for the same common resources. According to the above classification of species interactions, competition is simply a mutually negative interaction between species' populations, that arises, in this case, from the exploitation of common resources. When modeling competitive communities, one must be particularly careful in defining what a resource is, since the distinction with species is not always limpid. According to Grover [6] resources are "entities which contribute positively to population growth, and are consumed in the process". Two main classes of resources can be distinguished: *biotic* resources, that can reproduce and therefore follow some growth law, and *abiotic* resources, which cannot reproduce and must be supplied to the ecosystem from the outside.

1.2 Competitive Lotka-Volterra equations

The competitive Lotka-Volterra equations are a modified version of the famous predator-prey equations, which represent the first mathematical model of population dynamics. Similarly to the latter equations, competitive Lotka Volterra is based on the law of mass actions, i.e. it assumes that the rate of change of a species abundance due to the interaction with another species is proportional to the product of the two species' abundances.
Differently from the predator-prey model, however, the population growth in absence of other species is assumed to follow a logistic curve:

$$\dot{n} = rn\left(1 - \frac{n}{K}\right)$$

where $n(t)$ is the abundance at time t, r is the *intrinsic growth rate* and K is called the *carrying capacity* of the species, which represents value at which $n(t)$ saturates for $t \to \infty$. According to these two assumptions, the equations for a system of species interacting via competitive exclusion takes the form:

$$\dot{n_i} = r_i n_i \left(1 - \frac{n_i}{K_i} - \sum_{i \neq j} \alpha_{ij} n_j\right) = r_i n_i \left(1 - \sum_{i,j} \alpha_{ij} n_j\right) \qquad i = 1, ..., N$$

where $\alpha_{ij} > 0$ are the competition coefficients, and the minus sign is in agreement with the definition of competitive interaction given in Section 1.1. In the second equality, we have rewritten the logistic saturation term as an auto-interaction term, defining $\alpha_{ii} = 1/K_i$.

We observe that this model represents competition for common resources by means of a direct interaction between species' populations, without an explicit description of the resource dynamics, but rather representing their effect through the parameters r_i and α_{ij} only.
This has clear advantages in what concerns the mathematical tractability of the system. The drawback, however, lies in the predictive power of the model. First of all, the fact that only pairwise interactions are represented is a very strong, unrealistic assumption. Furthermore, the values of the interaction parameters $\alpha_{i \neq j}$ cannot be measured from species growing in isolation, nor estimated a priori, thus making it impossible to test the theory against real experimental data.

The limitations of the competitive Lotka-Volterra equations have lead the scientific community to look for alternative ways of modeling exploitative competition, such as the *consumer resource model* proposed by Robert MacArthur [7].

1.3 MacArthur's consumer-resource model

Differently from the competitive Lotka-Volterra, MacArthur model describes explicitly the dynamics of the resource population, in addition to the one of the species. Indeed, it consists of two coupled sets of differential equations:

$$\begin{cases} \dot{n}_\sigma = n_\sigma \left(\sum_{i=1}^{N_R} \alpha_{\sigma i}\, \mu_i(c_i) - \delta_\sigma \right) & \sigma = 1, ..., N_S \\ \dot{c}_i = s_i - \sum_{\sigma=1}^{N_S} n_\sigma\, \alpha_{\sigma i}\, \mu_i(c_i) & i = 1, ..., N_R \end{cases} \tag{1.1}$$

where $n_\sigma(\vec{x}, t)$ is the σ-th species population field, $c_i(\vec{x}, t)$ is the i-th resource population field, $\delta_\sigma > 0$ is the *death rate* of species σ, $s_i > 0$ is the *supply rate* of resource i, which is a constant in the case of abiotic resources, and $\alpha_{\sigma i} > 0$ are the *metabolic strategies*, which measure how much species σ relies on resource i for growth. The growth function $\mu_i(c_i)$ is usually required to satisfy the following properties:

- $\mu_i(c_i) \sim c_i$ for $c_i \ll 1$;
- $\mu_i(c_i) \to const.$ for $c_i \to \infty$;
- $\mu_i(c_i)$ is monotonically increasing in c_i.

Often a Monod function is chosen, particularly when modeling microbial populations:

$$\mu_i(c_i) = \frac{c_i}{c_i + K_i} \tag{1.2}$$

where K_i is called *half-saturation* constant.

We observe that in MacArthur the growth rate of species is no more a constant as it was in Lotka-Volterra, but it depends instead on resource availability $c_{i=1,...,N_R}$:

$$r_\sigma = r_\sigma(c_1, ..., c_{N_R}) = \sum_{i=1}^{N_R} \alpha_{\sigma i}\, \mu_i(c_i) \tag{1.3}$$

which is affected in turn by the consumption by the species.

In this sense, the resources are what mediates the interactions between the species in the ecosystem: thus one of the advantages of MacArthur model is that the growth rates, instead of being linear in the species populations as in Lotka-Volterra, are highly non linear. For instance, it is immediate to see that if any species' population grows, all other species are affected through the term (1.3).
The other major advantage is represented by the predictive capability of the resource-consumer model: indeed, the knowledge of the resource-dependent consumption and growth rates of each competitor population studied in isolation is sufficient to determine all system parameters, and thus the competitive dynamics. Therefore, predictions can be made and tested against real data.

To conclude, we show that the competitive Lotka-Volterra can be derived from MacArthur model under specific hypotheses, by exploiting a separation of species and resources evolution timescales. We consider a MacArthur system with biotic resources (then a predator-prey system), and we make the following assumptions:

- logistic resource growth rate: $s_i(c_i) = c_i \left(1 - \frac{c_i}{Q_i}\right)$
- species growth function: $\mu_i(c_i) = c_i$
- resources evolution occurs on much shorter timescales than species evolution $\Rightarrow \dot{c}_i \approx 0$

Then, $c_i(t)$ can be obtained from the resource equations:

$$\frac{c_i^2}{Q_i} + \left(\sum_\sigma n_\sigma \alpha_{\sigma i} - 1\right) c_i = 0 \quad \rightarrow \quad c_i = \left(1 - \sum_\sigma n_\sigma \alpha_{\sigma i}\right) Q_i$$

and it can be substituted in the species equations, yieldng:

$$\dot{n}_\sigma = n_\sigma r_\sigma \left(1 - \sum_{\rho=1}^{N_S} \hat{\alpha}_{\sigma\rho} n_\rho\right) \qquad \text{where:} \quad r_\sigma = \sum_{i=1}^{N_R} \alpha_{\sigma i} Q_i - \delta_\sigma \,, \;\; \hat{\alpha}_{\sigma\rho} = \frac{1}{r_\sigma} \sum_{i=1}^{N_R} \alpha_{\sigma i} \alpha_{\rho i} Q_i$$

In this perspective, MacArthur consumer-resource model can be considered as a generalisation of the competitive Lotka-Volterra equations. Notice also that, in this case, the interaction between the species encoded in the term $r_\sigma \, \hat{\alpha}_{\sigma\rho}$ is symmetric.

1.3.1 Competitive Exclusion Principle

An important result of the consumer-resource model concerns the levels of biodiversity admitted in a competitive community. According to the MacArthur equations (1.1), an arbitrary number of species cannot coexist given a fixed number of resources: as we are going to show, the number of species is bounded by the number of resources. To get an understanding of how this principle arises, we firstly illustrate a simple result, known as the *R* rule*, for a system of N_S species and 1 resource. In this case the equations read:

$$\begin{cases} \dot{n}_\sigma = n_\sigma \left(\alpha_\sigma \, \mu(c) - \delta_\sigma\right) & \sigma = 1, ..., N_S \\ \dot{c} = s - \displaystyle\sum_{\sigma=1}^{N_S} \alpha_\sigma \, \mu(c) \end{cases}$$

We define for each species σ:

$$R_\sigma^* \coloneqq \frac{\delta_\sigma}{\alpha_\sigma}$$

which can be interpreted as the value of $\mu(c)$ at which the species σ is at equilibrium (i.e. it holds $\dot{n_\sigma} = 0$, $\dot{c} = 0$). It is immediate to realise that if $\mu(c) > R_\sigma^*$, the population of species σ will increase, while if $\mu(c) < R_\sigma^*$ the population of species σ will decrease. Therefore, the species that has the smallest R_σ^* will survive and reach equilibrium, but all the other species will go extinct: species coexistence is allowed only in the eventuality that different species of the system are fine-tuned to have the same value of R_σ^*, which is obviously an unrealistic supposition. Indeed coexistence of all species can be expressed by the following condition:

$$\begin{cases} \dot{n_\sigma} = 0 \quad \forall \, \sigma \\ \dot{c} = 0 \;\rightarrow\; c = c^* \end{cases} \qquad \Leftrightarrow \quad \mu(c^*) = \delta_\sigma / \alpha_\sigma \quad \forall \, \sigma$$

which is a system of N_S equations in one unknown c^*, that admit no solution in the case of generic δ_σ, α_σ. By considering now a system with N_R resources (1.1), the coexistence condition becomes:

$$\begin{cases} \dot{n_\sigma} = 0 \quad \forall \, \sigma \\ \dot{c_i} = 0 \quad \forall \, i \quad \rightarrow \; c_i = c_i^* \end{cases} \qquad \Leftrightarrow \quad \sum_{i=1}^{N_R} \alpha_{\sigma i} \, \mu_i(c_i^*) = \delta_\sigma \quad \forall \, \sigma \tag{1.4}$$

which is a system of N_S equations in N_R unknowns $\{c_i^*\}_{i=1,...,N_R}$. It admits:

- unique solution if $N_S = N_R$;
- infinite solutions if $N_S < N_R$;
- no solution if $N_S > N_R$;

by reasoning in a similar way as in the previous case, we conclude that if a system starts with a number of species $N_S > N_R$, its evolution will lead to at least $N_S - N_R$ extinctions until the c_i^* solutions of the system (1.4) are reached and equilibrium is achieved. Therefore, at equilibrium, only a number of species $N_S \leq N_R$ can coexist: this result is known as *Competitive Exclusion Principle* (CEP), and it states that "complete competitors cannot coexist" [8], because the species having even a slight advantage on the others will necessarily outcompete them. The mathematical validity of this principle, under proper hypotheses, is unquestionable. However, comparison with real life ecosystems shows that such behavior is not actually encountered in nature, where we find extremely high levels of biodiversity with respect to those predicted by the theory.

An emblematic example is the so-called *paradox of the plankton* [9], which provides an extreme violation of the competitive exclusion principle. Indeed, a very high number of species of phytoplankton have been shown to coexist in an essentially isotropic and unstructured environment, despite feeding on the same limited number of resources (i.e. sunlight and some chemical compounds), which in certain periods of the year are also very scarce: the number of species can remarkably exceed that of resources, even up to an order of magnitude [10, 11].

1.3.2 Main hypotheses for a solution to the paradox

The Competitive Exclusion Principle is a pillar in ecology and natural sciences, and its origin can be conceptually traced back to "The Origin of Species" (1859) by Charles Darwin. It was rigorously formulated at the beginning of the 20th century, but it did not reach the majority of the scientific community until Gause's work (1934) [12]. Ever since, countless hypotheses have been formulated to explain the sharp contrast between theoretical expectation and the extremely high levels of biodiversity observed in natural communities [13, 14]. Most of them exploit the fact that real system may not satisfy the strict physical hypotheses over which the principle is grounded: indeed the consumer-resource model is obviously highly theoretical and it represents extreme simplification of an actual ecosystem.

Most likely, exploitative competition is not the only interaction taking place in a real ecosystem: predation is also possible, as well as parasitism and mutualism, and there might be a combination of such effects influencing the community structure. For instance, for what concerns phytoplankton, predation by zooplankton and viruses could be suppressing dominant competitors [15], while beneficial or mutualistic interactions may promote inferior competitors.
Another possibility could be that not all the actual resources present in the ecosystem have been considered. For instance, one could refer again to a mutualistic interaction such as cross-feeding, which is very common in microbial communities: this mechanism would produce additional resources that are typically difficult to detect and identify [16].
Lastly, without entering into detail, we mention that other mechanisms have been proposed, based mainly on behavioral effects altering the interactions between the species, which are able to regulate the overall dynamics of the system. In the literature, they are conventionally referred to as *additional limiting factors*.

Nevertheless, in strongly competitive systems we can admit that competition plays a major role, the other interactions being safely neglected. In such cases one could conjecture that the reason why CEP finds no confirmation in real systems must be searched elsewhere. Another line of thought for the resolution of this paradox is based on the fact that real ecosystem are not necessarily settled at dynamical equilibrium: rather, most biological system are far from it. Thus, our assumption is broken and the derivation proposed in (1.4) is not valid. As a consequence, if there is any spatial or temporal effect maintaining the system out of equilibrium, the CEP is not expected to hold.
In particular, the out of equilibrium behavior of the system might be forced by some external driving, such as temporal environmental fluctuations (e.g. weather driven) or spatial environmental heterogeneity. Indeed, no real habitat is truly spatially uniform: even the open ocean has a spatial structure which breaks, even only slightly, the homogeneity hypothesis. Otherwise, the out of equilibrium be-

havior may be the result of a self organized dynamics, which can induce oscillations and chaos, or lead to self-organized spatial segregation. There is indeed increasing evidence suggesting that spatial models are able to reproduce the higher biodiversity levels observed in natural communities without the need of invoking an underlying environmental heterogeneity [17, 18].

1.4 Spatial models: a brief overview

So far, we have briefly presented two models for exploitative competition which assume that the abundances have no spatial dependence, implying that the distributions can be essentially considered uniform: this mean-field approach represents however a drastic simplification.
There are, indeed, many reasons to believe that spatial effects cannot be simply discarded, and have instead a crucial influence on the dynamics of the system and on the structure of communities.

Intuitively, the interactions of an each individual with with other organisms or with the physical environment are necessarily constrained to its neighborhood, and therefore intrinsically spatial in nature. This consideration, however, would not be very relevant without empirical evidence or theoretical arguments revealing the fundamental role that spatial effects have on population dynamics. The laboratory experiments of Gause (1935) and Huffaker (1958), consisting in simple realizations of a two species predator-prey system, represent the earliest pieces of evidence supporting the idea that spatial effects are fundamental in determining the persistence of species, and suggesting that there may be some spatially-dependent mechanisms favoring biodiversity in natural ecosystems.
Clearly, this argument is strictly related to the previously discussed paradox, concerning the CEP and its sharp contrast with the high biodiversity levels observed in nature. This line of research was mainly developed by Tilman[1], both experimentally and theoretically [20].
Lastly, ecological spatial models are obviously necessary to describe migration and invasions, and are recently gaining growing interest in the context of conservation. Indeed, they can be used as means to study how habitat destruction and fragmentation, due to the human impact on natural environments, is affecting the diversity and persistence of populations [21], which is clearly a goal of the uttermost importance.

There exist many ways to introduce space into an ecological model. The first distinction that can be made is weather we describe space implicitly or explicitly. In the former case we can introduce spatial effects indirectly, for instance by means of some parameters correlated to spatial scales – e.g. in the MacArthur-Wilson model for island biogeography (1967) – or by specifying what fraction of the environment is occupied by each species, without defining how such patches are arranged in space – e.g. in the multispecies extensions of Levins metapopulation model (1969). Treating space explicitly obviously leads to more realistic and comprehensive results. In such case, we have the option of representing space as a continuum or as a discrete collection of sites. Besides, we can choose to keep track of each individual, making a distinction for every single organism, or we can consider individuals to be equivalent and only represent the population through its total abundance or density. The first class of methods is used in practice only in computer simulations, because they are essentially analytically intractable. Finally, the movement/migration in space can be represented as stochastic as a purely deterministic process.

The choice of the model depends on the specific objective of the study, besides the nature of the system to be described. For instance, interacting particle systems and cellular automata[2] are two examples of spatially explicit models that treat space as a discrete grid: the state of the system is in this case represented by the value of the population abundance at each point in space, and transition

[1] Tilman devoted much of his work to study the role of resource competition in community structure, and is also well known for his study concerning the *diversity-stability hypothesis*: thanks to a 20 years long experiment [19] he showed that the stability of a community is positively influenced by higher levels of biodiversity.

[2] Cellular automata models are usually set in discrete time, while interacting particle systems typically represent time as a continuous. See [22–24] for some early examples on the application of these well known physical models in theoretical ecology.

between states typically follows logic or stochastic rules, which can provide highly detailed predictions, with a downside concerning the mathematical tractability of the model – and difficulty in extracting the underlying mechanisms and principles.
Another class of models which is broadly used in ecology is represented by reaction-diffusion models – and their extensions to more general PDEs. Such models are based on an explicit representation of space by means of a continuous variable, and the evolution of the species abundances in time is determined by a set of differential equations.

1.4.1 Reaction-diffusion models in ecology

Reaction diffusion models were first introduced in theoretical ecology by Skellam, in the landmark paper "Random dispersal in theoretical populations" (1951) [25], which had a remarkable impact in the study of spatial ecology. He was the first to exploit the concept of random walk as a description of dispersal at the level of individual organisms, and to make the link to a diffusion equation description at the scale of the population abundances. In the cited paper, he proved the effectiveness of this approach by using empirical data related to the spread of the muskrat, a non-native species which was introduced in central Europe in the early 1900s. Moreover, he combined the diffusive representation of dispersal with the differential equation description of population dynamics, thus introducing reaction-diffusion equations into theoretical ecology[3].

The key idea is that, if one interprets the random dispersal of individuals in the environment as random walks, at a large enough spatial scale the population will exhibit a diffusive behavior which can be easily mathematically encoded by adding a Laplacian term to the equations ruling the population dynamics. A population with abundance n evolving and dispersing in a one-dimensional space can be therefore described by an equation of the kind:

$$\frac{\partial n}{\partial t} = f(x,t,n) + D\,\nabla^2 n$$

where the function $f(x,t,n)$ encodes the population dynamics, which typically includes characteristic parameters such as growth and death rates, while D is the diffusion coefficient. The system can be straightforwardly extended to higher dimensional spaces and to many interacting populations.
This method has both the advantages of a fair mathematical tractability – thanks to the deterministic evolution equations – and of including anyways a description of random processes. Moreover, it is sufficiently flexible, in the sense that it can be easily modified to account for more complex dispersal behaviors, that can be modeled e.g. by a density dependent diffusion coefficient.

Today, reaction-diffusion models are applied with three main purposes in ecology:

- the study of ecological invasions;
- the effect of size, shape and heterogeneity of the spatial domain on the persistence of species and on coexistence;
- the spontaneous formation of patterns in homogeneous space.

The latter phenomenon will be the topic of the next chapter: in particular, reaction-diffusion models will be treated in some detail in Section 2.3.1. A similar approach will be lastly adopted in Chapter 3, where a spatial version of the MacArthur model will be obtained by means of a reaction-diffusion-like extension of the MacArthur equations, and it will be used to study pattern initiation in a competitive ecosystem.

[3] See Chapter 2, Section 2.3.1 for an introduction to reaction-diffusion equations.

Chapter 2

Pattern formation

In this chapter I briefly introduce the topic of pattern formation. Given the broadness of the subject, only the most relevant methods pertaining to the purpose of this thesis are mentioned.
Pattern initiation is presented in Section 2.2, in which the classification of linear instabilities given by Hohenberg [5] is outlined, and in in Section 2.3 two types of models whose pattern-forming properties are frequently studied are shortly described. Lastly, in Section 2.4, the weakly nonlinear dynamics is considered, and the phenomenological amplitude equations are derived for a specific class of pattern forming systems.

2.1 Introduction

Patterns are widespread in nature. They consist in fairly regular spatially periodic structures that can be observed in inanimate systems, such as sand dunes, convection rolls, reacting and diffusing chemicals and even snowflakes to name but a few, and in living systems as well. They can be found at the level of single organisms, such as spots and stripes on animal coats, or they can appear in the distribution of plants or other living species at the ecosystem scale, which is the topic of this thesis.
Recently, much research activity has focused on modeling the processes responsible for their initiation and evolution, seeking to grasp a mechanism that could explain the appearance of very similar patterns in so many diverse systems.

From a physical point of view, pattern formation can be regarded as the process in which an out of equilibrium system passes from a homogeneous to a non-homogeneous state while tuning a suitable control parameter - or a set of parameters. This transition, which is referred to as *bifurcation*[1], usually occurs because the spatially homogeneous solution loses its stability, therefore any infinitesimal perturbation is able to drive the system far from it.
Calling r_c the critical value of the order parameter r of the system, suppose that the homogeneous solution is stable for $r < r_c$ and unstable for $r > r_c$. Being fluctuations unavoidable in any real system, the stable solution is never observed in practice for $r > r_c$, and we will see that this mechanism is able to explain the rising of spatially modulated solutions in physical systems.

The starting point when studying pattern formation consists in performing a linear stability analysis of the homogeneous solution (Section 2.2), which provides the following results:

- it determines the critical value of the control parameter;
- it gives some information about the expected emerging in-homogeneous state, identifying the relevant space and time scales of the pattern.

[1] A bifurcation is a qualitative change in the behavior of some dynamical system as a function of one or more parameters. It can refer, for example, to a change in the number or in the stability of the solutions of the system. It has a broader meaning with respect to the term "phase transition", which has a precise quantitative definition and pertains to infinite systems in thermodynamic equilibrium.

The fate of the instability is determined by the ensuing nonlinear dynamics, which can be studied by means of perturbative techniques (Section 2.4), and it depends on the type of bifurcation: in particular, on the stationary or oscillatory nature of the instability, on the range of unstable wave vectors and on the presence of conservation laws. If the control parameter $r > r_c$ is close enough to the critical value r_c, the dynamics typically terminates in a spatially periodic stationary state.

2.2 Linear stability analysis

More formally, let us consider a continuous-time and continuous-space dynamical model[2]. Such a system is defined by its evolution equation, which consists in a set of partial differential equations of the kind:

$$\partial_t\, u(x,t) = \mathcal{A}[u, \partial_x u, \partial_x^2 u, ...; r]$$

where:

- the field $u(x,t)$ depends on the temporal and spatial variables. It defines the state vector of the system, and it represents some physically relevant quantity through which the pattern can be observed. In general, the state field can have multiple components $u = (u_1,\, u_2 ... u_m)$, representing for instance the abundances of different species in an ecosystem.
- $\mathcal{A} = (\mathcal{A}_1, ... \mathcal{A}_m)$ are generic smooth functionals of the fields and of their spatial derivatives, and they are also dependent on the set of control parameters $r = r_1, ... r_p$.

Since we are describing physical systems in which a spatial structure spontaneously arises without being imposed by external constraints, we ask that the equations should satisfy some symmetries, such as isotropicity and homogeneity in space. Indeed, observed physical patterns typically occur in systems that have approximate Euclidean symmetry. We expect that some pattern with defined spatial periodicity may eventually emerge, breaking the underlying symmetry.
For this consideration to hold, we must also impose that the spatial domain is infinitely extended: as we will see, this has the consequence of providing continuous values for the wavenumbers k of the emerging pattern. Moreover, adopting an infinite domain allows us to avoid the complications arising from the shape of the boundaries influencing the nature of the emerging pattern.
In the following, we will consider the spatial dimension to be $d = 1$ for simplicity.

To start, we assume that there exists a time-independent solution to the PDEs for any r, and that it is invariant under all the spatial symmetries of the system. It consists thus of a stationary homogeneous state $u^* = u_1^*, ... u_m^*$ such that, for any equation labeled by i, it holds:

$$\partial_t\, u_i^* = 0 \qquad \Leftrightarrow \qquad \mathcal{A}_i[u^*, 0, ...0; r] = 0 \quad \forall\, r$$

We weakly perturb such solution and linearise the dynamical equations around u^*:

$$\begin{aligned} &u(x,t) = u^* + \delta u(x,t) \\ &\partial_t\, \delta u(x,t) \approx \mathcal{L}[u^* + \delta u, \partial_x \delta u, ...; r] \end{aligned} \tag{2.1}$$

where $\mathcal{L} = (\mathcal{L}_1, ... \mathcal{L}_m)$ are linear functionals of the fields $u_1, ... u_m$ and of their spatial derivatives, corresponding to the linear part of $\mathcal{A}$:

$$\mathcal{A}[u, \partial_x u, ...; r] = \mathcal{L}[u, \partial_x u, ...; r] + \mathcal{N}[u, \partial_x u, ...; r]$$

Thanks to its linearity, Eq. (2.1) can be easily solved with the help of Fourier analysis. The evolution of the single Fourier modes δu_k can be studied:

$$\delta u_{k,j}(x,t) \sim e^{\lambda t + ikx} \quad \forall\, j = 1, ... m$$

[2] As we have seen, an ecosystem can be modeled in such way. In this chapter, however, we discuss pattern formation adopting a general approach, which applies to any kind of pattern forming system.

where k is the wavenumber of the mode and j labels the field. Substituting $\partial_t \to \lambda$, $\partial_x \to ik$, the linearised equations turn into an eigenvalue problem:

$$\lambda\, \delta u_k = \mathbb{M}(k;r)\, \delta u_k \qquad \text{where} \quad \mathbb{M}(k;r) \text{ is a } m \times m \text{ matrix whose entries depend on } k \text{ and } r.$$

which yields a set of eigenvalues as a function of the wavenumber k and of the parameters r.
Let us focus on the eigenvalue with the largest real part, which we denote by $\lambda_+(k)$.
To have stability of the homogeneous solution for $r < r_c$ and instability for $r > r_c$, the leading growth rate of the Fourier modes must change as follows:

- $Re[\lambda_+(k)] < 0 \,\forall\, k$ for $r < r_c$
- $Re[\lambda_+(k_c)] = 0$ at some critical wavenumber k_c for $r = r_c$
- $Re[\lambda_+(k)] > 0$ in a band of wavenumbers $k_1 < k < k_2$ for $r > r_c$

where k_c is the wavenumber corresponding to the maximum of $Re[\lambda_+(k)]$ at the edge of the bifurcation (i.e. for $r \to r_c^+$) and we denote by $\bar{k} = \bar{k}(r)$ the most unstable wave vector when $r > r_c$. The temporal frequency is given by $w_c \coloneqq Im[\lambda_+(k_c)]$.

The type of instability is conventionally classified according to the behavior of the Fourier modes at the bifurcation [5], as illustrated in Fig. 2.1.
If $k_c = \bar{k} \neq 0$ the instability is spatially periodic, the unstable band being $k_1 < k < k_2$ (k_1, $k_2 \neq 0$): this is called a type I instability. If instead $k_c = \bar{k} = 0$, the instability is named of type III: it is spatially uniform, in the sense that no defined lengthscale can emerge, and the unstable band is given by $0 < k < k_2$. The intermediate case is represented by type II instability, in which $k_c \neq 0$ but $\bar{k} \neq k_c$ and $Re[\lambda_+(k = 0)] = 0 \,\forall\, r$, which is typically due to some conservation law. The unstable band is again $0 < k < k_2$, but the most unstable wave vector is now different from zero ($\bar{k} \neq 0$).

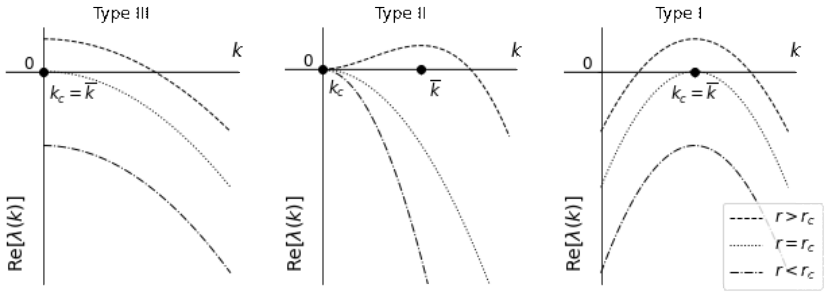

Type	k_c	$\bar{k}$
I	$k_c \neq 0$	$\bar{k} = k_c$
II	0	$\bar{k} \neq 0$
III	0	0

TAB. 2.1. Classification of linear instabilities according to Hohenberg [5].

Additionally, temporal instability must be taken into consideration: the pattern is stationary if $w_c = 0$ and oscillatory in time if $w_c \neq 0$.

2.2.1 Instability length and time scales

The above classification, based on the linear analysis of the system, allows to gain some preliminary information about the pattern that will emerge by setting $r > r_c$.

Firstly, since Fourier modes have a time dependence of the kind $e^{Re[\lambda(k)]t}$, the mode growing faster will be the one corresponding to the maximum of $\lambda_+(k)$, that is $\bar{k}$. In this sense, a clear difference between type III and type I-II instabilities can be noticed.
If $\bar{k} = 0$ there is no well-defined wavelength dominating over the others: therefore, we expect that many different lengthscales may appear, producing an initially confused pattern. If $\bar{k} \neq 0$, instead, there is a clear lengthscale $\bar{\lambda} = 2\pi/\bar{k}$ dominating the spatial pattern in the linear regime: such scale is equal to k_c for type I instabilities, while it depends on r for type II instabilities.

Similarly, another distinction can be made depending on the value of k_c. Indeed, if $k_c \neq 0$, the instability band is centered around k_c and it does not contain $k = 0$: this implies that, for $r - r_c \to 0^+$, all the unstable modes are vanishingly close to k_c, thus all unstable lengthscales are approximately equal to $2\pi/k_c$. If $k_c = 0$, instead, the instability band contains 0, therefore all modes with a wavelength larger than a certain threshold are unstable and contribute to the dynamics. This has important consequences on the nonlinear behavior of the system.

In all cases, the timescale for instability initiation is given by $\tau \sim 1/Re[\lambda_+(k_c)]$: when $t \ll \tau$ the behavior of the system can be considered linear with good approximation, while for $t \gtrsim \tau$ nonlinear terms become non negligible and the behavior of the system is determined by the non-linear dynamics.

2.3 Examples of pattern forming models

In this section I provide some relevant examples of pattern-forming models. The first one I briefly discuss is reaction-diffusion models, by reason of their analogy to the system which will be presented in this thesis: indeed they rely on the addition of diffusion terms to the dynamical equations governing the interaction of different chemical species. Secondly, I introduce the Swift-Hohenberg model, because it represents the simplest model producing type I stationary instabilities and thus it can be used as a starting point for the derivation of the amplitude equations governing such class of systems.

2.3.1 Reaction-diffusion models

In his famous 1952 paper "The Chemical Basis of Morphogenesis" [4], Alan Turing proposed a simple model to account for the formation of natural patterns. In his work, he showed that a steady state spatially heterogeneous pattern of chemical concentration with well-defined wavelength can spontaneously arise from a small perturbation of the homogeneous equilibrium state of a system of two reacting and diffusing chemicals. Even though Turing invoked this mechanism as a basis for the development of shape and structure in living organisms, biologists strongly disputed this theory. Many years later, in 1990, the first convincing evidence of an experimental Turing pattern was found (Castets *et al.*) and such mechanism eventually proved to be very effective in describing the formation of patterns in a variety of different contexts.

A famous class of pattern forming systems is indeed represented by reaction-diffusion models, which are mainly used - as the name states - to study the dynamics of reacting and diffusing chemicals.
In such models, each chemical species is described by means of its concentration field $u_i(x,t)$.
The evolution equations for n species read:

$$\partial_t u_i = R_i(u_1, ...u_n) + D_i \nabla^2 u_i \quad i = 1, ...n$$

and are determined by the reaction kinetics R_i, a nonlinear function of the concentrations which describes the interaction between species, and by the diffusive terms, characterized by the diffusion coefficients D_i. This model can exhibit all the types of linear instabilities we have previously outlined, by suitable choice of $R_1, ...R_n$ and $D_1, ...D_n$. Because we are interested in the formation of a spatially periodic pattern, our aim is to investigate the simplest conditions giving rise to a type I instability spectrum.
It is straightforward to notice that systems formed by one chemical alone cannot display the desired instability, since

$$\partial_t u = f(u) + D\nabla^2 u$$

and its linearisation yields:

$$\partial_t \delta u = \left(f'(u^*) + D\nabla^2\right) \delta u \quad \to \quad \lambda = f'(u^*) - k^2 D$$

which is a type III spectrum, having the maximum of λ in $k_c = 0$. We will then focus on a system of two chemicals, which is typically studied as the prototype for Turing patterns:

$$\begin{cases} \partial_t u = f(u,v) + D_u \nabla^2 u \\ \partial_t v = g(u,v) + D_v \nabla^2 v \end{cases}$$

where $u(x,t)$ and $v(x,t)$ are the concentrations of the two chemicals, and $D_u,\ D_v > 0$ are their diffusion coefficients. Being the diffusion isotropic, no preferred spatial direction can emerge in the analysis of the system, and all the relevant quantities will depend on the modulus of the wavenumber $k = |\mathbf{k}|$. For this reason, we can perform the linear stability analysis in one spatial dimension and rely on the generalisation to higher spatial dimensions to be straightforward. Through a redefinition of the spatial variable $x \to x/D_u$ we can get rid of a parameter:

$$\begin{cases} \partial_t u = f(u,v) + \nabla^2 u \\ \partial_t v = g(u,v) + d\,\nabla^2 v \end{cases} \tag{2.2}$$

and $d = D_v/D_u$ is now the control parameter of the system. We assume the existence of a homogeneous steady state $(u^*,\ v^*)$, such that $f(u^*, v^*) = 0 = g(u^*, v^*)$ linearise the system around it, by applying the following spatial disturbances:

$$\begin{cases} u(x,t) = u^* + \delta u(x,t) = u^* + \delta_u\, e^{\lambda t + ikx} \\ v(x,t) = v^* + \delta v(x,t) = v^* + \delta_v\, e^{\lambda t + ikx} \end{cases} \tag{2.3}$$

which we have already expressed as single harmonic modes, since the problem that we are going to study is linear. Eq. (2.2) becomes, at first order:

$$\begin{cases} \partial_t\, \delta u = \dfrac{df}{du}\Big|_{u^*,v^*}\delta u + \dfrac{df}{dv}\Big|_{u^*,v^*}\delta v + \nabla^2 \delta u \\ \partial_t\, \delta v = \dfrac{dg}{du}\Big|_{u^*,v^*}\delta u + \dfrac{dg}{dv}\Big|_{u^*,v^*}\delta v + d\,\nabla^2 \delta v \end{cases}$$

which corresponds to the eigenvalue problem:

$$\lambda\, \vec{\delta} = (\mathbb{J} - k^2 \mathbb{D})\, \vec{\delta} \equiv \mathbb{M}(k)\, \vec{\delta}$$

where $\vec{\delta} = (\delta_u,\ \delta_v)$, $\mathbb{J}$ is the Jacobian of the reaction kinetics and $\mathbb{D} = \begin{pmatrix} 1 & 0 \\ 0 & d \end{pmatrix}$ is the diffusion matrix. Solving in λ:

$$\begin{aligned} \det\big(\mathbb{M}(k) - \lambda \mathbb{I}\big) = 0 \quad &\Leftrightarrow \quad \lambda^2 - \lambda\, \mathrm{Tr}(\mathbb{M}) + \det(\mathbb{M}) = 0 \\ &\Leftrightarrow \quad \lambda_\pm(k) = \frac{\mathrm{Tr}(\mathbb{M}) \pm \sqrt{\big(\mathrm{Tr}(\mathbb{M})\big)^2 - 4\det(\mathbb{M})}}{2} \end{aligned}$$

At this point, one must introduce some constraints on stability. Asking that u^* is an actual stable equilibrium of the spatially independent system is equivalent to imposing its stability under spatially uniform perturbations, which are obtained by setting $k = 0$ in (2.3). This occurs if the real part of both eigenvalues is strictly negative, in such a way that the perturbation decays exponentially fast to zero.

Pattern formation arises if, in addition to the previous condition, that ensures the stability of the underlying equilibrium, u^* is also linearly unstable under heterogeneous perturbations ((2.3) with $k > 0$), in such a way that the spatial perturbations will grow in time - more precisely, the modes corresponding to unstable wavenumbers k will grow and produce a pattern in space, as explained in the previous sections. This holds if at least one eigenvalue has positive real part for some $k > 0$.

$$Re[\lambda_+(k > 0)] > 0 \quad \Rightarrow\ u^* \text{ is unstable under heterogeneous perturbations}$$

The above inequalities imply that the cross terms $\frac{df}{dv}\big|_{u^*,v^*}$ and $\frac{dg}{du}\big|_{u^*,v^*}$ must be non-vanishing and have opposit sign, and additionally:

$$\begin{cases} \frac{df}{du}\big|_{u^*,v^*} > 0 \\ \frac{dg}{dv}\big|_{u^*,v^*} < 0 \\ d > 1 \quad \Leftrightarrow \quad D_v > D_u \end{cases} \quad \vee \quad \begin{cases} \frac{df}{du}\big|_{u^*,v^*} < 0 \\ \frac{dg}{dv}\big|_{u^*,v^*} > 0 \\ d < 1 \quad \Leftrightarrow \quad D_u > D_v \end{cases}$$

Referring to the *activator* as the species that promotes growth and as the *inhibitor* as the one that leads to a concentration decay, this result can be summarised by stating that the inhibitor must diffuse faster than the activator in order for the pattern to form. This property is known as *local activation with long-range inhibition*, and it is an example of a scale-dependent feedback mechanism.

2.3.2 Swift-Hohenberg model

The Swift-Hohenberg model (SH) represents the simplest nonlinear model displaying type I_s linear instability. It is defined by the following PDE in the field $u(x,t)$:

$$\partial_t u = \left(r - (\partial_x^2 + k_c^2)^2\right) u - u^3 \equiv \mathcal{L}\, u + \mathcal{N}[u]\,, \quad k_c \neq 0 \tag{2.4}$$

where r is the bifurcation parameter, $\mathcal{N}[u] = u^3$ is the nonlinear part and $\mathcal{L} = \left(r - (\partial_x^2 + k_c^2)^2\right)$ is indeed a linear operator producing type-I_s instabilities.
To prove it, let us study the linear behavior of the system around the homogeneous solution $u^* = 0$, by applying a perturbation of the form $\delta u(x,t) = Ae^{\lambda t + ikx}$, with A constant. Since $u = u^* + \delta u = \delta u$, at linear order:

$$\begin{aligned} &\lambda\, u \approx \left(r - \partial_x^4 - k_c^4 - 2k_c^2\partial_x^2\right) u = \left(r - k^4 - k_c^4 + 2k_c^2 k^2\right) u = \left(r - (k^2 - k_c^2)^2\right) u \\ &\Rightarrow \lambda(k) = r - (k^2 - k_c^2)^2 \end{aligned} \tag{2.5}$$

which is real and has global maximum in $k = k_c \neq 0$, therefore the linear instability is spatially periodic and stationary in time.

Besides, it can be noticed that the additional cubic term in the SH equation (2.4) is the lowest-order nonlinear term preserving the invariance of $\mathcal{L}$ with respect to the field inversion $u \to -u$.
A quadratic term breaking the $u \to -u$ symmetry can otherwise be added, leading to the generalised Swift-Hohenberg equation:

$$\partial_t u = \left[r - (\partial_x^2 + k_c^2)^2\right] u + \rho u^2 - u^3 \tag{2.6}$$

We observe, however, that the quadratic term alone cannot guarantee the saturation of the unstable amplitude, because it contributes to $\partial_t u$ with a constant sign, independent of the sign of u. Therefore, the cubic term must be also kept. This can be seen more rigorously from the amplitude equations that will be presented in the next section.

2.4 Amplitude equations

The linear analysis presented in Section 2.2 provides a classification of linear instabilities whose validity is limited to short timescales $t < \tau$, beyond which the effect of the nonlinear terms become no longer negligible. An analytical approach for the solution of the full equations is however mostly unfeasible.

Near the threshold, though, the behavior of the system can be described by means of phenomenological equations, thanks to the fact that the nonlinearities are weak and the spatial and temporal modulations of the amplitude are slow.
It turns out that these model equations have - broadly speaking - universal forms, meaning that they depend only on general properties of the system, such as the linear instability type, the symmetries and conservation laws: hence, they can both provide an explanation for the fact that similar patterns are observed in systems of completely different nature, and they can be used as a mean to get insight into the outcome of instability in a given physical system.
The notion of universality, which is rigorous and quantitatively defined for critical points in equilibrium statistical mechanics, is however highly qualitative in this context, and it is yet unclear how far this analogy can be pushed for what concerns pattern formation.

Exploiting this generality, in Section 2.4.1 we shall derive the the Ginzburg-Landau envelope equation, that describes systems with type-I linear instability and with symmetries $x \to -x$, $x \to x + \bar{x}$, by starting from the simplest model that displays such features: the SH model discussed in Section 2.3.2. A symmetry-based approach for their derivation, which brings out their universal character, will be instead presented in Section 2.4.2.

2.4.1 Amplitude equations derivation from the SH model

Let us determine the scalings for a type-I instability. Firstly, we want to understand what is the order of magnitude of the unstable k interval given by (2.5) very close to the bifurcation, i.e. for $0 < r \ll 1$ (having rescaled r in such a way that $r_c = 0$). The unstable wavenumber values will be very close to k_c if r is very small, therefore we can express k as $k = k_c + k_x$ with $|k_x| \ll k_c$ and expand:

$$\begin{aligned} \lambda(k) &= r - \left((k_c + k_x)^2 - k_c^2\right)^2 = r - (k_x^2 + 2k_c k_x)^2 = r - k_x^4 - 4k_c^2 k_x^2 - 4k_c k_x^3 \approx \\ &\approx r - 4k_c^2 k_x^2 + O(k_x^3) \end{aligned} \tag{2.7}$$

Thus if $k_c \sim O(1)$ we see that $\lambda(k) = 0$ for $k_x \sim \sqrt{r}$ and we have found the scaling of the unstable wavenumber band. As for the temporal scale, $\lambda(k)$ is clearly of order $\lambda(k_c) = r$ for $r \to 0^+$.
A type-I bifurcation is therefore characterized by a k instability range of order $\sim \sqrt{r}$ and a growth rate of order r.

The effect of such an unstable wavenumber interval can be interpreted as the introduction of a modulation in the amplitude of the carrier wave $e^{ik_c x}$, varying slowly in time and space:

$$u(x,t) = A(x,t)e^{ik_c x} + c.c. \quad \text{with A depending weakly on } x \text{ and } t. \tag{2.8}$$

The modulation is weak because the wavenumbers corresponding to positive λ_+ have a small variability for $r \to 0$. To get an intuition of this fact, we can consider a simple example. Suppose we have two unstable wavenumber modes falling in the instability region around k_c (Fig. 2.1).

$$u(x) = a_1 \cos(k_1 x) + a_2 \cos(k_2 x) = (a_1 + a_2)\cos(\delta k\, x)\cos(k_0 x) + (a_1 - a_2)\sin(\delta k\, x)\sin(k_0 x)$$

Then, having defined $k_0 = (k_1 + k_2)/2$ and $\delta k = (k_2 - k_1)/2$. Since $k_0 \sim k_c$ and $\delta k \sim |k_x| \ll k_c$, the above solution represents an oscillation of wavenumber k_0 modulated by a weakly varying amplitude.

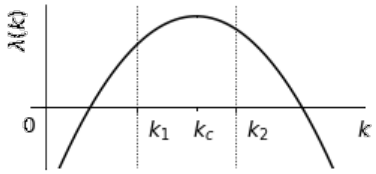

FIG. 2.1. Schematic illustration of a system displaying two unstable wavenumber modes k_1, k_2 in the instability region.

Therefore, due to the scaling we found above, we expect that the spatial variable appears in the carrier wave as $k_c x$ and in the amplitude according to the scaling $\sqrt{r}\,x$, while the time variable can be enclosed the slowly varying amplitude as $\lambda(k_c)\,t \approx rt$.

In order to formally treat this problem, a multiscale expansion can be performed. Using the more convenient notation $r = \epsilon^2\,\hat{r}$ with $\epsilon^2 \ll 1$, $\hat{r} = const > 0$, we can define the slow variables as follows:

$$\begin{cases} X = \epsilon\, x \\ T = \epsilon^2 t \end{cases}$$

in contrast with the fast variables:

$$\begin{cases} \tilde{x} = x \\ \tilde{t} = t \end{cases}$$

Therefore (2.8) becomes:

$$u(X, T, \tilde{x}, \tilde{t}) = A(X, T)\, e^{ik_c\tilde{x}} + c.c. \tag{2.9}$$

which naturally encodes the different temporal and spatial scales. Applying the chain rule to the temporal and spatial derivatives in (2.4) and using the fact that $u(X, T, \tilde{x}, \tilde{t})$ is independent of $\tilde{t}$, the equation becomes:

$$\epsilon^2\,\partial_T u = \epsilon^2 \hat{r}\,u - \left(\partial_{\tilde{x}}^2 + \epsilon^2\,\partial_X^2 + 2\epsilon\,\partial_{\tilde{x}}\partial X + k_c^2\right)^2 u - u^3$$

If the solution is expanded in powers of ϵ:

$$u = u_1\epsilon + u_2\epsilon^2 + u_3\epsilon^3 + ...$$

$$\begin{aligned} \epsilon^2\left(\partial_T u_1\epsilon + ...\right) &= \epsilon^2\hat{r}\left(u_1\epsilon + ...\right) - \left(\partial_{\tilde{x}}^2 + \epsilon^2\,\partial_X^2 + 2\epsilon\,\partial_{\tilde{x}}\partial X + k_c^2\right)^2\left(u_1\epsilon + u_2\epsilon^2 + u_3\epsilon^3 + ...\right) - \left(u_1\epsilon + ...\right)^3 \\ &= \epsilon^2\hat{r}\left(u_1\epsilon + ...\right) - \big[(\partial_{\tilde{x}}^2 + k_c^2)^2 + 4\epsilon(\partial_{\tilde{x}}^2 + k_c^2)\partial_{\tilde{x}}\partial X + \\ &\qquad + 2\epsilon^2(3\partial_{\tilde{x}}^2 + k_c^2)\partial_X^2 + 4\epsilon^3\partial_{\tilde{x}}\partial_X^3 + \epsilon^4\partial_X^4\big]\left(u_1\epsilon + u_2\epsilon^2 + u_3\epsilon^3 + ...\right) + \\ &\qquad - \left(u_1\epsilon + ...\right)^3 \end{aligned}$$

The equation is then analysed order by order:

$$\text{at } O(\epsilon) \qquad (\partial_{\tilde{x}}^2 + k_c^2)^2 u_1 = 0 \quad \rightarrow \quad u_1 = A_1(X, T)e^{ik_c\tilde{x}} + c.c.$$

$$\begin{aligned} \text{at } O(\epsilon^2) \qquad & (\partial_{\tilde{x}}^2 + k_c^2)^2 u_2 = -4(\partial_{\tilde{x}}^2 + k_c^2)\partial_{\tilde{x}}\partial_X u_1 - (\partial_{\tilde{x}}^2 + k_c^2)^2 u_1 = 0 \\ & \rightarrow \quad u_2 = A_2(X, T)e^{ik_c\tilde{x}} + c.c. \end{aligned}$$

where, in the last equality of the $O(\epsilon^2)$ equation, the solution for u_1 was substituted. Proceeding similarly, one finds the following equation for the third order:

$$\begin{aligned} \text{at } O(\epsilon^3) \qquad (\partial_{\tilde{x}}^2 + k_c^2)^2 u_3 &= \hat{r}u_1 - \partial_T u_1 2(3\partial_{\tilde{x}}^2 + k_c^2)\partial_X^2 u_1 - u_1^3 = \\ &= \left(\hat{r} - \partial_T + 4\,k_c^2\,\partial_X^2\right) u_1 - u_1^3 \end{aligned}$$

Using $u_1 = A_1(X,T)e^{ik_c\tilde{x}} + c.c.$ and calling $A_1 \to A$ for simplicity.

$$u_1^3 = (A(X,T)e^{+ik_c\tilde{x}} + \overline{A(X,T)}\, e^{-ik_c\tilde{x}})^3 = A^3 e^{3ik_c\tilde{x}} + 3|A|^2\,\overline{A}\, e^{ik_c\tilde{x}} + c.c.$$

The equation at $O(\epsilon^3)$ becomes:

$$(\partial_{\tilde{x}}^2 + k_c^2)^2 u_3 = \left(\hat{r}A - \partial_T A + 4\,k_c^2\,\partial_X^2 A - 3|A|^2\,\overline{A}\right) e^{ik_c\tilde{x}} - A^3 e^{3ik_c\tilde{x}} + c.c.$$

therefore it contains a term which is proportional to the solution of the homogeneous equation, and would introduce secular terms in the solution, i.e. terms which grow without bound, that would break down the perturbative approach we have adopted. Thanks to the separation of scales, however, the vanishing of such term can be imposed by putting to zero its coefficient:

$$\hat{r}A - \partial_T A + 4\,k_c^2\,\partial_X^2 A - 3|A|^2\,\overline{A} \equiv 0 \quad \Rightarrow \quad \partial_T A = \hat{r}A + 4\,k_c^2\,\partial_X^2 A - 3|A|^2\,\overline{A}$$

This is the Ginzburg-Landau equation (GL) at lowest order in the amplitude. The values of the coefficients here are specific of the SH model, whereas in general the coefficients are not fixed and depend on the microscopic details of the system. For instance, if we considered the generalised SH equations, we would find:

$$\partial_T A = \hat{r}A + 4\,k_c^2\,\partial_X^2 A - \left(3\sigma - \frac{38}{9}\frac{\rho^2}{k_c^4}\right)|A|^2\,\overline{A}$$

labeling with σ the coefficient of the u^3 term in the generalised SH equations. From the above equation it is clear that if the cubic term is absent from Eq. (2.6), the nonlinearity will not be able to saturate the linear instability and the amplitude of the pattern will continue to grow. For the nonlinearity to counteract the linear behavior, it is necessary that $3\sigma - \frac{38}{9}\frac{\rho^2}{k_c^4} > 0$.

2.4.2 Symmetry based derivation of the amplitude equations

To better grasp the universality of SH equations, we outline a symmetry-based derivation.
Starting from the basic assumption (2.8), of which we justified the validity, we want to obtain the envelope equations of a system displaying type I_s instability and satisfying the spatial homogeneity and isotropicity symmetries.

The linear part of the envelope equations can be derived quite simply from the basic requirements on the linear growth rate of type I_s instabilities.
Indeed, considering a mode $u(x,t) = A_0\, e^{\lambda t + ikx}$ with wavenumber close to k_c, $k = k_c + k_x$, we can expand the growth rate $\lambda(k)$ in terms of $|k_x| \ll k_c$. The requirement that $k = k_c$ (i.e. $k_x = 0$) corresponds to the maximum growth rate sets the first order term of the expansion to zero. Moreover, remembering that we can always rescale the control parameter r in such a way that k_c becomes unstable at $r = 0$, the growth rate near the bifurcation can be written in full generality as:

$$\lambda(k) = \tau_0^{-1}(r - \xi_0^2 k_x^2) + O(k_x^3) \tag{2.10}$$

at lowest order in k_x, where the real constants τ_0 and ξ_0 represent some typical temporal and spatial scales of the individual system under consideration, and depend on its microscopic details.
We notice indeed that this result is perfectly consistent with the one derived by expanding the linear growth rate predicted by the SH model (2.7). Therefore, the same scalings can be exploited, allowing to interpret the above considered Fourier as follows:

$$u(x,t) = A_0\, e^{\lambda t + ik_x x + ik_c x} = A_0\, e^{\hat{\lambda}\epsilon^2 t + i\hat{k_x}\epsilon x + ik_c x} = A_0\, e^{\hat{\lambda}T + i\hat{k_x}X} e^{ik_c x} \equiv A(X,T)\, e^{ik_c x}$$

where A is a complex amplitude depending on the slow variables X, T.
Thus, we see that Eq. (2.10) could have been derived from a partial differential equation in u, which can be recovered by making the substitutions $\lambda \to \epsilon^2\partial_T$, $k_x \to -i\epsilon\partial_X$ that bring us back from Fourier space to real space.

$$\epsilon^2\,\tau_0\,\partial_T u = ru + \epsilon^2\,\xi_0^2\,\partial_X^2 u \tag{2.11}$$

We can also rewrite $r = \epsilon^2 \hat{r}$ according to the consistent scaling for r. Since there is no explicit dependence on x, the carrier wave factor $e^{ik_c x}$ can be simplified and the equation holds for the complex amplitude alone:

$$\tau_0 \, \partial_T A = \hat{r} A + \xi_0^2 \, \partial_X^2 A \tag{2.12}$$

which is the linear part of the GL equations. To look for the nonlinear terms, we consider the symmetries of our system.

Translation in space
Exploiting the separation of scales, invariance under translation in x corresponds to the invariance under two symmetries: translation in X and phase shift in A.

$$x \to x + \phi \quad \Rightarrow \quad \begin{array}{l} X \to X + \epsilon\phi \\ A \to A \, e^{i\phi} \end{array}$$

Reflection in space
Similarly:

$$x \to -x \quad \Rightarrow \quad \begin{array}{l} X \to -X \\ A \to \overline{A} \end{array}$$

Translation in time
Time translational symmetry must also hold, for the obvious freedom to choose the temporal origin.

$$t \to t + \tau \quad \Rightarrow \quad T \to T + \epsilon^2 \tau$$

Since both A and its spatial derivatives are expected to be small close to the bifurcation, we must look for the lowest order nonlinear terms preserving the symmetries listed above. Starting from phase shift, the quadratic terms A^2, $\overline{A}^2$ and $|A|^2$ all transform in a different way from $\partial_T A$. Among the cubic terms A^3, $\overline{A}^3$, $|A|^2\overline{A}$ and $|A|^2 A$, the only one transforming in the appropriate way is the latter, indeed:

$$\hat{r} A e^{i\phi} + \xi_0^2 \, \partial_X^2 A e^{i\phi} - g_0 |A|^2 e^{i\phi} e^{-i\phi} A e^{i\phi} = e^{i\phi} \left(\hat{r} A + \xi_0^2 \, \partial_X^2 A - g_0 |A|^2 A \right) \equiv \tau_0 \, \partial_T A e^{i\phi}$$

Invariance under complex conjugation fixes its coefficient g_0 to be real:

$$\begin{aligned} \hat{r} \, \overline{A} + \xi_0^2 \, \partial_X^2 \overline{A} - g_0 |A|^2 \overline{A} &\equiv \tau_0 \, \partial_T \overline{A} \\ &= \overline{\hat{r} A + \xi_0^2 \, \partial_X^2 A - g_0 |A|^2 A} \end{aligned} \quad \Leftrightarrow \quad \overline{g_0} \equiv g_0 \quad \Leftrightarrow \quad g_0 \in \mathbb{R}$$

Invariance under translation in X and T trivially implies that g_0 must be independent of both variables, i.e. it is a constant. If the nonlinearity has to saturate the linear instability, we must further require that $g_0 > 0$. The amplitude equations therefore read:

$$\tau_0 \, \partial_T A = \hat{r} A + \xi_0^2 \, \partial_X^2 A - g_0 |A|^2 A \tag{2.13}$$

which can be written in universal form by rescaling:

$$\begin{array}{l} X \to X/\xi_0 \\ T \to T/\tau_0 \\ A \to A \, g_0^{1/3} \end{array} \quad \Rightarrow \quad \partial_T A = (\hat{r} + \partial_X^2) \, A - |A|^2 A$$

Which is the GL equation at lowest order.

Chapter 3

Spatially-extended MacArthur's model

In this chapter, I try to derive a spatial extension of the MacArthur consumer-resource model by adopting an approach similar to reaction diffusion models: diffusion-like terms are added to the equations of the system, with the aim of achieving a type I linear instability.
Many attempts are outlined, until the desired result is obtained and presented in Section 3.5.
An alternative approach based on non-local resource optimization is discussed in Section 3.6.

3.1 Introductory trivial model

To begin to investigate the effect of diffusion terms on MacArthur equations, I will start with a truly basic model: I consider a 1-dimensional spatial domain, and I study the dynamics of one species alone, characterized by some rate r:

$$\dot{n} = r\, n - \partial_x J \tag{3.1}$$

where $n = n(x,t)$ is the population density field. As for the diffusion term $\partial_x J$, I am considering a density dependent diffusion coefficient $\mathcal{D}(n) = D - \widetilde{D}\, n$ with D, $\widetilde{D}$ positive constants:

$$-\partial_x J = \partial_x \left[\mathcal{D}(n)\, \partial_x n\right] = \partial_x \left[(\, D - \widetilde{D}\, n\,)\, \partial_x n\right] = D\, \partial_x^2 n - \widetilde{D} \left[(\partial_x n)^2 + n \partial_x^2 n\right] \tag{3.2}$$

Such term represents a simple dispersal motion, characterized by the diffusion coefficient D, with the addition of an overcrowding effect, modeled by a negative diffusion coefficient $-\widetilde{D}\, n$ which is linearly proportional to the population density n. In such a way, for high enough population densities, the overall diffusion coefficient $\mathcal{D}(n)$ becomes more and more negative as n grows, thus producing a further increase in the concentration of the population.
As we shall see in the following, indeed, this assumption allows for a richer dynamics with respect to simple diffusion alone, thanks to the fact that $\mathcal{D}(n)$ can change sign.

Let us perform the linear stability analysis for this simple equation, to discover if it can give rise to a spatial instability.

Uniform equilibrium

Firstly, the equilibrium solution n_* must be determined. In the following, we adopt an asterisk as notation for the equilibrium states.

$$\begin{cases} \dot{n_*} = 0 \\ \partial_x n_* = 0 \end{cases} \quad \Rightarrow \quad r\, n_* = 0 \quad \Leftrightarrow \quad n_* = 0$$

Stability under uniform perturbation

I perturb the equilibrium as follows:

$$n(t) = n_* + \delta n(t) \qquad \text{with} \quad \delta n(t) = \delta\, e^{\lambda t} \tag{3.3}$$

Substituting such perturbation in Eq. (3.1):

$$\dot{\delta n} = r(n_* + \delta n) = r\,\delta n$$
$$\lambda\,\delta n = r\,\delta n$$

Therefore the equilibrium is stable $\Leftrightarrow \lambda = r < 0$, and r actually plays the role of a death rate.

Non-uniform perturbation

Now I look for instability under non-uniform perturbations, which are expressed as Fourier modes:

$$n(x,t) = n_* + \delta n(x,t) \qquad \text{with} \quad \delta n(x,t) = \delta\, e^{\lambda t + ikx} \tag{3.4}$$

Substituting in Eq. (3.1):

$$\delta\dot{n} = r(n_* + \delta n) + D\,\partial_x^2\delta n - \widetilde{D}\left[(\partial_x\delta n)^2 + (n_* + \delta n)\,\partial_x^2\delta n\right]$$

Neglecting $(\delta n)^2$:

$$\delta\dot{n} = r(n_* + \delta n) + D\,\partial_x^2\delta n - \widetilde{D}\left[n_*\,\partial_x^2 n\right]$$

I observe that, by substituting the equilibrium value $n_* = 0$, the overcrowding contribution disappears, hence the system does not show instability under spatial perturbations, since the perturbations decay with rate:

$$\lambda = r - k^2 D < 0 \quad \forall\, k$$

We can attempt to modify this model in such a way that the equilibrium value becomes different from zero.

3.1.1 Basic one-species model

The simplest way to allow for a positive equilibrium value is to add a constant growth supply $\mu > 0$. Calling d the death rate, the equation becomes:

$$\dot{n} = \mu - d\,n + \partial_x\left[\left(D - \widetilde{D}n\right)\,\partial_x n\right] \tag{3.5}$$

We underline that the opposite possibility, i.e writing $\dot{n} = \mu\,n - d + \partial_x J$, would lead to finding $d < 0$, $\mu < 0$ which is equivalent to the considered case.

Uniform equilibrium

In this case the equilibrium of the system is:

$$\begin{cases} \dot{n} = 0 \\ \partial_x n = 0 \end{cases} \quad \Rightarrow \quad \mu - d\,n_* = 0 \quad \Leftrightarrow \quad n_* = \mu/d$$

Stability under uniform perturbation

By substituting the uniform perturbation (3.3) into Eq. (3.5):

$$\delta\dot{n} = \mu - d(n_* + \delta n) = -d\,\delta n$$
$$\lambda\,\delta n = -d\,\delta n$$

Therefore the equilibrium is stable if $\lambda = -d < 0 \Leftrightarrow d > 0$.

Non-uniform perturbation

Substituting the perturbation (3.4) in Eq. (3.5) and linearising around n_* yields:

$$\begin{aligned}\delta\dot{n} &= \mu - d\,(n_* + \delta n) + D\,\partial_x^2\delta n - \widetilde{D}\left[(\partial_x\delta n)^2 + (n_* + \delta n)\,\partial_x^2\delta n\right] = \\ &= \mu - d\,(n_* + \delta n) + D\,\partial_x^2\delta n - \widetilde{D}\,n_*\,\partial_x^2\delta n = \\ &= -d\,\delta n + (D - \widetilde{D}\mu/d)\,\partial_x^2\delta n\end{aligned}$$

where in the last line I substituted the equilibrium value. Taking the derivatives of the perturbation I find:

$$\lambda\,\delta n = -d\,\delta n - k^2\left(D - \widetilde{D}\,\mu/d\right)\delta n$$

The system is therefore unstable if:

$$\lambda = -d + k^2\left(\widetilde{D}\,\mu/d - D\right) > 0 \tag{3.6}$$

Being $-d < 0$ as required by the stability of the uniform equilibrium, $\widetilde{D}\,\mu/d - D$ must necessarily be > 0 for instability to hold.

$$\lambda > 0 \quad \Leftrightarrow \quad \begin{cases} \widetilde{D}\,\mu/d - D > 0 \\ k^2 > \dfrac{d}{\widetilde{D}\mu/d - D} \end{cases} \tag{3.7}$$

In conclusion, thanks to the presence of the overcrowding term, a spatial instability is allowed for:

$$\text{wavenunmbers } k > \sqrt{\frac{d}{\widetilde{D}\mu/d - D}} \quad \rightarrow \quad \text{wavelengths } < 2\pi\sqrt{\frac{\widetilde{D}\mu/d - D}{d}}$$

However, this is not the desired outcome, since it is not a type I instability. On the contrary, this result is somewhat pathological, because it leads to the instability of all the microscopic wavelengths, which is clearly physically meaningless. Indeed, it would lead to the formation of patterns with a strong dependence on initial conditions, and therefore not robust.

3.2 MacArthur 1s 1r

At this point, I move on to the analysis of the simplest case of an actual MacArthur model. I consider the evolution equations for one species and one resource, with the addition of a diffusion-like term to the species dynamics, equal to the one presented in the previous section.
In the following, I will always consider an infinitely extended spatial domain: I perform the linear stability analysis in one spatial dimension and, thanks to isotropicity, the generalisation to a two dimensional space will be straightforward[1].
The considered evolution equations read:

$$\begin{cases} \dot{n} = [\mu(c) - d]\, n + \partial_x \left[(\, D - \widetilde{D}\, n\,)\, \partial_x n \right] \\ \dot{c} = s - \mu(c)\, n \end{cases} \tag{3.8}$$

where $n(x,t)$ is the field representing the abundance of the species, $c(x,t)$ is the one for the resource, $d > 0$ is the death rate, $s > 0$ is the resource supply rate, and the growth rate is represented by a positive and monotonically increasing function of the resource abundance: $\mu(c) > 0$, $\frac{d\mu}{dc} > 0 \; \forall\, c$.

Uniform equilibrium

In this case the equilibrium of the system is the pair $(n_*,\, c_*)$ such that:

$$\begin{cases} \dot{n_*} = 0 \\ \dot{c_*} = 0 \\ \partial_x n_* = 0 \\ \partial_x c_* = 0 \end{cases} \quad \Leftrightarrow \quad \begin{cases} \mu(c_*) = d, \quad \rightarrow\, c_* = \mu^{-1}(d) \\ n_* = s/\mu(c_*) = s/d \end{cases} \tag{3.9}$$

Stability under uniform perturbation

We introduce the uniform perturbation:

$$\begin{pmatrix} n(t) \\ c(t) \end{pmatrix} = \begin{pmatrix} n_* \\ c_* \end{pmatrix} + \begin{pmatrix} \delta n(t) \\ \delta c(t) \end{pmatrix} \qquad \text{with} \quad \begin{pmatrix} \delta n(t) \\ \delta c(t) \end{pmatrix} = \vec{\delta}\, e^{\lambda t} \tag{3.10}$$

By substituting such uniform perturbation into Eq. (3.8):

$$\begin{cases} \delta\dot{n} = [\mu(c_* + \delta c) - d]\, (n_* + \delta n) \\ \delta\dot{c} = s - \mu(c_* + \delta c)\, (n_* + \delta n) \end{cases}$$

We can expand in a Taylor series the growth function around the equilibrium value:

$$\mu(c_* + \delta c) = \mu(c_*) + \frac{d\mu}{dc}\Big|_{c_*} \delta c + ...$$

and neglect δ^2 terms:

$$\begin{cases} \delta\dot{n} = [\mu(c_*) - d]\, (n_* + \delta n) + \frac{d\mu}{dc}\Big|_{c_*} n_*\, \delta c \\ \delta\dot{c} = s - \mu(c_*)\, (n_* + \delta n) - \frac{d\mu}{dc}\Big|_{c_*} n_*\, \delta c \end{cases} \qquad \begin{cases} \delta\dot{n} = \frac{s}{d}\, \frac{d\mu}{dc}\Big|_{c_*} \delta c \\ \delta\dot{c} = -d\, \delta n - \frac{s}{d}\, \frac{d\mu}{dc}\Big|_{c_*} \delta c \end{cases}$$

Where in the second step the the equilibrium values (3.9) were substituted. Making explicit the perturbation form:

$$\begin{cases} \lambda\, \delta n = \frac{s}{d}\, \frac{d\mu}{dc}\Big|_{c_*} \delta c \\ \lambda\, \delta c = -d\, \delta n - \frac{s}{d}\, \frac{d\mu}{dc}\Big|_{c_*} \delta c \end{cases}$$

[1] As already underlined, being the diffusion isotropic, no preferred spatial direction can emerge in the analysis of the system and, regardless of the dimension of space, all the relevant quantities will depend on the modulus of the wavenumber $k = |\mathbf{k}|$.

This is an eigenvalue problem in λ:

$$\lambda\,\vec{\delta} = \mathbb{J}\,\vec{\delta} \qquad \text{with} \quad \mathbb{J} = \begin{pmatrix} 0 & \frac{s}{d}\frac{d\mu}{dc}\big|_{c_*} \\ -d & -\frac{s}{d}\frac{d\mu}{dc}\big|_{c_*} \end{pmatrix} = \begin{pmatrix} 0 & \mathcal{A} \\ -d & -\mathcal{A} \end{pmatrix} \tag{3.11}$$

where I defined for shortness of notation $\mathcal{A} = \frac{s}{d}\frac{d\mu}{dc}\big|_{c_*}$, which is a positive quantity since s, d, $\frac{d\mu}{dc}\big|_{c_*} > 0$ for definition.

$$\det\left(\mathbb{J} - \lambda\mathbb{I}\right) = \lambda\left(\mathcal{A} + \lambda\right) + d\,\mathcal{A} = \lambda^2 + \lambda\,\mathcal{A} + d\,\mathcal{A} = 0 \qquad \Leftrightarrow \qquad \lambda_\pm = \frac{-\mathcal{A} \pm \sqrt{\mathcal{A}^2 - 4\mathcal{A}\,d}}{2}$$

Let us consider the stability of the equilibrium. Being:

$$\mathcal{A} > 0,\ -4\mathcal{A}d < 0 \quad \text{and} \quad \sqrt{\mathcal{A}^2 - 4\mathcal{A}\,d} < \mathcal{A}$$

$$\Rightarrow \quad \begin{matrix} Re[\lambda_-] < 0 \\ Re[\lambda_+] < 0 \end{matrix}$$

the homogeneous solution is stable to uniform perturbations for all values of the system parameters.

Non-uniform perturbation

If we consider now a non-uniform perturbation of the kind:

$$\begin{pmatrix} n(x,t) \\ c(x,t) \end{pmatrix} = \begin{pmatrix} n_* \\ c_* \end{pmatrix} + \begin{pmatrix} \delta n(x,t) \\ \delta c(x,t) \end{pmatrix} \qquad \text{with} \quad \begin{pmatrix} \delta n(x,t) \\ \delta c(x,t) \end{pmatrix} = \vec{\delta}\, e^{\lambda t + ikx} \tag{3.12}$$

and we substitute it into the linearised system, we obtain:

$$\begin{cases} \delta\dot{n} = \left[\mu(c_*) - d\right](n_* + \delta n) + \dfrac{d\mu}{dc}\big|_{c_*} n_*\,\delta c + (D - \widetilde{D}\,n_*)\,\partial_x^2\delta n \\ \delta\dot{c} = s - \mu(c_*)\,(n_* + \delta n) - \dfrac{d\mu}{dc}\big|_{c_*} n_*\,\delta c \end{cases}$$

Using the equilibrium solution (3.9) yields:

$$\begin{cases} \delta\dot{n} = \dfrac{s}{d}\dfrac{d\mu}{dc}\big|_{c_*}\delta c + \left(D - \widetilde{D}\,\dfrac{s}{d}\right)\partial_x^2\delta n \\ \delta\dot{c} = -d\,\delta n - \dfrac{s}{d}\dfrac{d\mu}{dc}\big|_{c_*}\delta c \end{cases} \qquad \begin{cases} \lambda\,\delta n = \dfrac{s}{d}\dfrac{d\mu}{dc}\big|_{c_*}\delta c - k^2\left(D - \widetilde{D}\,\dfrac{s}{d}\right)\delta n \\ \lambda\,\delta c = -d\,\delta n - \dfrac{s}{d}\dfrac{d\mu}{dc}\big|_{c_*}\delta c \end{cases}$$

where in the second step the perturbation form was explicitely used. This corresponds to the eigenvalue problem:

$$\lambda\,\vec{\delta} = \left(\mathbb{J} - k^2\mathbb{D}\right)\vec{\delta} \qquad \text{with} \quad \mathbb{D} = \begin{pmatrix} D - \widetilde{D}\frac{s}{d} & 0 \\ 0 & 0 \end{pmatrix} \quad \text{and } \mathbb{J} \text{ defined in (3.24)}$$

$$\begin{aligned} \det\left(\mathbb{J} - k^2\mathbb{D} - \lambda\mathbb{I}\right) &= \left[\lambda + k^2\left(D - \widetilde{D}\frac{s}{d}\right)\right](\mathcal{A} + \lambda) + d\,\mathcal{A} = \\ &= \lambda^2 + \lambda\left[\mathcal{A} + k^2\left(D - \widetilde{D}\frac{s}{d}\right)\right] + \mathcal{A}\left[d + k^2\left(D - \widetilde{D}\frac{s}{d}\right)\right] = \\ &= \lambda^2 + \lambda\left(\mathcal{A} + k^2\mathcal{D}\right) + \mathcal{A}\left(d + k^2\mathcal{D}\right) \end{aligned}$$

where I have renamed the parameters, for shortness:

$$\begin{aligned} \mathcal{A} &\coloneqq \frac{s}{d}\frac{d\mu}{dc}\bigg|_{c_*} > 0 \\ \mathcal{D} &\coloneqq D - \widetilde{D}\frac{s}{d} \end{aligned} \tag{3.13}$$

Therefore:

$$\begin{aligned} &\det\left(\mathbb{J}-k^2\mathbb{D}-\lambda\mathbb{I}\right)=0 \\ \Leftrightarrow\quad &\lambda_\pm=\frac{1}{2}\left(A\pm\sqrt{A^2+B}\right)=\frac{1}{2}\left(-\mathcal{A}-k^2\mathcal{D}\pm\sqrt{\left(-\mathcal{A}-k^2\mathcal{D}\right)^2-4\mathcal{A}\left(d+k^2\mathcal{D}\right)}\right) \end{aligned} \tag{3.14}$$

where I further defined the following functions of k^2:

$$\begin{aligned} &A(k^2)\coloneqq-\mathcal{A}-k^2\mathcal{D} \\ &h(k^2)\coloneqq-4\mathcal{A}\left(d+k^2\mathcal{D}\right) \end{aligned}$$

Spatial instability

Instability occurs when at lest one of the two eigenvalues has positive real part $Re[\lambda_\pm]>0$.
Calling the argument of the square root $\Delta(k^2)\coloneqq g^2-4h=(-\mathcal{A}-k^2\mathcal{D})^2-4\mathcal{A}(d+k^2\mathcal{D})$, I observe that there are three possible instability cases:

$$\begin{aligned} &\text{if } \Delta<0: \quad Re[\lambda_+]=Re[\lambda_-]=\frac{1}{2}A>0\Leftrightarrow A>0 \\ &\text{if } \Delta>0: \quad Re[\lambda_-]=\lambda_-=\frac{1}{2}(A-\sqrt{(A^2+B)})>0\Leftrightarrow A>0\wedge B<0 \\ &\qquad\qquad (\text{indeed } B<0\Rightarrow\sqrt{(A^2+B)})<A) \\ &\text{if } \Delta>0: \quad Re[\lambda_+]=\lambda_+=\frac{1}{2}(A+\sqrt{(A^2+B)})>0\Leftrightarrow A>0\vee(A<0\wedge B>0) \\ &\qquad\qquad (\text{indeed } B>0\Rightarrow\sqrt{(A^2+B)})>|A|) \end{aligned}$$

Now I study the sign of $A(k^2)$ and $B(k^2)$:

$$\begin{aligned} A>0 \quad&\Leftrightarrow\quad -\mathcal{A}-k^2\mathcal{D}>0 \quad\Leftrightarrow\quad \begin{cases}\mathcal{D}<0\\ k^2>-\mathcal{A}/\mathcal{D}\end{cases} \\ A<0 \quad&\Leftrightarrow\quad -\mathcal{A}-k^2\mathcal{D}<0 \quad\Leftrightarrow\quad \mathcal{D}>0\vee\begin{cases}\mathcal{D}<0\\ k^2<-\mathcal{A}/\mathcal{D}\end{cases} \\ B>0 \quad&\Leftrightarrow\quad d+k^2\mathcal{D}<0 \quad\Leftrightarrow\quad \begin{cases}\mathcal{D}<0\\ k^2>-d/\mathcal{D}\end{cases} \\ B<0 \quad&\Leftrightarrow\quad d+k^2\mathcal{D}>0 \quad\Leftrightarrow\quad \mathcal{D}>0\vee\begin{cases}\mathcal{D}<0\\ k^2<-d/\mathcal{D}\end{cases} \end{aligned}$$

Therefore:

$$\begin{aligned} &\text{if } \Delta<0: \quad Re[\lambda_+]=Re[\lambda_-]>0\Leftrightarrow\begin{cases}\mathcal{D}<0\\ k^2>-\mathcal{A}/\mathcal{D}\end{cases} \\ &\text{if } \Delta>0: \quad Re[\lambda_-]=\lambda_->0\Leftrightarrow\begin{cases}\mathcal{D}<0\\ \mathcal{A}-d<0\\ -\mathcal{A}/\mathcal{D}<k^2<-d/\mathcal{D}\end{cases} \\ &\text{if } \Delta>0: \quad Re[\lambda_+]=\lambda_+>0\Leftrightarrow\begin{cases}\mathcal{D}<0\\ \mathcal{A}-d>0\\ k^2>-d/\mathcal{D}\end{cases}\vee\begin{cases}\mathcal{D}<0\\ \mathcal{A}-d<0\\ k^2>-\mathcal{A}/\mathcal{D}\end{cases} \end{aligned} \tag{3.15}$$

In conclusion, $\mathcal{D} < 0$ is a necessary condition for instability (indeed if $\mathcal{D} > 0$ we easily realize that $Re[\lambda_\pm] < 0$), and the regions of instability in k also depend on the sign of $\mathcal{A} - d$.
Obviously the sign of Δ itself depends on k^2, therefore I should solve also $\Delta(k^2) > 0$ or < 0 and substitute it in (3.15), however these inequalities depend on the existence of roots and give rise to many other conditions on parameters, therefore I just calculate the zeros to get an idea, and then rely on plots:

$$\Delta(k^2) = (-\mathcal{A} - k^2\mathcal{D})^2 - 4\mathcal{A}(d + k^2\mathcal{D}) = \mathcal{D}^2k^4 - 2\mathcal{A}\mathcal{D}k^2 + \mathcal{A}(\mathcal{A} - 4d) = 0 \quad \Leftrightarrow \quad k^2_\pm = -\frac{-\mathcal{A} \pm \sqrt{\mathcal{A}d}}{\mathcal{D}}$$

If $\mathcal{D} < 0$ (that holds when we have instability), k^2_- is negative and therefore we expect $\Delta(k^2)$ to have at most one root (k_+).

As a check, I plot $Re[\lambda_\pm]$ in the different instability cases listed in (3.15):

- Fig. 3.1: case $\mathcal{D} < 0$, $\mathcal{A} - d > 0$ so we expect only λ_+ instability for $k > \sqrt{-d/\mathcal{D}}$
- Fig. 3.2: case $\mathcal{D} < 0$, $\mathcal{A} - d < 0$ so we expect: λ_+ instability for $k > \sqrt{-\mathcal{A}/\mathcal{D}}$ (3.16)
  λ_- instability for $\sqrt{-\mathcal{A}/\mathcal{D}} < k < \sqrt{-d/\mathcal{D}}$
- Fig. 3.3: case $\mathcal{D} > 0$ so we expect no instability.

The discontinuity in the plotted functions is due to the fact that the real part of the eigenvalues is taken, therefore when $\Delta(k^2) = 0$ $Re[\lambda_\pm]$ is a quadratic function of k, but when $\Delta(k^2) \neq 0$ there is an additional square root of $\Delta = -\mathcal{D}k^4 - 2\mathcal{A}\mathcal{D}k^2 + const$ that modifies the slope of the function.
I also plot the case in which the only zero of $\Delta(k^2)$ is $k_+ = 0$ (Fig. 3.4): in this case there is no discontinuity in the domain $k > 0$.

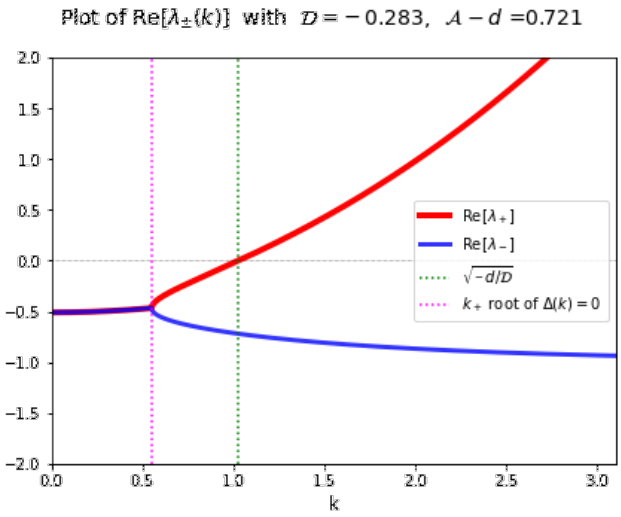

FIG. 3.1. Plot of the real parts of the eigenvalues $\lambda_+(k)$ and $\lambda_-(k)$ (in red and blue, respectively), in the case of parameters $\mathcal{D} < 0$, $\mathcal{A} - d > 0$. Consistently with the calculations, instability occurs for wavenumbers larger than a threshold value.

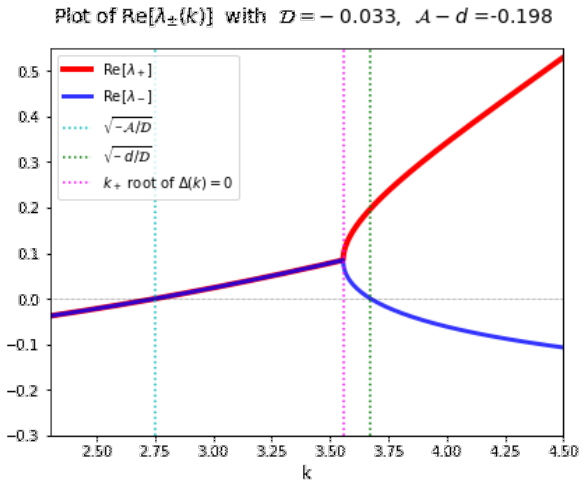

FIG. 3.2. Plot of the real parts of the eigenvalues $\lambda_+(k)$ and $\lambda_-(k)$ (in red and blue, respectively), in the case of parameters $\mathcal{D} < 0$, $\mathcal{A} - d < 0$. As expected, $Re[\lambda_+(k)]$ is positive for all k larger than a threshold value, while $Re[\lambda_-(k)] > 0$ in a limited interval of wavenumbers.

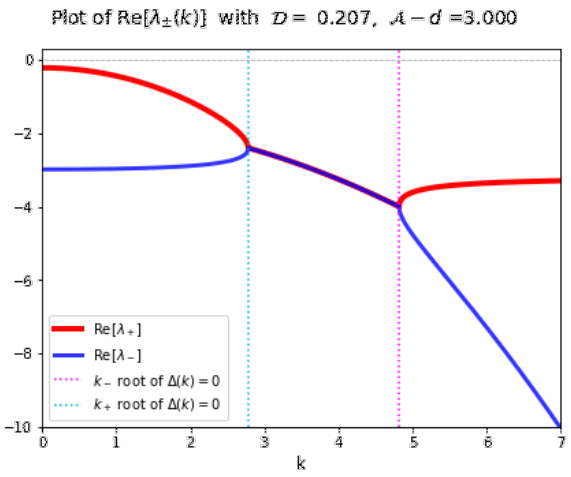

FIG. 3.3. Plot of the real parts of the eigenvalues $\lambda_+(k)$ and $\lambda_-(k)$ (in red and blue, respectively), in the case of $\mathcal{D} > 0$. In this case both eigenvalues have negative real part $\forall\, k$, thus no instability is allowed. $\Delta(k)$ has two zeros.

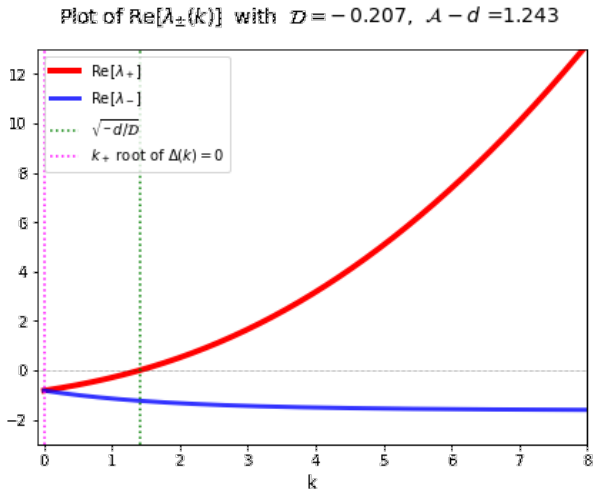

FIG. 3.4. Plot of the real parts of the eigenvalues $\lambda_+(k)$ and $\lambda_-(k)$ (in red and blue, respectively), in the case in which $\mathcal{A} = 4d \Rightarrow k_+ = 0$ and $\mathcal{D} < 0 \Rightarrow k_-$ is not real.

Expansion for k $\gg 1$

To better understand the behavior of $\lambda_\pm$ for large k, I Taylor expand the eigenvalues:

$$\begin{aligned}\sqrt{\Delta} &= \sqrt{\left(-\mathcal{A}-k^2\mathcal{D}\right)^2 - 4\mathcal{A}\left(d+k^2\mathcal{D}\right)} = \sqrt{k^4\mathcal{D}^2 - 2\mathcal{A}\mathcal{D}k^2 + \mathcal{A}(\mathcal{A}-4\,d)} = \\ &= |\mathcal{D}|k^2\sqrt{1-2\frac{\mathcal{A}}{\mathcal{D}}\frac{1}{k^2}+O\left(\frac{1}{k^4}\right)} = |\mathcal{D}|\,k^2\left(1-\frac{\mathcal{A}}{\mathcal{D}}\frac{1}{k^2}+O\left(\frac{1}{k^4}\right)\right) \\ &= |\mathcal{D}|\,k^2 - \mathcal{A}\,sgn(\mathcal{D}) + O\left(\frac{1}{k^2}\right)\end{aligned} \tag{3.17}$$

$$\lambda_\pm = \frac{1}{2}\left[-\mathcal{A}\left(1\pm sgn(\mathcal{D})\right) + k^2|\mathcal{D}|\left(-sgn(\mathcal{D})\pm 1\right) + O\left(\frac{1}{k^2}\right)\right]$$

Therefore, for $\mathcal{D} < 0$ (when instability is allowed):

$$\lambda_\pm = \frac{1}{2}\left[\mathcal{A}\left(-1\pm 1\right) - k^2\mathcal{D}\left(1\pm 1\right) + O\left(\frac{1}{k^2}\right)\right] \quad \Rightarrow \quad \lambda_+ \approx k^2|\mathcal{D}|\,, \quad \lambda_- \approx -\mathcal{A} \quad \text{for } k \gg 1$$

while for $\mathcal{D} > 0$ (when instability is not allowed):

$$\lambda_\pm = \frac{1}{2}\left[-\mathcal{A}\left(1\pm 1\right) - k^2\mathcal{D}\left(-1\pm 1\right) + O\left(\frac{1}{k^2}\right)\right] \quad \Rightarrow \quad \lambda_+ \approx -\mathcal{A}\,, \quad \lambda_- \approx -k^2|\mathcal{D}| \quad \text{for } k \gg 1$$

Again, we have found a nonphysical result which is analogue to the one obtained in Section 3.1.1: the spatial instability is allowed for all wavelengths minor than a certain threshold value.

3.3 MacArthur 2s 1r

Let us see how the instability behavior changes if we allow two species into the model. The evolution equations read:

$$\begin{cases} \dot{n_1} = (\alpha_1 \mu(c) - d_1)\, n_1 + \partial_x J_1 \\ \dot{n_2} = (\alpha_2 \mu(c) - d_2)\, n_2 + \partial_x J_2 \\ \dot{c} = s - (\alpha_1\, n_1 + \alpha_2\, n_2)\mu(c) \end{cases} \quad \text{with} \quad \partial_x J_\sigma = \partial_x \left[(\, D_\sigma - \sum_\rho D_{\sigma\rho} n_\rho \,)\, \partial_x n_\sigma \right] \text{ for } \sigma = 1, 2 \tag{3.18}$$

where $d_1, d_2 > 0$ are the death rates, $s > 0$ is the resource supply rate, α_1, α_2 are positive constants and the growth function is $\mu(c) > 0$ with $\frac{d\mu}{dc} > 0 \, \forall c$. The diffusion coefficients $D_\sigma > 0$ account for simple diffusion, while $D_{\sigma\rho} > 0$ reproduce the overcrowding effect.

Analogue calculations, relative to the generalisation of MacArthur's model in the case of three species and one resource, are reported in Appendix A.

Uniform equilibrium

The equilibrium of the system is $(n_1^*,\, n_2^*,\, c^*)$ such that:

$$\begin{cases} \dot{n_1}^* = \dot{n_2}^* = \dot{c}^* = 0 \\ \partial_x n_1^* = \partial_x n_2^* = \partial_x c^* = 0 \end{cases} \quad \Leftrightarrow \quad \begin{cases} \mu(c^*) = d_1/\alpha_1, \\ n_1^* = s/d_1, \\ n_2^* = 0 \end{cases} \quad \vee \quad \begin{cases} \mu(c^*) = d_2/\alpha_2, \\ n_2^* = s/d_2, \\ n_1^* = 0 \end{cases} \tag{3.19}$$

Stability under uniform perturbation

Let us choose the first equilibrium and linearize the system around it:

$$\begin{pmatrix} n_1(t) \\ n_2(t) \\ c(t) \end{pmatrix} = \begin{pmatrix} n_1^* \\ n_2^* \\ c^* \end{pmatrix} + \begin{pmatrix} \delta n_1(t) \\ \delta n_2(t) \\ \delta c(t) \end{pmatrix} \quad \text{with} \quad \begin{pmatrix} \delta n_1(t) \\ \delta n_2(t) \\ \delta c(t) \end{pmatrix} = \vec{\delta}\, e^{\lambda t}\,, \quad \begin{pmatrix} n_1^* \\ n_2^* \\ c^* \end{pmatrix} = \begin{pmatrix} s/d_1 \\ 0 \\ \mu^{-1}(d_1/\alpha_1) \end{pmatrix} \tag{3.20}$$

By substituting such perturbation into Eq. (3.18):

$$\begin{cases} \delta\dot{n_1} = [\alpha_1\, \mu(c^* + \delta c) - d_1]\, (n_1^* + \delta n_1) \\ \delta\dot{n_2} = [\alpha_2\, \mu(c^* + \delta c) - d_2]\, (n_2^* + \delta n_2) \\ \dot{\delta c} = s - [\alpha_1\, (n_1^* + \delta n_1) + \alpha_2\, (n_2^* + \delta n_2)]\, \mu(c^* + \delta c) \end{cases}$$

Expanding $\mu(c^* + \delta c) = \mu(c^*) + \frac{d\mu}{dc}\big|_{c^*} \delta c + \ldots$ and neglecting δ^2 terms:

$$\begin{cases} \delta\dot{n_1} = [\alpha_1\, \mu(c^*) - d_1]\, (n_1^* + \delta n_1) + \alpha_1 \dfrac{d\mu}{dc}\Big|_{c^*} n_1^*\, \delta c \\ \delta\dot{n_2} = [\alpha_2\, \mu(c^*) - d_2]\, (n_2^* + \delta n_2) + \alpha_2 \dfrac{d\mu}{dc}\Big|_{c^*} n_2^*\, \delta c \\ \delta\dot{c} = s - [\alpha_1\, (n_1 * + \delta n_1) + \alpha_2\, (n_2 * + \delta n_2)]\, \mu(c^*) - \dfrac{d\mu}{dc}\Big|_{c^*} (\alpha_1\, n_1^* + \alpha_2\, n_2^*)\ \delta c \end{cases}$$

Substituting the equilibrium values (3.20):

$$\begin{cases} \delta\dot{n_1} = \lambda\, \delta n_1 = \dfrac{\alpha_1 s}{d_1} \dfrac{d\mu}{dc}\Big|_{c^*} \delta c \\ \delta\dot{n_2} = \lambda\, \delta n_2 = \left(\dfrac{\alpha_2}{\alpha_1} d_1 - d_2 \right) \delta n_2 \\ \dot{\delta c} = \lambda\, \delta c = -d_1\, \delta n_1 - \dfrac{\alpha_2}{\alpha_1} d_1\, \delta n_2 - \dfrac{\alpha_1 s}{d_1} \dfrac{d\mu}{dc}\Big|_{c^*} \delta c \end{cases}$$

This corresponds to the eigenvalue problem:

$$\lambda\,\vec{\delta} = \mathbb{J}\,\vec{\delta} \quad \text{with } \mathbb{J} = \begin{pmatrix} 0 & 0 & \frac{\alpha_1 s}{d_1}\frac{d\mu}{dc}\Big|_{c^*} \\ 0 & \frac{\alpha_2}{\alpha_1}d_1 - d_2 & 0 \\ -d_1 & -\frac{\alpha_2}{\alpha_1}d_1 & -\frac{\alpha_1 s}{d_1}\frac{d\mu}{dc}\Big|_{c^*} \end{pmatrix} = \begin{pmatrix} 0 & 0 & \mathcal{A} \\ 0 & \frac{\alpha_2}{\alpha_1}d_1 - d_2 & 0 \\ -d_1 & -\frac{\alpha_2}{\alpha_1}d_1 & -\mathcal{A} \end{pmatrix} \tag{3.21}$$

where I defined $\mathcal{A} \coloneqq \frac{\alpha_1 s}{d_1}\frac{d\mu}{dc}\Big|_{c^*} > 0$ to simplify notation. Let us solve the system:

$$\det\left(\mathbb{J} - \lambda\mathbb{I}\right) = \left(\frac{\alpha_2}{\alpha_1}d_1 - d_2 - \lambda\right)\det\begin{pmatrix} -\lambda & \mathcal{A} \\ -d_1 & -(\mathcal{A}+\lambda) \end{pmatrix} = \left(\frac{\alpha_2}{\alpha_1}d_1 - d_2 - \lambda\right)\left(\lambda^2 + \mathcal{A}\lambda + \mathcal{A}d_1\right) = 0$$

$$\Leftrightarrow \qquad \begin{cases} \lambda_0 = \dfrac{\alpha_2}{\alpha_1}d_1 - d_2 \\ \lambda_\pm = \dfrac{-\mathcal{A} \pm \sqrt{\mathcal{A}^2 - 4\mathcal{A}d_1}}{2} \end{cases}$$

Then the equilibrium $(n_1^*,\, n_2^*,\, c^*)$ is stable if:

$$\begin{cases} Re[\lambda_0] < 0 \quad \Leftrightarrow \quad \dfrac{\alpha_2}{\alpha_1}d_1 - d_2 < 0 \\ Re[\lambda_\pm] < 0 \end{cases}$$

Since the second inequality is always verified (being $4\mathcal{A}d_1 > 0$), the only stability constraint is that the parameters of the system should satisfy:

$$\frac{\alpha_2}{\alpha_1}d_1 - d_2 < 0 \tag{3.22}$$

Non-uniform perturbation

I consider the following perturbation around the equilibrium values $(n_1^*,\, n_2^*,\, c^*)$ reported in (3.20).

$$\begin{pmatrix} n_1(x,t) \\ n_2(x,t) \\ c(x,t) \end{pmatrix} = \begin{pmatrix} n_1^* \\ n_2^* \\ c^* \end{pmatrix} + \begin{pmatrix} \delta n_1(x,t) \\ \delta n_2(x,t) \\ \delta c(x,t) \end{pmatrix} \qquad \text{with} \qquad \begin{pmatrix} \delta n_1(x,t) \\ \delta n_2(x,t) \\ \delta c(x,t) \end{pmatrix} = \vec{\delta}\, e^{\lambda t + ikx}$$

Substituting it in the linearized equations of the system yields:

$$\begin{cases} \delta\dot{n}_1 = \dfrac{\alpha_1 s}{d_1}\dfrac{d\mu}{dc}\Big|_{c^*}\delta c + (\partial_x J_1)_{lin} \\ \delta\dot{n}_2 = \left(\dfrac{\alpha_2}{\alpha_1}d_1 - d_2\right)\delta n_2 + (\partial_x J_2)_{lin} \\ \delta\dot{c} = -d_1\,\delta n_1 - \dfrac{\alpha_2}{\alpha_1}d_1\,\delta n_2 - \dfrac{\alpha_1 s}{d_1}\dfrac{d\mu}{dc}\Big|_{c^*}\delta c \end{cases}$$

where the linearised diffusion term reads:

$$\begin{aligned} (\partial_x J_1)_{lin} &= \left(D_1 - D_{11}\frac{s}{d_1}\right)\partial_x^2\,\delta n_1 \\ (\partial_x J_2)_{lin} &= \left(D_2 - D_{22}n_2^* - D_{21}n_1^*\right)\partial_x^2\,\delta n_2 = \left(D_2 - D_{21}\frac{s}{d_1}\right)\partial_x^2\,\delta n_2 \end{aligned} \tag{3.23}$$

Indeed:

$$\begin{aligned} \partial_x J_1 &= D_1\partial_x^2 n_1 - D_{11}\left[(\partial_x n_1)^2 + n_1\partial_x^2 n_1\right] - D_{12}\left[(\partial_x n_1)(\partial_x n_2) + n_2\partial_x^2 n_1\right] = \\ &= D_1\partial_x^2\delta n_1 - D_{11}\left[(\partial_x\delta n_1)^2 + (n_1^* + \delta n_1)\partial_x^2\delta n_1\right] - D_{12}\left[(\partial_x\delta n_1)(\partial_x\delta n_2) + (n_2^* + \delta n_2)\partial_x^2\delta n_1\right] \approx \\ &\approx \left(D_1 - D_{11}n_1^* - D_{12}n_2^*\right)\partial_x^2\,\delta n_1 \end{aligned}$$

and similarly:

$$\partial_x J_2 \approx (D_2 - D_{22} n_2^* - D_{21} n_1^*)\, \partial_x^2\, \delta n_2$$

Substituting the equilibrium values into the above expressions leads to the expression written above (3.23). The corresponding eigenvalue problem reads:

$$\lambda\, \vec{\delta} = (\mathbb{J} - k^2 \mathbb{D})\, \vec{\delta} \qquad \text{with} \quad \mathbb{D} = \begin{pmatrix} D_1 - D_{11}\frac{s}{d_1} & 0 & 0 \\ 0 & D_2 - D_{21}\frac{s}{d_1} & 0 \\ 0 & 0 & 0 \end{pmatrix}, \quad \mathbb{J} \text{ defined in (3.21).}$$

$$\begin{aligned} &\det\left(\mathbb{J} - k^2\mathbb{D} - \lambda\mathbb{I}\right) = \\ &= \left[\frac{\alpha_2}{\alpha_1} d_1 - d_2 - k^2\left(D_2 - D_{21}\frac{s}{d_1}\right) - \lambda\right] \det\begin{pmatrix} -\left[\lambda + k^2\left(D_1 - D_{11}\frac{s}{d_1}\right)\right] & \mathcal{A} \\ -d_1 & -(\mathcal{A}+\lambda) \end{pmatrix} = \\ &= \left[\frac{\alpha_2}{\alpha_1} d_1 - d_2 - k^2\left(D_2 - D_{21}\frac{s}{d_1}\right) - \lambda\right] \left\{\lambda^2 + \lambda\left[\mathcal{A} + k^2\mathcal{D}\right] + \mathcal{A}\left[d_1 + k^2\mathcal{D}\right]\right\} \end{aligned}$$

where I defined:

$$\mathcal{A} \coloneqq \frac{\alpha_1 s}{d_1}\frac{d\mu}{dc}\bigg|_{c^*} > 0$$

$$\mathcal{D} \coloneqq D_1 - D_{11}\frac{s}{d_1}$$

$$\det\left(\mathbb{J} - k^2\mathbb{D} - \lambda\mathbb{I}\right) = 0 \quad \Leftrightarrow \quad \begin{cases} \lambda_0 = \dfrac{\alpha_2}{\alpha_1} d_1 - d_2 - k^2\left(D_2 - D_{21}\dfrac{s}{d_1}\right) \\ \lambda_\pm = \dfrac{1}{2}\left(-\mathcal{A} - k^2\mathcal{D} \pm \sqrt{\left[-\mathcal{A} - k^2\mathcal{D}\right]^2 - 4\mathcal{A}\left[d_1 + k^2\mathcal{D}\right]}\right) \end{cases}$$

Spatial instability

It can be easily noticed that λ_0 is equivalent to the eigenvalue (3.6) obtained for the basic model in Section 3.1.1: indeed both are quadratic functions where the constant is required to be negative by the equilibrium stability condition, while the k^2 coefficient depends on the difference between the simple diffusion coefficient and the overcrowding diffusion coefficient times n^*.

$$\begin{aligned} \text{Basic model:} \quad & \lambda = -d + k^2\left(D_{21}\, s/d_1 - D_2\right) \\ \text{MA2s1r:} \quad & \lambda_0 = \frac{\alpha_2}{\alpha_1} d_1 - d_2 + k^2\left(\widetilde{D}\,\mu/d - D\right) \end{aligned}$$

Likewise, with $\mathcal{D}$ accounting for the difference between a simple diffusion coefficient and an overcrowding term, $\lambda_\pm$ is equal to the eigenvalues (3.14) found in Section 3.2 for the MacArthur model with 1 species and 1 resource, with the only difference of having $d_1 \to d$ and $\alpha_1\mu \to \mu$.

$$\text{MA1s1r:} \quad \lambda_\pm = \frac{1}{2}\left[-\frac{s}{d}\frac{d\mu}{dc}\Big|_{c_*} - k^2\mathcal{D} \pm \sqrt{\left(-\frac{s}{d}\frac{d\mu}{dc}\Big|_{c_*} - k^2\mathcal{D}\right)^2 - 4\frac{s}{d}\frac{d\mu}{dc}\Big|_{c_*}\left(d + k^2\mathcal{D}\right)}\right]$$

$$\text{with } \mathcal{D} = D - \widetilde{D}s/d$$

$$\text{MA2s1r:} \quad \lambda_\pm = \frac{1}{2}\left[-\frac{\alpha_1 s}{d_1}\frac{d\mu}{dc}\Big|_{c^*} - k^2\mathcal{D} \pm \sqrt{\left(-\frac{\alpha_1 s}{d_1}\frac{d\mu}{dc}\Big|_{c^*} - k^2\mathcal{D}\right)^2 - 4\frac{\alpha_1 s}{d_1}\frac{d\mu}{dc}\Big|_{c^*}\left(d + k^2\mathcal{D}\right)}\right]$$

$$\text{with } \mathcal{D} = D_1 - D_{11}s/d_1$$

Therefore the instability conditions for the MacArthur for 2 species and 1 resource (MA2s1r) are the ones found for :

$\lambda_0 \rightarrow$ Basic model (3.7)
$\lambda_\pm \rightarrow$ MA1s1r (3.16)

and we have not yet obtained the desired result.

We then seek to modify the system in such a way that they follow the desired behavior, i.e. they become positive in a limited interval of wavenumber values.
In the next section, we analyse a fully general two-reactants model, allowing both diffusion coefficients to become negative, trying to understand which feature of the MacArthur model generates the unwanted result.

3.4 General two-reactants model with overcrowding diffusion

We want to study the instability of a system of two reactants, in the more general case in which overcrowding diffusion is allowed for both: with respect to the previous cases, we are allowing the resource to diffuse into the environment as well, and we admit that it might be subject to an overcrowding effect too.
We leave the reaction dynamics unspecified to achieve a greater generality. This allows us both to see if the pathological behavior of the MacArthur model can be cured by adding a more complex dispersal behavior, and to elucidate the reasons of such undesired result.

We consider the following evolution equations:

$$\begin{cases} \dot{n} = f(n,c) + \partial_x \left[(\, D_0 - D_1\, n\,)\, \partial_x n \right] \\ \dot{c} = g(n,c) + \partial_x \left[(\, \bar{D}_0 - \bar{D}_1\, c\,)\, \partial_x c \right] \end{cases}$$

where f is the reaction dynamics of the species, g is that of the resource, and the diffusion coefficients D_0, D_1, $\bar{D}_0$, $\bar{D}_1$ are all non-negative. The following notation is adopted:

- the subscript 0 labels the simple diffusion coefficients;
- the subscript 1 labels the overcrowding diffusion coefficients;
- an overline indicates the coefficients describing the dispersal behavior of the resource.

We denote the linearisation of the above system about the uniform equilibrium $(n^*,\, c^*)$ as follows[2]:

$$\lambda\, \vec{\delta} = (\mathbb{J} - k^2 \mathbb{D})\, \vec{\delta} \qquad \text{with} \quad \mathbb{J} = \begin{pmatrix} f_n & f_c \\ g_n & g_c \end{pmatrix}, \quad \mathbb{D} = \begin{pmatrix} D & 0 \\ 0 & \bar{D} \end{pmatrix} \tag{3.24}$$

having defined:

$$D = D_0 - n^* D_1, \quad \bar{D} = \bar{D}_0 - c^* \bar{D}_1$$

Both the linearised diffusion coefficients can be either positive or negative, thanks to the effect of overcrowding. The solution for the system is:

$$\det\left(\mathbb{J} - k^2\mathbb{D} - \lambda \mathbb{I}\right) = \lambda^2 + \lambda g(k^2) + h(k^2) = 0 \qquad \Leftrightarrow \qquad \lambda_\pm(k^2) = \frac{-g(k^2) \pm \sqrt{g^2(k^2) - 4h(k^2)}}{2}$$

with:

$$g(k^2) = k^2(D + \bar{D}) - \mathrm{tr}(\mathbb{J})$$
$$h(k^2) = k^4 D\bar{D} - k^2(\bar{D} f_n + D g_c) + \det(\mathbb{J})$$

[2]The calculations are identical to the ones reported in the previous sections, therefore I skipped them for brevity. See Section 3.2 for more details.

Therefore, the stability of the uniform equilibrium $(n^*,\, c^*)$ requires that $\lambda_\pm(k^2=0)<0$, which implies in turn:

$$\mathrm{tr}(\mathbb{J})<0 \quad \wedge \quad \det(\mathbb{J})>0$$

Spatial instability

As we have seen, instability under spatially heterogeneous perturbations arises if $\lambda_\pm(k^2)>0$ for some value of the wavenumber k:

$$\begin{aligned} \lambda_+>0 \quad &\Leftrightarrow \quad g<0 \vee \begin{cases} g>0 \\ h<0 \end{cases} \\ \lambda_->0 \quad &\Leftrightarrow \quad \begin{cases} g<0 \\ h>0 \end{cases} \end{aligned} \tag{3.25}$$

where:

$$\begin{aligned} g(k^2) &= k^2(D+\bar{D}) - \mathrm{tr}(\mathbb{J}) \\ h(k^2) &= k^4 D\bar{D} - k^2(\bar{D}f_n + Dg_c) + \det(\mathbb{J}) \end{aligned} \tag{3.26}$$

with $\mathrm{tr}(\mathbb{J})<0$ and $\det(\mathbb{J})>0$ as required by the stability of the equilibrium $(n^*,\, c^*)$.

We observe that the addition of a diffusion term to the equation for the resources has modified the shape of the h function in (3.26) by introducing a k^4 term. Therefore, h has become a quadratic function of k^2, which, for given signs of the coefficients, could become negative in a limited interval of the wavenumber domain, and might therefore lead to the solution of our problem.

Study of g

Being $\mathrm{tr}(\mathbb{J})<0$, $g(k^2)=g_1k^2+g_0$ is a linear function of k^2 with positive intercept g_0, therefore:

$$\begin{aligned} &\text{if } g_1>0: \quad && g>0\,\forall\, k \\ &\text{if } g_1<0: \quad && \begin{cases} g>0 & \text{for } k<\bar{k} \\ g<0 & \text{for } k>\bar{k} \end{cases} \qquad \text{where } \bar{k}=\frac{\mathrm{tr}(\mathbb{J})}{g_1}=\frac{\mathrm{tr}(\mathbb{J})}{D+\bar{D}} \end{aligned}$$

Study of h

Being $\det(\mathbb{J})>0$, $h(k^2)=h_2k^4+h_1k^2+h_0$ is a quadratic function of k^2 with positive intercept h_0. Depending on the signs of h_2 and h_1, different possibilities are found:

$$\begin{aligned} &\text{if } h_2>0 \text{ and } h_1>0: && h>0\,\forall\, k \\ &\text{if } h_2>0,\, h_1<0 \text{ and } \min(h)>0: && h>0\,\forall\, k \\ &\text{if } h_2>0,\, h_1<0 \text{ and } \min(h)<0: && \begin{cases} h<0 & \text{for } k_-<k<k_+ \\ h>0 & \text{for } k>k_+ \vee k<k_- \end{cases} \\ &\text{if } h_2<0: && \begin{cases} h<0 & \text{for } k<k_+ \\ h>0 & \text{for } k>k_- \end{cases} \end{aligned}$$

where the roots of $h(k^2)$ are:

$$k_\pm=\frac{-h_1\pm\sqrt{h_1^2-4h_2h_0}}{2h_2} \tag{3.27}$$

Expansion for k $\gg 1$

So far we have not made any assumption about the signs of D, $\bar{D}$ and the form of f_n, f_c, g_n, g_c. Indeed, in full generality, before diving deeper into the study of the sign of $Re[\lambda_\pm]$, we ask ourselves if there is some requirement that we can impose on this system, such that an instability appears in some limited range $[k_1, k_2]$ of wavenumbers. To do so, we perform an expansion for large k values and we look at the sign of the leading k^2 term.

$$\begin{aligned}\Delta(k^2) = g^2 - 4h &= k^4(\bar{D}-D)^2 + 2k^2(\bar{D}-D)(f_n-g_c) + (f_n-g_c)^2 + 4g_n f_c = \\ &= k^4(\bar{D}-D)^2\left[1 + \frac{2}{k^2}\frac{f_n-g_c}{\bar{D}-D} + \frac{1}{k^4}\frac{(f_n-g_c)^2+4g_nf_c}{(\bar{D}-D)^2}\right]\end{aligned}$$

$$\begin{aligned}\sqrt{\Delta(k^2)} &= k^2|\bar{D}-D|\sqrt{1 + \frac{2}{k^2}\frac{f_n-g_c}{\bar{D}-D} + \frac{1}{k^4}\frac{(f_n-g_c)^2+4g_nf_c}{(\bar{D}-D)^2}} \approx \\ &\approx k^2|\bar{D}-D|\left[1 + \frac{1}{k^2}\frac{f_n-g_c}{\bar{D}-D} + O\left(\frac{1}{k^4}\right)\right] = k^2|\bar{D}-D| + \mathrm{sgn}(\bar{D}-D)\,(f_n-g_c) + O\left(\frac{1}{k^2}\right)\end{aligned}$$

Therefore:

$$\lambda_\pm \approx \frac{1}{2}\left[k^2\left(-(\bar{D}+D) \pm |\bar{D}-D|\right) + f_n + g_c \pm \mathrm{sgn}(\bar{D}-D)\,(f_n-g_c)\right] + O\left(\frac{1}{k^2}\right)$$

Thus, for $k \gg 1$, the eigenvalues at leading order behave like a quadratic function of k^2, whose coefficient depends in particular on the sign of $\bar{D} - D$.

For $\bar{D} - D > 0$:

$$\begin{aligned}\lambda_+ &\approx -D\,k^2 + f_n + O\left(\frac{1}{k^2}\right) \\ \lambda_- &\approx -\bar{D}\,k^2 + g_c + O\left(\frac{1}{k^2}\right)\end{aligned} \tag{3.28}$$

For $\bar{D} - D < 0$:

$$\begin{aligned}\lambda_+ &\approx -\bar{D}\,k^2 + g_c + O\left(\frac{1}{k^2}\right) \\ \lambda_- &\approx -D\,k^2 + f_n + O\left(\frac{1}{k^2}\right)\end{aligned}$$

In conclusion:

- if D, $\bar{D} < 0$ we observe that both eigenvalues grow like $\lambda_\pm \sim +k^2$, therefore surely instability is not limited to a finite k interval.
- if D, $\bar{D} > 0$ we find the desired behavior $\lambda_\pm \sim -k^2$.
- if $D < 0$, $\bar{D} > 0$ we are in the case $\bar{D} - D > 0$ therefore $\lambda_- \sim -k^2$ but $\lambda_+ \sim +k^2$.
- if $D > 0$, $\bar{D} < 0$ we are in the case $\bar{D} - D < 0$ therefore, again, $\lambda_- \sim -k^2$ and $\lambda_+ \sim +k^2$.

Then, the only case of interest to us is represented by D, $\bar{D} > 0$, and we can restrict our analysis to this case.

Instability: case $D, \bar{D} > 0$

Let us consider the case of interest $D, \bar{D} > 0$, for which $\lambda_\pm$ follows the desired trend $\sim -k^2$ for $k \gg 1$. For such signs of $D, \bar{D}$:

$$g_1 < 0 \quad \Rightarrow \quad g > 0 \, \forall \, k$$

The behavior of $h(k^2)$, instead, depends also on the values of f_n, f_c, g_n, g_c :

$$h_2 > 0$$
$$h_1 = \bar{D} f_n + D g_c$$

Therefore Eq. (3.25) implies that:

$$Re[\lambda_+] > 0 \quad \Leftrightarrow \quad \begin{cases} \bar{D} f_n + D g_c < 0 \\ (\bar{D} f_n + D g_c)^2 - 4 D \bar{D} \det(\mathbb{J}) > 0 \\ k_- < k < k_+ \end{cases} \tag{3.29}$$

in which case instability is allowed in the limited range $[k_-, k_+]$ (3.27).

3.4.1 Specification to the MacArthur reaction dynamics

Let us discuss this result in the case of the reaction dynamics of the MacArthur model. In such case:

$$\mathbb{J} = \begin{pmatrix} f_n & f_c \\ g_n & g_c \end{pmatrix} = \begin{pmatrix} 0 & \mathcal{A} \\ -d & -\mathcal{A} \end{pmatrix} \quad \Rightarrow \quad \begin{matrix} \det(\mathbb{J}) = d\mathcal{A} > 0 \\ \mathrm{tr}(\mathbb{J}) = -\mathcal{A} < 0 \end{matrix} \quad \text{with } \mathcal{A} \text{ defined in (3.13)}$$

and the conditions on stability are automatically met. Substituting the given expressions into (3.26):

$$g(k^2) = k^2(D + \bar{D}) + \mathcal{A}$$
$$h(k^2) = k^4 D\bar{D} + k^2 D\mathcal{A} + d\mathcal{A}$$

Recalling that the instability occurs in a limited interval $\Leftrightarrow$ $D, \bar{D} > 0$, it is immediate to realise that both functions are always positive, therefore instability to spatial perturbations cannot occur.
From another perspective, if one considers:

- $D < 0$, $\bar{D} > 0 \Rightarrow \bar{D} - D > 0$ and (3.28) yields $\lambda_+ \sim +k^2$;
- $D > 0$, $\bar{D} < 0 \Rightarrow \bar{D} - D < 0$ and (3.28) gives the same trend $\lambda_+ \sim +k^2$;
- $D < 0$, $\bar{D} < 0$ and in both cases $\bar{D} - D \lessgtr 0$ (3.28) yields $\lambda_+ \sim +k^2$.

thus instability is allowed, in some cases, but it is not constrained to a limited interval in the wavenumbers, consistently with the results of Section 3.2.

In conclusion, the desired instability behavior is not encountered by using the MacArthur reaction dynamics and adding diffusion to both the species and the resource, neither by allowing both coefficients to become negative. In order to solve the problem, a more effective modification of the diffusion-like terms will be introduced in the next section.

3.5 Adding stabilizing terms to the MacArthur's model

In this section, the effects of adding other stabilizing terms to the dynamical equations presented in Section 3.2 are analysed. Two modifications are made: one affecting once more the dispersal behavior, and the other consisting in an additional density-dependent inhibition term.

3.5.1 The Janzen-Connell effect

The latter approach can be interpreted as resulting from the presence of host-specific pathogens in the ecosystem, inducing the *Janzen-Connell effect*. This mechanism is held responsible for the maintenance of high diversity levels in the tree communities of tropical forests, thanks to a negative feedback mechanism supported by host-specific pathogens, that prevent seedlings from growing in proximity of parent trees, thus diminishing the local crowding within each species. This effect acts as a regulator which favors species coexistence. Let us briefly sketch how to incorporate the Janzen-Connell effect into MacArthur's model [18]. The starting point consists in writing three sets of differential equations, describing the coupled evolution of the populations of species, resources and pathogens, the latter being indicated by p and labeled by the index a:

$$\begin{cases} \dot{n}_\sigma = n_\sigma \left(\sum_{i=1}^{N_R} \alpha_{\sigma i}\, \mu_i(c_i) - \delta_\sigma - \sum_{a=1}^{N_P} A_{\sigma a} p_a \right) & \sigma = 1, ..., N_S \\ \dot{c}_i = s_i - \sum_{\sigma=1}^{N_S} n_\sigma\, \alpha_{\sigma i}\, \mu_i(c_i) & i = 1, ..., N_R \\ \dot{p}_a = p_a \sum_{\sigma=1}^{N_S} B_{a\sigma} n_\sigma - k_a p_a^2 & a = 1, ..., N_P \end{cases}$$

where $N_P \equiv N_S$ and the matrices $A_{\sigma a}$, $B_{a\sigma}$ must be diagonal for the parasites to be host-specific. The presence of pathogens counteracts the growth of species, as visible from the negative sign of the species-pathogen interaction in the first set of equations. This interaction is encoded in the positive degradation matrix $A_{\sigma a}$. The pathogens, on the other hand, benefit from the host population, as visible from the last set of equations, in which pathogens grow proportionally to the species population, with growth rates encoded by the benefit matrix $B_{a\sigma}$. Finally, the last term in the pathogen equations serves as a limit to their population growth, $1/k_a$ defining the carrying capacity of pathogen species a. The above system can be greatly simplified by exploiting a separation of scales: indeed, the pathogens naturally have a much faster growth scale with respect to the ones of species and resources, and thus reach stationary much sooner. This allows to write:

$$p_a \sum_{\sigma=1}^{N_S} B_{a\sigma} n_\sigma - k_a p_a^2 = 0$$

and extract the stationary solution for the pathogen population. One can prove that, by substituting it in the full evolution equations, the following effective model is obtained:

$$\begin{cases} \dot{n}_\sigma = n_\sigma \left[\sum_{i=1}^{N_R} \alpha_{\sigma i}\, \mu_i(c_i) - \delta_\sigma - \sum_{\rho}^{N_S} \left(\sum_{a=1}^{N_P} \frac{A_{\sigma a} B_{a\rho}}{k_a} \right) n_\rho \right] & \sigma = 1, ..., N_S \\ \dot{c}_i = s_i - \sum_{\sigma=1}^{N_S} n_\sigma\, \alpha_{\sigma i}\, \mu_i(c_i) & i = 1, ..., N_R \end{cases}$$

and by renaming $\epsilon_{\sigma\rho} \coloneqq \sum_{a=1}^{N_P} \frac{A_{\sigma a} B_{a\rho}}{k_a}$, one finds:

$$\begin{cases} \dot{n}_\sigma = n_\sigma \left[\sum_{i=1}^{N_R} \alpha_{\sigma i}\, \mu_i(c_i) - \delta_\sigma - \sum_{\rho}^{N_S} \epsilon_{\sigma\rho} n_\rho \right] & \sigma = 1, ..., N_S \\ \dot{c}_i = s_i - \sum_{\sigma=1}^{N_S} n_\sigma\, \alpha_{\sigma i}\, \mu_i(c_i) & i = 1, ..., N_R \end{cases}$$

which is the classical MacArthur model with the addition of a negative-signed quadratic term in the species populations, that has the effect of limiting their growth.
Notice also that, since the benefit and degradation matrices are assumed to be diagonal, $\epsilon_{\sigma\rho}$ is diagonal as well.

3.5.2 Stabilizing squared laplacian term

The second modification which will be introduced follows the same line of reasoning proposed in Section 3.4, i.e. the idea that the introduction of a quartic order term into the function h (3.26) could lead to a finite instability interval. This can be achieved by directly inserting a squared laplacian term in the dynamical equations, that clearly leads to the appearance of a k^4 term when Fourier decomposing the perturbation.
Finally, an overcrowding diffusion term for the resource population is also included, allowing for a greater generality of analysis. It is indeed reasonable to expect that this term, coupled with the squared laplacian one, will further introduce higher powers of k into the function h.

Since the system to be studied depends now on a large number of parameters, the analysis will be carried out by switching them off progressively, aiming to determine the minimal set of parameters that admit the wanted result.

3.5.3 Linear stability analysis

Limiting our analysis to the simple case of one species and one resource, the the modified MacArthur's dynamical equations read:

$$\begin{cases} \dot{n} = (\alpha c - d - \epsilon n)\, n + \partial_x \left[(D_0 - D_1 n)\ \partial_x n \right] - \beta\, \partial_x^4 n \\ \dot{c} = s - \alpha c\, n + \bar{D}\, \partial_x^2 c \end{cases} \tag{3.30}$$

where $d > 0$ is the death rate, $\alpha > 0$ is the growth rate, $s > 0$ is the resource supply rate and $\epsilon \geq 0$ is the coefficient of the n^2 term related to pathogens. As for the diffusion coefficients, we have $D_0 \geq 0$ simple diffusion coefficient and $D_1 \geq 0$ overcrowding coefficient for species, while $\bar{D} \geq 0$ accounts for the the simple diffusion of resources.
Notice that we have restricted the growth rate function $\mu(c)$ to be a linear function of c, to simplify the calculations:

$$\mu(c) = \alpha\, c\,, \quad \text{with } \alpha > 0$$

indeed, as clearly evident from the previous analyses, the form of μ does not affect the nature of the instability, as long as it is monotonically increasing in c.

Uniform equilibrium

The equilibrium of the system is $(n_*,\, c_*)$ such that:

$$\begin{cases} \dot{n_*} = 0 \\ \dot{c_*} = 0 \\ \partial_x n_* = 0 \\ \partial_x c_* = 0 \end{cases} \quad \Leftrightarrow \quad \begin{cases} \epsilon \neq 0 \\ n_* = \dfrac{-d + \sqrt{d^2 + 4\epsilon s}}{2\epsilon} \\ c_* = \dfrac{s}{\alpha}\dfrac{1}{n_*} = \dfrac{d + \sqrt{d^2 + 4\epsilon s}}{2\alpha} \end{cases} \vee \begin{cases} \epsilon = 0 \\ n_* = s/d \\ c_* = \dfrac{s}{\alpha}\dfrac{1}{n_*} = d/\alpha \end{cases} \tag{3.31}$$

Stability under uniform perturbation

Substituting the uniform perturbation (3.10) into Eq. (3.30) yields:

$$\lambda\, \vec{\delta} = \mathbb{J}\, \vec{\delta} \qquad \text{with} \quad \mathbb{J} = \begin{pmatrix} -n_*\epsilon & n_*\alpha \\ -c_*\alpha & -n_*\alpha \end{pmatrix} = \begin{pmatrix} -n_*\epsilon & n_*\alpha \\ -s/n_* & -n_*\alpha \end{pmatrix} \tag{3.32}$$

Solving in λ:

$$\det(\mathbb{J}-\lambda\mathbb{I}) = \lambda^2+n_*(\epsilon+\alpha)\lambda+\alpha(s+\epsilon\, n_*^2) = 0 \Leftrightarrow \lambda_\pm = \frac{1}{2}\left[-n_*(\alpha+\epsilon) \pm \sqrt{n_*^2(\alpha+\epsilon)^2 - 4\alpha(s+\epsilon\, n_*^2)}\right]$$

Being $n_*(\alpha+\epsilon) > 0$, λ_- is clearly negative, while $\alpha(s+\epsilon\, n_*^2) > 0$ implies that λ_+ is negative as well. Therefore the uniform equilibrium is stable for all values of the parameters: in particular, I stress that $\epsilon = 0$ does not break the stability.

Non-uniform perturbation

Substituting the non-uniform perturbation (3.12) into the system in Eq. (3.30), we linearise the diffusion terms as follows:

$$\begin{aligned}
&\partial_x[(D_0 - D_1 n)\,\partial_x n] - \beta\,\partial_x^4 n = \partial_x[(D_0 - D_1 n_* - D_1\delta n)\,\partial_x\delta n] - \beta\,\partial_x^4\delta n \approx (D_0 - D_1 n_*)\,\partial_x^2\delta n - \beta\,\partial_x^4\delta n \\
&\qquad\qquad \to\ -k^2(D_0 - D_1 n_*)\,\delta n - k^4\beta\,\delta n \\
&\bar{D}\,\partial_x^2 c = \bar{D}\,\partial_x^2\delta c \ \to\ -k^2\bar{D}\delta c
\end{aligned}$$

where the arrows indicate the transition into Fourier space. Thus Eq. (3.30) becomes:

$$\lambda\,\vec{\delta} = (\mathbb{J} - k^2\mathbb{D}_1 - k^4\mathbb{D}_2)\,\vec{\delta} \qquad \text{with} \quad \mathbb{D}_1 = \begin{pmatrix} D_0 - D_1 n_* & 0 \\ 0 & \bar{D} \end{pmatrix}, \quad \mathbb{D}_2 = \begin{pmatrix} \beta & 0 \\ 0 & 0 \end{pmatrix}, \quad \text{and } \mathbb{J} \text{ defined in (3.32)} \tag{3.33}$$

Solving in λ:

$$\det(\mathbb{J} - \widetilde{\mathbb{D}} - \lambda\mathbb{I}) = \lambda^2 + g(k^2)\lambda + h(k^2) = 0 \quad \Leftrightarrow \quad \lambda_\pm = \frac{1}{2}\left[-g(k^2) \pm \sqrt{g^2(k^2) - 4h(k^2)}\right] \tag{3.34}$$

Where I adopted the same notation as in Section 3.4 for the coefficient functions of the characteristic polynomial:

$$\begin{aligned}
g(k^2) &= \beta\,k^4 + (\bar{D} + D)\,k^2 + n_*(\alpha+\epsilon) \\
h(k^2) &= \beta\bar{D}\,k^6 + (\alpha\beta n_* + D\bar{D})\,k^4 + n_*(\alpha D + \epsilon\bar{D})\,k^2 + \alpha(s+\epsilon\, n_*^2)
\end{aligned} \tag{3.35}$$

and I defined for shortness $D \coloneqq D_0 - D_1 n_*$.

3.5.4 Instability

To perform the linear instability analysis, as usual, we need to study the sign of the functions $g(k^2)$ and $h(k^2)$ according to Eq. (3.25).

Study of $g(k^2)$

$g(k^2)$ is a quadratic function of k^2: $g(k^2) = g_2k^4 + g_1k^2 + g_0$, with

- $g_2 = \beta > 0$
- $g_1 = \bar{D} + D$ can be $\gtrless 0$
- $g_0 = \alpha(s+\epsilon\, n_*^2) > 0$

Then if $g_1 > 0 \quad \Rightarrow \quad g > 0\,\forall k$

if $\begin{cases} g_1 < 0 \\ \min(g) > 0 \end{cases} \quad \Rightarrow \quad g > 0\,\forall k$

if $\begin{cases} g_1 < 0 \\ \min(g) < 0 \end{cases} \quad \Rightarrow \quad \begin{array}{l} g > 0 \text{ for } k < k_- \text{ and } k > k_+ \\ g < 0 \text{ for } k_- < k < k_+ \end{array}$

Where k_-^2, k_+^2 are the positive roots of $g(k^2)$

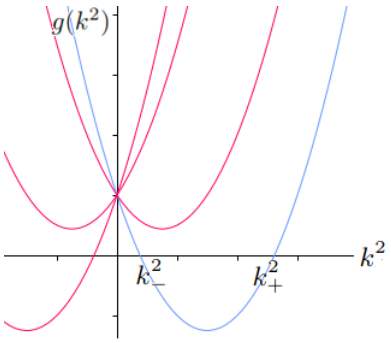

FIG. 3.5. Visual sketch of the possible behaviors of the function $g(k^2)$.

Study of $h(k^2)$

$h(k^2)$ is a cubic function of k^2: $h(k^2) = h_3k^6 + h_2k^4 + h_1k^2 + h_0$, with

- $h_3 = \beta\bar{D} > 0$
- $h_2 = \alpha\beta n_* + D\bar{D}$ can be $\gtrless 0$
- $h_1 = n_*(\alpha D + \epsilon\bar{D})$ can be $\gtrless 0$
- $h_0 = \alpha(s + \epsilon\, n_*^2) > 0$

$$\text{Then if } \begin{cases} h_1 > 0 \\ h_2 > 0 \end{cases} \quad \Rightarrow \quad h > 0\,\forall k$$

$$\text{if } \begin{cases} h_1 < 0 \vee h_2 < 0 \\ \min(h) > 0 \end{cases} \quad \Rightarrow \quad h > 0\,\forall k$$

$$\text{if } \begin{cases} h_1 < 0 \vee h_2 < 0 \\ \min(h) < 0 \end{cases} \quad \Rightarrow \quad \begin{array}{l} h > 0 \text{ for } k < \overline{k}_- \text{ and } k > \overline{k}_+ \\ h < 0 \text{ for } \overline{k}_- < k < \overline{k}_+ \end{array}$$

Where $\overline{k}_-^2, \overline{k}_+^2$ are the positive roots of $h(k^2)$

Then the general instability conditions follow from Eq. (3.25):

$$\begin{aligned} Re[\lambda_+] > 0 \quad \Leftrightarrow \quad & \begin{cases} g_1 < 0 \\ \min(g) < 0 \\ k_- < k < k_+ \end{cases} \vee \begin{cases} g_1 > 0 \vee \begin{cases} g_1 < 0 \\ \min(g) > 0 \end{cases} \vee \begin{cases} g_1 < 0 \\ \min(g) < 0 \\ k < k_- \vee k > k_+ \end{cases} \\ h_1 < 0 \vee h_2 < 0 \\ \min(h) < 0 \\ \overline{k}_- < k < \overline{k}_+ \end{cases} \\ Re[\lambda_-] > 0 \quad \Leftrightarrow \quad & \begin{cases} g_1 < 0 \\ \min(g) < 0 \\ k_- < k < k_+ \\ \begin{cases} h_1 > 0 \\ h_2 > 0 \end{cases} \vee \begin{cases} h_1 < 0 \vee h_2 < 0 \\ \min(h) > 0 \end{cases} \vee \begin{cases} h_1 < 0 \vee h_2 < 0 \\ \min(h) < 0 \\ k < \overline{k}_- \vee k > \overline{k}_+ \end{cases} \end{cases} \end{aligned} \tag{3.36}$$

Let us try to understand the behavior of the model in simplified cases, by switching off some parameters of the system.

Case $D_1 = 0$

$D_1 = 0 \Rightarrow D = D_0 > 0$, therefore:

$$g(k^2) = \beta\, k^4 + D_0\, k^2 + n_*(\alpha + \epsilon)$$
$$h(k^2) = \beta\bar{D}\, k^6 + (\alpha\beta n_* + D_0\bar{D})\, k^4 + n_*(\alpha D_0 + \epsilon\bar{D})\, k^2 + \alpha(s + \epsilon\, n_*^2)$$

Then all coefficients g_2, g_1, g_0, h_3, h_2, h_1, h_0 are positive $\Rightarrow$ g, $h > 0\,\forall k$ and consequently there is no instability (Fig. 3.6). This also allows us to observe that $D = D_0 - D_1 n_* < 0$ is a necessary condition for instability, while the specific value of D_0 alone does not seem to be very influential.

$$D = D_0 - D_1 n_* > 0 \quad \Rightarrow \quad \text{no spatial instability.} \tag{3.37}$$

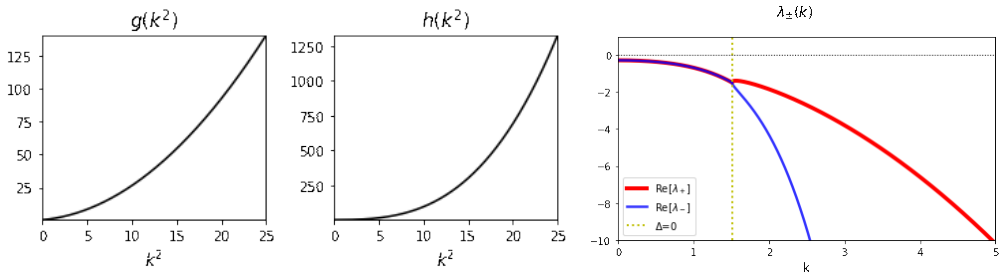

FIG. 3.6. Plots of h, g and $Re[\lambda_\pm]$ for parameter values $D_1 = 0$, $D_0 = 0.2$, $\beta = 0.2$, $\bar{D} = 0.4$, $\alpha = 0.3$, $\epsilon = 0.6$, $d = 0.4$, $s = 0.5$. In this case $g_1 = 0.6$, $h_2 = 0.12$, $h_1 = 0.19$, therefore $h(k^2)$ and $g(k^2)$ have no minimum in the domain $k^2 > 0$.

Case $\beta = 0$

When $\beta = 0$ we fall back to the case studied in Section 3.4, with $\mathbb{J}$ given by (3.32) $\Rightarrow$ f_n, $g_c < 0$. We immediately conclude, from (3.29), that instability is never allowed in a limited wavenumber range in this case.

Case $\epsilon = 0$

In this case the uniform equilibrium solution takes the simplest form

$$n_* = s/d$$

and the functions (3.35) become:

$$g(k^2) = \beta\, k^4 + (\bar{D} + D)\, k^2 + \alpha s/d$$
$$h(k^2) = \beta\bar{D}\, k^6 + (\alpha\beta s/d + D\bar{D})\, k^4 + \alpha D s/d\, k^2 + \alpha s$$

Having clarified that D must necessarily be < 0, the signs of the coefficients are the following:

- $g_2 > 0$, $g_1 \gtrless 0$ and $g_0 > 0$;
- $h_3 > 0$, $h_2 \gtrless 0$, $h_1 < 0$ and $h_0 > 0$.

Therefore:

$$
\begin{aligned}
Re[\lambda_+] > 0 \quad \Leftrightarrow \quad & \begin{cases} g_1 < 0 \\ \min(g) < 0 \\ k_- < k < k_+ \end{cases} \vee \begin{cases} g_1 > 0 \vee \begin{cases} g_1 < 0 \\ \min(g) > 0 \end{cases} \vee \begin{cases} g_1 < 0 \\ \min(g) < 0 \\ k < k_- \vee k > k_+ \end{cases} \\ \min(h) < 0 \\ \overline{k}_- < k < \overline{k}_+ \end{cases} \\
Re[\lambda_-] > 0 \quad \Leftrightarrow \quad & \begin{cases} g_1 < 0 \\ \min(g) < 0 \\ k_- < k < k_+ \\ \min(h) > 0 \vee \begin{cases} \min(h) < 0 \\ k < \overline{k}_- \vee k > \overline{k}_+ \end{cases} \end{cases}
\end{aligned}
\tag{3.38}
$$

Some examples are plotted in the figures below.

In conclusion, instability is allowed with $\epsilon = 0$, for suitable choices of the other system parameters.

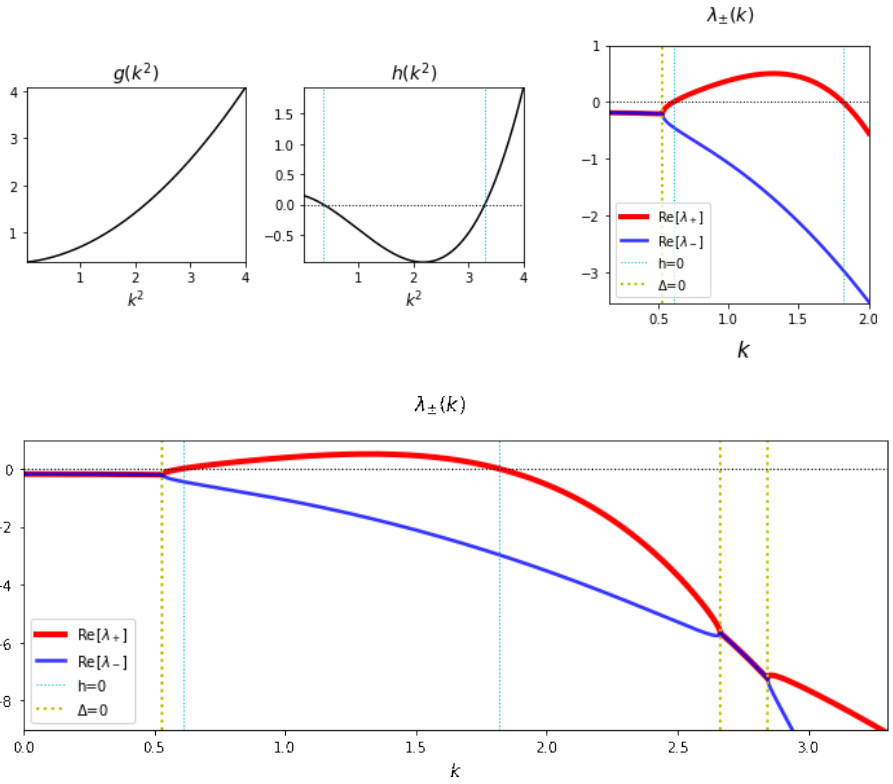

FIG. 3.7. Plots of h, g and $Re[\lambda_\pm]$ for parameter values $\epsilon = 0$, $D_1 = 0.7$, $D_0 = 0.2$ ($\Rightarrow D = -0.675$), $\beta = 0.2$, $\bar{D} = 0.8$, $\alpha = 0.3$, $d = 0.4$, $s = 0.5$.
In this case $g_1 = 0.12$, $h_2 = -0.46$, $h_1 = -0.25$, therefore $g(k^2)$ has no minimum in the domain $k^2 > 0$, while $\min(h) = -0.95$ in $k^2 = 2.18$ and $h(k^2)$ has two roots $\overline{k}_-^2$, $\overline{k}_+^2$ in the domain $k^2 > 0$.
As expected, instability occurs in the range $\overline{k}_- < k < \overline{k}_+$, where $Re[\lambda_+] > 0$.

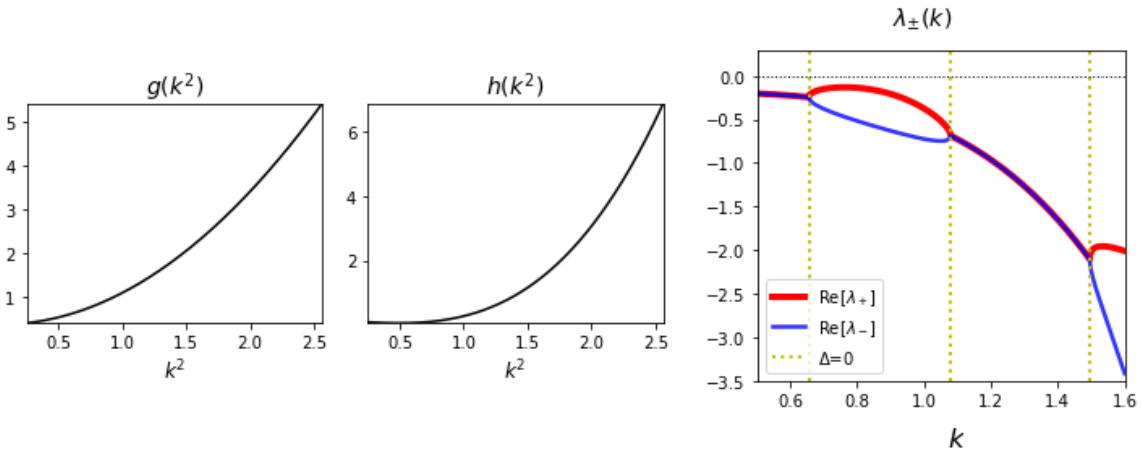

FIG. 3.8. Plots of h, g and $Re[\lambda_\pm]$ for parameter values $\epsilon = 0$, $D_1 = 0.7$, $D_0 = 0.2$ ($\Rightarrow D = -0.675$), $\beta = 0.8$, $\bar{D} = 0.6$, $\alpha = 0.3$, $d = 0.4$, $s = 0.5$.
In this case $g_1 = -0.08$, $h_2 = -0.11$, $h_1 = -0.25$, therefore $\min(g) = 0.37$ in $k^2 = 0.05$ and $\min(h) = 0.06$ in $k^2 = 0.49$: the two functions have no roots in the domain $k^2 > 0$.
No instability is found, consistently with (3.38).

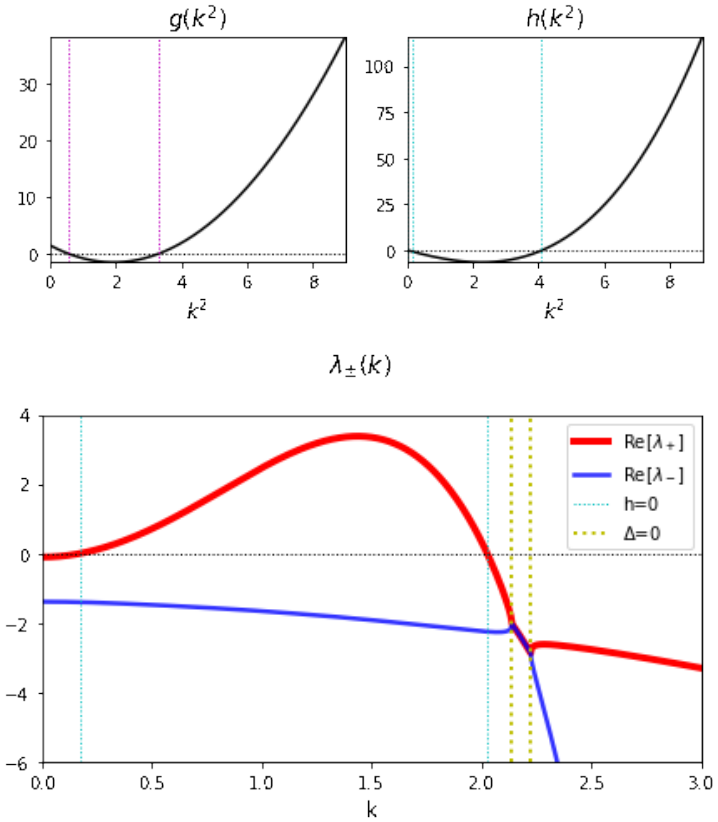

FIG. 3.9. Plots of h, g and $Re[\lambda_\pm]$ for parameter values $\epsilon = 0$, $D_1 = 0.7$, $D_0 = 0.2$ ($\Rightarrow D = -0.675$), $\beta = 0.8$, $\bar{D} = 0.2$, $\alpha = 0.3$, $d = 0.1$, $s = 0.5$.
In this case $g_1 = -3$, $h_2 = 0.54$, $h_1 = -5$, therefore $\min(g) = -1.5$ in $k^2 = 1.9$ and $\min(h) = -6.4$ in $k^2 = 2.28$. Therefore, consistently with (3.38), instability occurs for λ_+ in the range $\overline{k}_- < k < \overline{k}_+$, since $\overline{k}_-^2 < k_-^2 < k_+^2 < \overline{k}_+^2$.

Case $\epsilon = 0$ and $\bar{D} = 0$

Let us try to simplify even more the analysis by putting $\bar{D}$ to zero as well. In this case (3.35) becomes:

$$\begin{aligned} g(k^2) &= \beta\, k^4 + D\, k^2 + \alpha s/d \\ h(k^2) &= \alpha\beta s/d\, k^4 + \alpha D s/d\, k^2 + \alpha s \end{aligned} \tag{3.39}$$

Both functions are quadratic functions of k^2 with coefficients $g_2, h_2 > 0,\ g_1, h_1 < 0,\ g_0, h_0 > 0$ (assuming $D < 0$). Therefore their roots are always positive, when they exist. They can be studied easily:

$$\text{if } \min(g) = \frac{\alpha s}{d} - \frac{D^2}{4\beta} < 0 \quad \rightarrow \quad \exists \text{ roots of } g\text{: } k_\pm^2 = \frac{1}{2\beta}\left(-D \pm \sqrt{D^2 - 4\alpha\beta s/d}\right) > 0$$
$$\text{if } \min(h) = \frac{\alpha s}{d}\left(d - \frac{D^2}{4\beta}\right) < 0 \quad \rightarrow \quad \exists \text{ roots of } h\text{: } \overline{k}_\pm^2 = \frac{1}{2\beta}\left(-D \pm \sqrt{D^2 - 4\beta d}\right) > 0$$

and both g and h have the minimum in $k^2_{min} = -\frac{D}{2\beta}$.

Moreover, the ordering of the roots depends on the values of parameters α, s and d:

$$\text{if } d > \frac{\alpha s}{d} \quad \rightarrow \quad k_+^2 > \overline{k}_+^2 \text{ and } k_-^2 < \overline{k}_-^2 \quad \rightarrow \quad k_- < \overline{k}_- < \overline{k}_+ < k_+$$
$$\text{if } d < \frac{\alpha s}{d} \quad \rightarrow \quad k_+^2 < \overline{k}_+^2 \text{ and } k_-^2 > \overline{k}_-^2 \quad \rightarrow \quad \overline{k}_- < k_- < k_+ < \overline{k}_+$$

The instability conditions (3.38) become:

$$Re[\lambda_+] > 0 \quad \Leftrightarrow \quad \begin{cases} \dfrac{\alpha s}{d} < \dfrac{D^2}{4\beta} \\ k_- < k < k_+ \end{cases} \vee \begin{cases} \dfrac{\alpha s}{d} > \dfrac{D^2}{4\beta} \vee \begin{cases} \dfrac{\alpha s}{d} < \dfrac{D^2}{4\beta} \\ k < k_- \vee k > k_+ \end{cases} \\ d < \dfrac{D^2}{4\beta} \\ \overline{k}_- < k < \overline{k}_+ \end{cases}$$

$$Re[\lambda_-] > 0 \quad \Leftrightarrow \quad \begin{cases} \dfrac{\alpha s}{d} < \dfrac{D^2}{4\beta} \\ k_- < k < k_+ \end{cases} \vee \begin{cases} d > \dfrac{D^2}{4\beta} \vee \begin{cases} d < \dfrac{D^2}{4\beta} \\ k < \overline{k}_- \vee k > \overline{k}_+ \end{cases} \end{cases}$$

	parameters	instability	instability range
a.	$\frac{\alpha s}{d} > \frac{D^2}{4\beta} \wedge d > \frac{D^2}{4\beta}$	no	
b.	$d < \frac{D^2}{4\beta} < \frac{\alpha s}{d} \vee d < \frac{\alpha s}{d} < \frac{D^2}{4\beta}$	$Re[\lambda_+]$	$\overline{k}_- < k < \overline{k}_+$
c.	$\frac{\alpha s}{d} < \frac{D^2}{4\beta} < d$	$Re[\lambda_+]$, $Re[\lambda_-]$	$k_- < k < k_+$
d.	$\frac{\alpha s}{d} < d < \frac{D^2}{4\beta}$	$Re[\lambda_+]$ $Re[\lambda_-]$	$k_- < k < k_+$ $k_- < k < \overline{k}_-,\ \overline{k}_+ < k < k_+$

TAB. 3.1. Instability conditions for $\epsilon = 0$, $\bar{D} = 0$.

Let us study the different cases.

$$\text{if} \quad \frac{\alpha s}{d} > \frac{D^2}{4\beta},\, d > \frac{D^2}{4\beta}: \quad g,\, h > 0\, \forall k \;\Rightarrow\; \text{NO INSTABILITY}$$

$$\text{if} \quad \frac{\alpha s}{d} > \frac{D^2}{4\beta} > d: \quad Re[\lambda_+] > 0 \text{ in the range } \overline{k}_- < k < \overline{k}_+$$

$$\text{if} \quad \frac{\alpha s}{d} < \frac{D^2}{4\beta} < d: \quad Re[\lambda_+],\, Re[\lambda_-] > 0 \text{ in the range } k_- < k < k_+$$

$$\text{if} \quad \frac{\alpha s}{d} < \frac{D^2}{4\beta},\, d < \frac{D^2}{4\beta}: \quad Re[\lambda_+] > 0 \;\Leftrightarrow\; k_- < k < k_+ \vee \begin{cases} k < k_- \vee k > k_+ \\ \overline{k}_- < k < \overline{k}_+ \end{cases}$$

$$Re[\lambda_-] > 0 \;\Leftrightarrow\; \begin{cases} k_- < k < k_+ \\ k < \overline{k}_- \vee k > \overline{k}_+ \end{cases}$$

$$\text{Then if} \quad d > \frac{\alpha s}{d}: \quad Re[\lambda_+] > 0 \;\Leftrightarrow\; k_- < k < k_+$$

$$Re[\lambda_-] > 0 \;\Leftrightarrow\; k_- < k < \overline{k}_- \vee \overline{k}_+ < k < k_+$$

$$\text{if} \quad d < \frac{\alpha s}{d}: \; Re[\lambda_+] > 0 \;\Leftrightarrow\; \overline{k}_- < k < \overline{k}_+$$

The results are summarized in Tab. 3.1 and some examples are plotted for each possible case.

We remark that the obtained instabilities can be classified as stationary linear instabilities of type I (labeled I_s instabilities) in the cases **b.** and **d.** of Tab. 3.1, with the exception of case **c.**. In the latter case, the instability is still of type I, however the eigenvalues are not real in proximity of k_c, as visible from Fig. 3.13, therefore the instability is oscillatory in time (I_o).

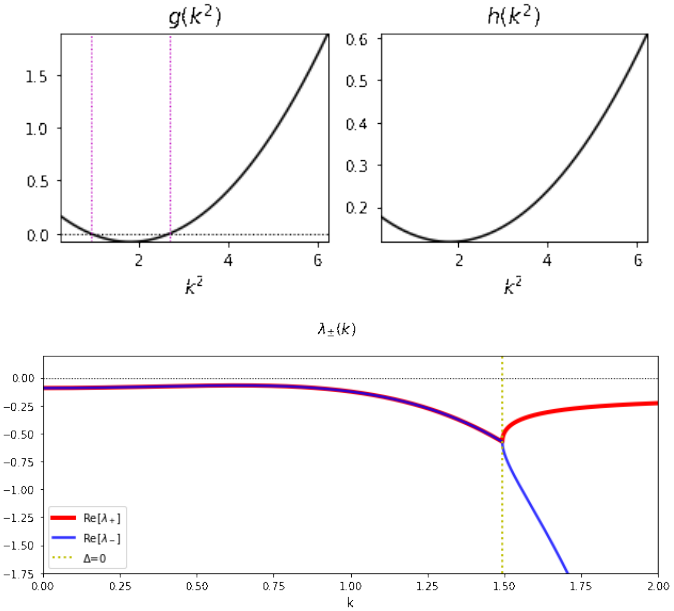

FIG. 3.10. Plots of h, g and $Re[\lambda_\pm]$ for parameter values $\epsilon = 0$, $\bar{D} = 0$, $D_1 = 0.7$, $D_0 = 0.2$ ($\Rightarrow D = -0.24$), $\beta = 0.3$, $\alpha = 0.3$, $d = 0.8$, $s = 0.5$.
In this case $\min(g) = 0.14$ and $\min(h) = 0.14$, indeed g and h are positive $\forall\, k^2$.
$d = 0.8 > \frac{\alpha s}{d} = 0.19 > \frac{D^2}{4\beta} = 0.05$ therefore we are in case **a.** of Tab. 3.1: as expected, there is no instability.

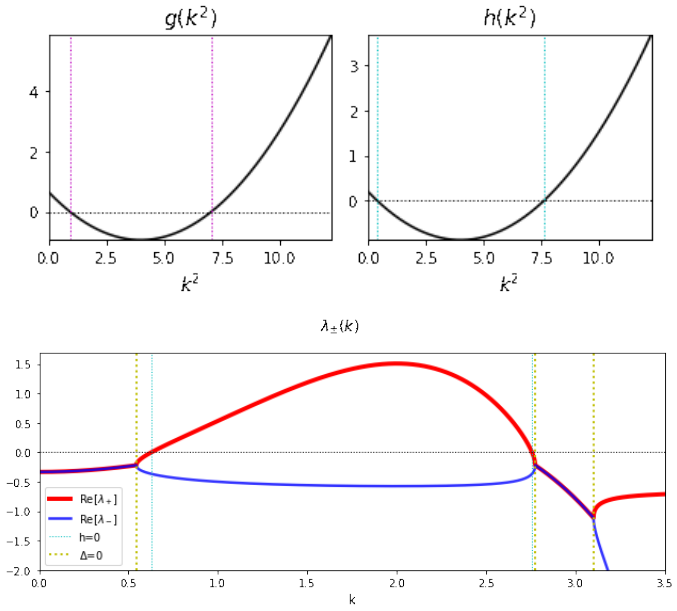

FIG. 3.11. Plots of h, g and $Re[\lambda_\pm]$ for parameter values $\epsilon = 0$, $\bar{D} = 0$, $D_1 = 0.6$, $D_0 = 0.2$ ($\Rightarrow D = -0.8$), $\beta = 0.1$, $\alpha = 0.4$, $d = 0.3$, $s = 0.5$.
In this case $\min(g) = -0.93$ and $\min(h) = -0.86$, indeed both functions have two zeros in the domain $k^2 > 0$.
$d = 0.3 < \frac{\alpha s}{d} = 0.67 < \frac{D^2}{4\beta} = 1.6$ therefore we are in case **b.** of Tab. 3.1.
As expected, instability occurs for $Re[\lambda_+]$ in the range $\overline{k}_- < k < \overline{k}_+$.

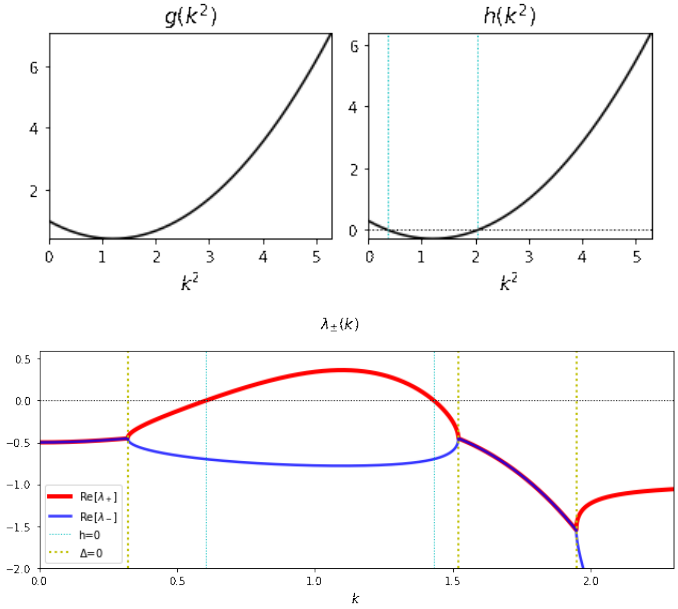

FIG. 3.12. Plots of h, g and $Re[\lambda_\pm]$ for parameter values $\epsilon = 0$, $\bar{D} = 0$, $D_1 = 0.7$, $D_0 = 0.2$ ($\Rightarrow D = -0.97$), $\beta = 0.4$, $\alpha = 0.6$, $d = 0.3$, $s = 0.5$.
In this case $\min(g) = 0.4$ and $\min(h) = -0.3$, indeed only h has zeros in the domain $k^2 > 0$.
$d = 0.3 < \frac{D^2}{4\beta} = 0.6 < \frac{\alpha s}{d} = 1$ therefore we are in case **b.** of Tab. 3.1.
Instability occurs for $Re[\lambda_+]$ in the range $\overline{k}_- < k < \overline{k}_+$.

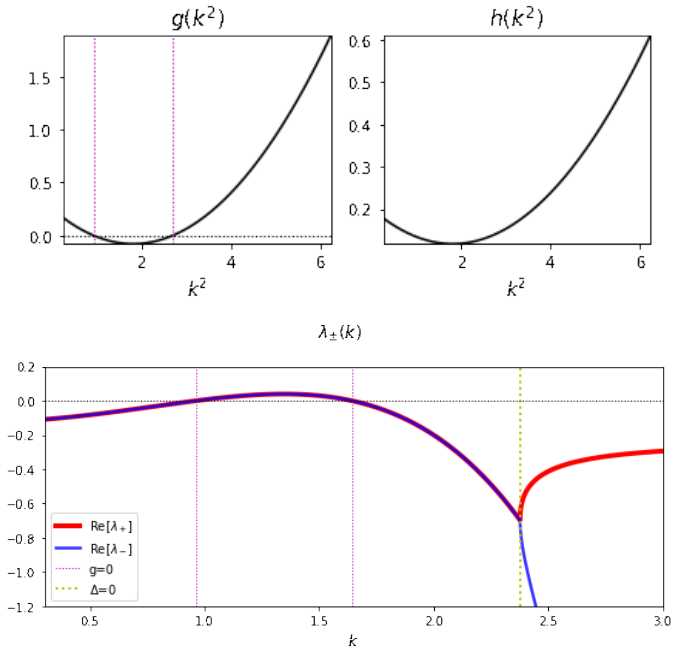

FIG. 3.13. Plots of h, g and $Re[\lambda_\pm]$ for parameter values $\epsilon = 0$, $\bar{D} = 0$, $D_1 = 0.9$, $D_0 = 0.2$ ($\Rightarrow D = -0.36$), $\beta = 0.1$, $\alpha = 0.4$, $d = 0.8$, $s = 0.5$. In this case $\min(g) = -0.08$ and $\min(h) = 0.12$, indeed only g has zeros in the domain $k^2 > 0$. $\frac{\alpha s}{d} = 0.25 < \frac{D^2}{4\beta} = 0.33 < d = 0.8$ therefore we are in case **c.** of Tab. 3.1.
As expected, instability occurs for $Re[\lambda_+] \equiv Re[\lambda_-]$ in the range $k_- < k < k_+$: this means that both eigenvalues have non-vanishing imaginary part for all wavenumbers k belonging to such interval, therefore the instability is oscillatory in time.

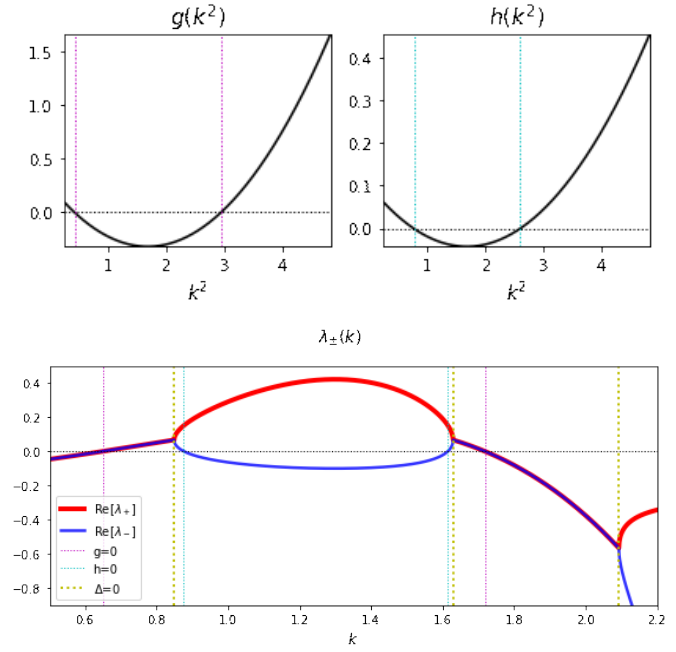

FIG. 3.14. Plots of h, g and $Re[\lambda_\pm]$ for parameter values $\epsilon = 0$, $\bar{D} = 0$, $D_1 = 0.7$, $D_0 = 0.2$ ($\Rightarrow D = -0.675$), $\beta = 0.2$, $\alpha = 0.2$, $d = 0.4$, $s = 0.5$. In this case $\min(g) = -0.32$ and $\min(h) = -0.04$, indeed both functions have two zeros in the domain $k^2 > 0$. $\frac{\alpha s}{d} = 0.25 < d = 0.4 < \frac{D^2}{4\beta} = 0.57$ therefore we are in case **d.** of Tab. 3.1.
Instability occurs for $Re[\lambda_+]$ in the range $k_- < k < k_+$ and for λ_- in the ranges $k_- < k < \overline{k}_-$, $\overline{k}_+ < k < k_+$. Even though the eigenvalues have non-vanishing imaginary part in the disjoints intervals $[k_-, \overline{k}_-]$ and $[\overline{k}_+, k_+]$, they are both real in the central interval containing k_c: therefore $\lambda_+(k_c)$ is real and the instability is stationary in time.

Case $\bar{D} = 0$

In the case $\bar{D} = 0$ and $\epsilon \neq 0$, (3.35) becomes:

$$g(k^2) = \beta\, k^4 + D\, k^2 + n_*(\alpha + \epsilon)$$
$$h(k^2) = \alpha\beta n_*\, k^4 + n_*\alpha D\, k^2 + \alpha(s + \epsilon\, n_*^2)$$

where we must consider now the equilibrium value:

$$n_* = \frac{-d + \sqrt{d^2 + 4\epsilon s}}{2\epsilon}$$

The signs of coefficients do not change with respect to Section 3.5.4 (having assumed $D < 0$).
The minima of g and h are:

$$\min(g) = (\alpha + \epsilon)n_* - \frac{D^2}{4\beta}$$
$$\min(h) = \alpha(s + \epsilon(n_*)^2) - \frac{D^2\alpha n_*}{4\beta}$$

and both are found in $k^2_{min} = -\frac{D}{2\beta}$.

$$\text{if } \min(g) < 0 \quad \rightarrow \quad \exists \text{ roots of } g\text{: } k^2_\pm = \frac{1}{2\beta}\left(-D \pm \sqrt{D^2 - 4\beta n_*(\alpha + \epsilon)}\right) > 0$$
$$\text{if } \min(h) < 0 \quad \rightarrow \quad \exists \text{ roots of } h\text{: } \bar{k}^2_\pm = \frac{1}{2\beta}\left(-D \pm \sqrt{D^2 - 4\beta(\epsilon n_* + s/n_*)}\right) > 0$$

Therefore the behavior of the system does not qualitatively change if we switch on the ϵ parameter, the major difference being the change in the equilibrium value.

The instability conditions of Eq. (3.25) read:

$$Re[\lambda_+] > 0 \quad \Leftrightarrow \quad \begin{cases} (\alpha + \epsilon)n_* < \dfrac{D^2}{4\beta} \\ k^2_- < k^2 < k^2_+ \end{cases} \vee \begin{cases} (\alpha + \epsilon)n_* > \dfrac{D^2}{4\beta} \vee \begin{cases} (\alpha + \epsilon)n_* < \dfrac{D^2}{4\beta} \\ k^2 < k^2_- \vee k^2 > k^2_+ \end{cases} \\ (s/n_* + \epsilon\, n_*) > \dfrac{D^2}{4\beta} \\ k^2_1 < k^2 < k^2_2 \end{cases}$$
$$Re[\lambda_-] > 0 \quad \Leftrightarrow \quad \begin{cases} (\alpha + \epsilon)n_* < \dfrac{D^2}{4\beta} \\ k^2_- < k^2 < k^2_+ \\ (s/n_* + \epsilon\, n_*) > \dfrac{D^2}{4\beta} \vee \begin{cases} (s/n_* + \epsilon\, n_*) < \dfrac{D^2}{4\beta} \\ k^2 < k^2_1 \vee k^2 > k^2_2 \end{cases} \end{cases} \tag{3.40}$$

An example is plotted in Fig. 3.15.

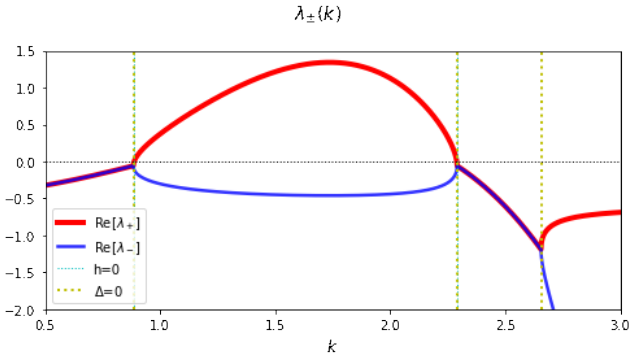

FIG. 3.15. Plot of $Re[\lambda_\pm]$ for parameter values $\bar{D} = 0$, $D_1 = 0.9$, $D_0 = 0.2$ ($\Rightarrow D = -1.2$), $\beta = 0.2$, $\alpha = 0.4$, $\epsilon = 0.2$, $d = 0.2$, $s = 0.8$. In this case $\min(g) = -0.88$ and $\min(h) = -0.62$, indeed both functions have two zeros in the domain $k^2 > 0$. Instability is found for $Re[\lambda_+]$ in the range $\overline{k_-} < k < \overline{k}_+$.

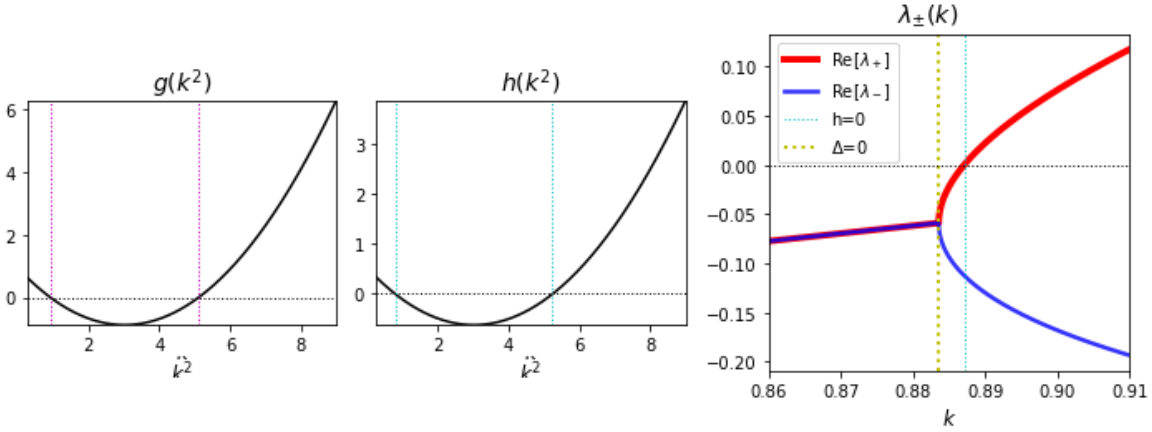

FIG. 3.16. Left, center : Plots of and g and h relative to the parameter values reported in Fig. 3.15. **Right:** zoom of Fig. 3.15 around $\bar{k_-}$.

3.5.5 Expansion for k $\gg 1$

$$\Delta = g^2 - 4h = k^8\beta^2 + 2k^6\beta(D-\bar{D}) + k^4\left[(D-\bar{D})^2 - 2\beta(f_n - g_c)\right] - 2k^2(D-\bar{D})(f_n-g_c) + (f_n-g_c)^2 + 4g_n f_c =$$
$$= k^8\beta^2\left[1 + \frac{2}{k^2\beta}(D-\bar{D}) + \frac{1}{k^4\beta^2}\left((D-\bar{D})^2 - 2\beta(f_n-g_c)\right) - \frac{2}{k^6\beta^2}(D-\bar{D})(f_n-g_c) + \frac{1}{k^8\beta^2}\left((f_n-g_c)^2 + 4g_n f_c\right)\right]$$

$$\sqrt{\Delta} \approx k^4\beta\left[1 + \frac{1}{k^2\beta}(D-\bar{D}) - \frac{1}{k^4\beta}(f_n-g_c) - \frac{1}{k^6\beta^2}(D-\bar{D})(f_n-g_c) + O\left(\frac{1}{k^6}\right)\right] =$$
$$= k^4\beta + k^2(D-\bar{D}) - (f_n-g_c) + O\left(\frac{1}{k^2}\right)$$

$$\lambda_\pm \approx \frac{1}{2}\left[k^4\beta(-1\pm 1) + k^2\left(-(D+\bar{D}) \pm (D-\bar{D})\right) + f_n + g_c \pm (g_c - f_n)\right] + O\left(\frac{1}{k^2}\right)$$

Therefore:

$$\lambda_+ \approx -\bar{D}k^2 + g_c + O\left(\frac{1}{k^2}\right)$$
$$\lambda_- \approx -k^4\beta - Dk^2 + f_n + O\left(\frac{1}{k^2}\right)$$

We notice that the introduction of the $-\beta\,\partial_x^4 n$ term has succesfully stabilized the system, ensuring that the instability, when allowed, occurs for a limited range of wavenumbers.

In conclusion, the desired instability behavior is obtained through the spatial extension of MacArthur's model here proposed: the minimal additional parameters required in order to observe a type I instability starting from the MacArthur's one species and one resource dynamics are β, relative to the stabilizing squared laplacian term, and the overcrowding diffusion coefficient D_1.

The other dispersal parameters $\bar{D}$ and D_0, accounting for the simple diffusion of consumer and resource, as well as the parameter ϵ related to the Janzen-Connel effect, are instead superfluous.
D_0, in particular, influences the stability of the system only through the combination $D = D_0 + n^* D_1$, which is required to be negative for spatial instability to be allowed.

The instability conditions valid for the above mentioned minimal set of parameters are summarized in Tab. 3.1: specifically, a stationary instability appears in the cases classified as **b.** and **d.**, while the instability is oscillatory in time in the case **c.**.

3.6 Non-local MacArthur's model

Up to now we have assumed that resource utilization by a consumer occurs only at the exact point in which the consumer is located. If we relax this assumption, we can model non-local consumption of resources as follows:

$$\alpha\, c(x,t) \quad \rightarrow \quad \int_{-\infty}^{+\infty} \phi(x-y)\, c(y,t)\, \mathrm{d}y = (c * \phi)\,(x,t) \tag{3.41}$$

where $\phi(x-y)$ is the kernel function, and $(c*\phi)\,(x,t)$ is the convolution of the resource population field with the kernel. In this case, $\phi(x-y)$ it is a bell-shaped distribution function in the variable y, peaked in $y = x$. The hypotheses on such function are the following:

- $\phi : \mathbb{R} \rightarrow \mathbb{R}^+$ the distribution function is a real, non negative function;
- $\phi(x) = \phi(-x)$ the distribution function is even;

It is immediate to observe that by setting $\phi(x-y) \rightarrow \alpha\, \delta(x-y)$ the local model is recovered.

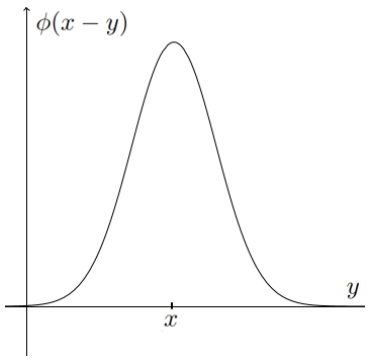

FIG. 3.17. Example of a resource utilization distribution.

The equations for this model are obtained by substituting (3.41) into the MacArthur equations studied in Section 3.5, without the squared laplacian term ($\beta = 0$) :

$$\begin{cases} \dot{n}(x,t) = [(c*\phi)\,(x,t) - d - \epsilon\, n(x,t)]\, n(x,t) + \partial_x \left[(\, D_0 - D_1\, n(x,t)\,)\, \partial_x n(x,t) \right] \\ \dot{c}(x,t) = s - n(x,t)\,(c*\phi)\,(x,t) + \bar{D}\, \partial_x^2 c(x,t) \end{cases} \tag{3.42}$$

Uniform equilibrium

The uniform equilibrium of the system is $(n_0,\, c_0)$ such that:

$$\begin{cases} (c_0 * \phi)\,(x,t) - d - \epsilon\, n_0 = 0 \\ s - n_0\,(c_0 * \phi)\,(x,t) = 0 \end{cases}$$

$$\text{with:}\quad (c_0 * \phi)\,(x,t) = \int_{-\infty}^{+\infty} \phi(x-y)\, c_0\, \mathrm{d}y = c_0 \int_{-\infty}^{+\infty} \phi(-z)\, \mathrm{d}z = c_0 \int_{-\infty}^{+\infty} \phi(z)\, \mathrm{d}z = c_0\, \widetilde{\phi}(k=0) \tag{3.43}$$

where a change of variables is performed in the second step, and then the parity of ϕ is exploited. Being $\phi(z) > 0\, \forall z$, $\widetilde{\phi}(k=0)$ is a positive constant. Therefore:

$$\begin{cases} c_0\, \widetilde{\phi}(0) - d - \epsilon\, n_0 = 0 \\ s - n_0\, c_0\, \widetilde{\phi}(0) = 0 \end{cases}$$

which yields the same solutions of (3.31) with the substitution $\alpha \to \widetilde{\phi}(0)$:

$$\begin{cases} \epsilon \neq 0 \\ n_0 = \dfrac{-d + \sqrt{d^2 + 4\epsilon s}}{2\epsilon} \\ c_0 = \dfrac{s}{n_0\, \widetilde{\phi}(0)} = \dfrac{d + \sqrt{d^2 + 4\epsilon s}}{2\widetilde{\phi}(0)} \end{cases} \vee \begin{cases} \epsilon = 0 \\ n_0 = s/d \\ c_0 = d/\widetilde{\phi}(0) \end{cases}$$

Stability under uniform perturbation

Substituting an uniform perturbation of the form (3.10) into Eq. (3.42) yields:

$$\begin{cases} \dot{\delta n}(t) = (n_0 + \delta n(t)) \left[\big((c_0 + \delta c) * \phi\big) - d - \epsilon\, (n_0 + \delta n) \right] \\ \dot{\delta c}(t) = s - (n_0 + \delta n(t)) \big((c_0 + \delta c) * \phi\big) \end{cases}$$

where:

$$\big((c_0 + \delta c) * \phi\big)(x,t) = \int_{-\infty}^{+\infty} \phi(x-y)\, \big(c_0 + \delta c(t)\big)\, \mathrm{d}y = \big(c_0 + \delta c\big) \int_{-\infty}^{+\infty} \phi(z)\, \mathrm{d}z = \big(c_0 + \delta c\big)\, \widetilde{\phi}(0)$$

$$\Rightarrow \quad \lambda\, \vec{\delta} = \mathbb{J}\, \vec{\delta} \qquad \text{with} \quad \mathbb{J} = \begin{pmatrix} -n_0 \epsilon & n_0\, \tilde{\phi}(0) \\ -s/n_0 & -n_0\, \tilde{\phi}(0) \end{pmatrix}$$

The eigenvalues are:

$$\lambda_\pm = \frac{-n_0 \big(\widetilde{\phi}(0) + \epsilon\big) \pm \sqrt{n_0^2 \big(\widetilde{\phi}(0) + \epsilon\big)^2 - 4\, \widetilde{\phi}(0)\, \big(s + \epsilon n_0^2\big)}}{2}$$

Being all the MacArthur parameters positive by definition, and $\widetilde{\phi}(0) > 0$:

if the eigenvalues are complex: $Re[\lambda_\pm] = -n_0(\widetilde{\phi}(0) + \epsilon)/2 < 0$

if they are real: $\lambda_- = [-n_0(\widetilde{\phi}(0) + \epsilon) - \sqrt{\Delta}]/2 < 0\,,$

$\lambda_+ = [-n_0(\widetilde{\phi}(0) + \epsilon) + \sqrt{\Delta}]/2 < 0$, being $\sqrt{\Delta} < n_0(\widetilde{\phi}(0) + \epsilon)\,.$

Thus the uniform equilibrium is always stable.

Non-uniform perturbation

Substituting a spatially dependent perturbation with the form (3.12) into Eq. (3.42):

$$\begin{cases} \dot{\delta n} = (n_0 + \delta n)\left[(c * \phi) - d - \epsilon\,(n_0 + \delta n)\right] + \partial_x\left[(D_0 - D_1(n_0 + \delta n))\,\partial_x \delta n\right] \\ \dot{\delta c} = s - (n_0 + \delta n)\,(c * \phi) + \bar{D}\,\partial_x^2 \delta c \end{cases}$$

the convolution becomes, by substituting $c(x,t) = c_0 + \bar{\delta} e^{\lambda t + ikx}$ and changing the integration variable:

$$(c * \phi)\,(x,y) = \int \phi(x-y)\,\left[c_0 + \delta c(y,t)\right]\,\mathrm{d}y = c_0\,\widetilde{\phi}(0) + \bar{\delta} e^{\lambda t + ikx} \int \phi(z) e^{ikz}\,\mathrm{d}z = c_0\,\widetilde{\phi}(0) + \delta c\,\widetilde{\phi}(k)$$

Then, at linear order:

$$\begin{cases} \lambda\,\delta n = -\epsilon\,n_0\,\delta n + n_0\,\widetilde{\phi}(k)\,\delta c - k^2 D\,\delta n \\ \lambda\,\delta c = -c_0\,\widetilde{\phi}(k)\,\delta n - n_0\,\widetilde{\phi}(k)\,\delta c - k^2 \bar{D}\,\delta c \end{cases}$$

where I defined $D \coloneqq D_0 - D_1 n_0$. The eigenvalues can be determined by solving:

$$\begin{aligned} &\lambda\,\vec{\delta} = (\mathbb{J} - k^2 \mathbb{D})\,\vec{\delta} \qquad \text{with} \quad \mathbb{D} = \begin{pmatrix} D & 0 \\ 0 & \bar{D} \end{pmatrix}, \ \text{and} \ \mathbb{J} = \begin{pmatrix} -n_0\epsilon & n_0\,\tilde{\phi}(k) \\ -s/n_0 & -n_0\,\tilde{\phi}(k) \end{pmatrix} \\ &\lambda_\pm = \frac{-g \pm \sqrt{g^2 - 4h}}{2} \\ &\text{with:} \quad g(k) = \left(D + \bar{D}\right)\,k^2 + n_0\epsilon + n_0\,\widetilde{\phi}(k) \\ &\qquad\quad h(k) = D\bar{D}\,k^4 + n_0\epsilon\bar{D}\,k^2 + \widetilde{\phi}(k)\left(n_0 D\,k^2 + s + \epsilon\,n_0^2\right) \end{aligned} \tag{3.44}$$

Properties of $\widetilde{\phi}(k)$

The hypothesis that $\phi(x)$ is an even function ensures that $\widetilde{\phi}$ is a real and even function of k:

$$\begin{aligned} \widetilde{\phi}(k) &= \int_{-\infty}^{+\infty} \phi(x)\,e^{ikx}\,\mathrm{d}x = \int_0^{+\infty} \phi(x)\,e^{ikx}\,\mathrm{d}x + \int_{-\infty}^{0} \phi(x)\,e^{ikx}\,\mathrm{d}x = \\ &= \int_0^{+\infty} \phi(x)\,e^{ikx}\,\mathrm{d}x + \int_0^{+\infty} \phi(x)\,e^{-ikx}\,\mathrm{d}x = \int_0^{+\infty} \phi(x)\,\left(e^{ikx} + e^{-ikx}\right)\,\mathrm{d}x = \\ &= 2\int_0^{+\infty} \phi(x)\,\cos(kx)\,\mathrm{d}x \end{aligned} \tag{3.45}$$

$$\Rightarrow \quad \widetilde{\phi}(k) \in \mathbb{R}, \quad \widetilde{\phi}(k) = \widetilde{\phi}(-k)$$

3.6.1 Hypotheses on the Fourier transform of the kernel

Having analysed the linear stability of the model as a function of a generic kernel $\phi(x)$ in B, we can now make some hypothesis on its form and see if it leads to the desired results.

The easiest case is represented by a Gaussian kernel function:

$$\phi(x) = \alpha \exp\left(-\frac{x^2}{2\sigma^2}\right) \quad \rightarrow \quad \widetilde{\phi}(k) = \alpha\,\sigma \exp\left(-\frac{\sigma^2 k^2}{2}\right) \equiv \phi_0 \exp\left(-\frac{\sigma^2 k^2}{2}\right) > 0\,\forall\,k$$

and the study of the sign of $\mathrm{Re}[\lambda_\pm(k)]$ in terms of its Fourier transform is reported in **??**. Let's recall the results of the linear instability analysis in this case.

Since $\widetilde{\phi}(k) > 0\,\forall\,k$, when $D > 0$ the functions $g(k)$, $h(k) > 0\,\forall\,k$, and instability is never allowed.
If $D < 0$, instead, considering for simplicity the case $\epsilon = 0$, $\bar{D} = 0$ we obtain (B.7) :

$$\widetilde{\phi}(k) < -A(k) \quad \vee \quad \begin{cases} \widetilde{\phi}(k) > -A(k) \\ k > \bar{k} \end{cases} \qquad \text{where } A(k) = \frac{D}{n_0}k^2,\ \bar{k} = \sqrt{-\frac{sD}{n_0}}$$

and instability is found $\forall\,k > \bar{k}$, as plotted in figure Fig. 3.18. As already discussed in the previous sections, this is not a desired behavior.

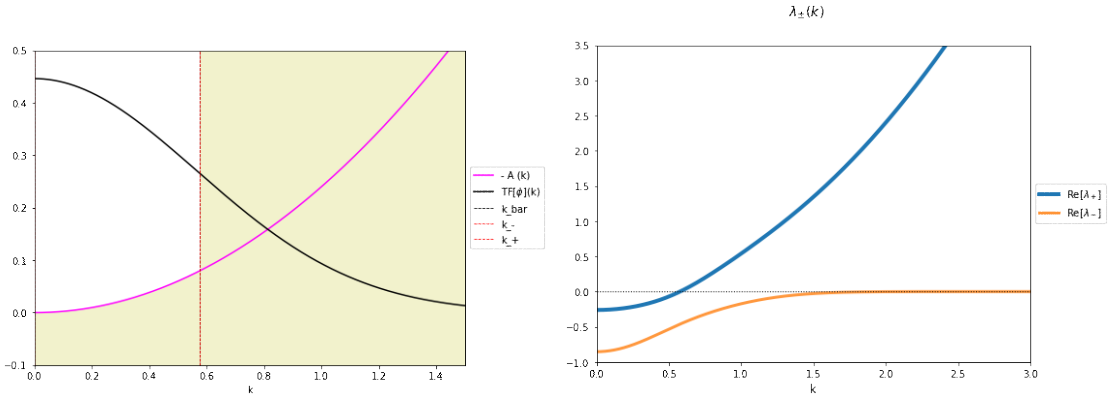

FIG. 3.18. The Fourier transform of the kernel function is positive $\forall\, k$.

An attempt to cure this problem could be to select a slightly modified kernel function, having at least one zero, in such a way that $\widetilde{\phi}(k) < 0$ for some k and still $\widetilde{\phi}(k) \to 0$ like an exponential for $k \to \infty$, so that the expansion (B.12) still holds. Then, instability would be allowed for some k even when $D > 0$, and in such case from (B.12) we would expect the eigenvalues to be negative for large wavenumber values.

For example, if we considered a kernel function whose Fourier transform has the shape plotted in Fig. 3.19, we would find instability for $D > 0$ in an interval $k_1 < k < k_2$.
In case $\widetilde{\phi}(k)$ had more than one zero, the behavior could be more complicated and more than one instability interval could be found for the wavenumber k (Fig. 3.20).

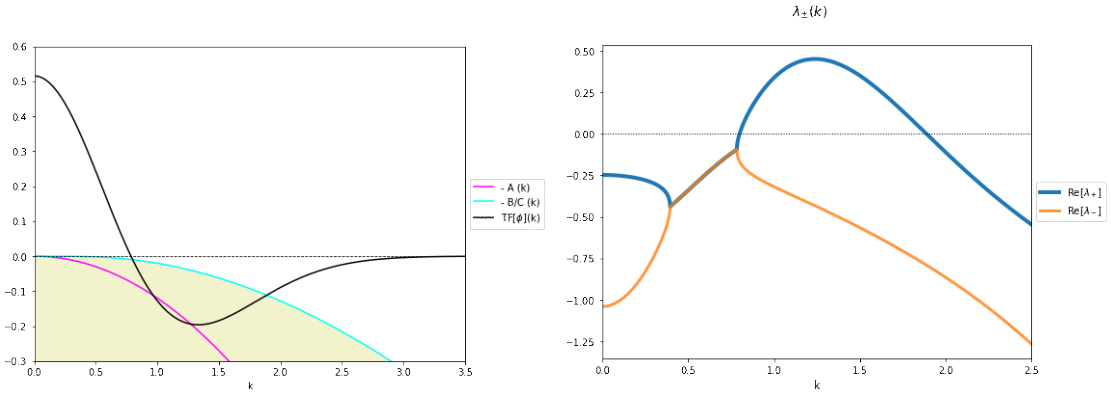

FIG. 3.19. The Fourier transform of the kernel function has one zero.

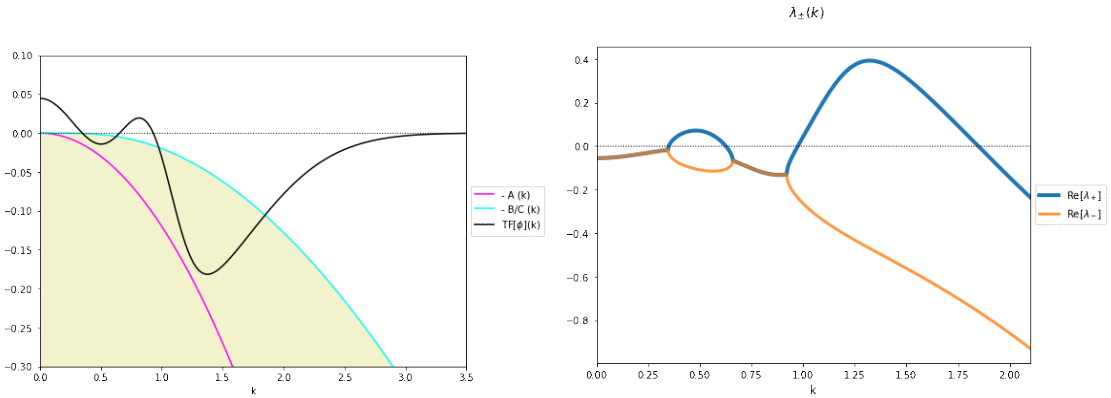

FIG. 3.20. The Fourier transform of the kernel function has two zeros.

Chapter 4

Numerical integration and results

In this chapter, I will describe the code developed for the numerical integration of the system (Section 4.1) and I will present the result that I have obtained by integrating the SH equation (Section 4.2) and the spatial extension of the MacArthur model provided in Section 3.5 (Section 4.3).

4.1 Numerical implementation

The first aspect that must be taken into account when numerically implementing the integration of a PDE concerns the discretization of the spatial domain. The one-dimensional spatially infinite domain is approximated by a lattice of N_x discrete sites, each spaced by a distance dx, with periodic boundary conditions. The total length of the domain is therefore:

$$L = N_x \cdot dx$$

which must be large enough for such approximation to hold. This has important consequences on the allowed wavenumbers k: in case of infinite domain they take continuous values, but if the domain is finite, only a limited number of modes is allowed, which are the modes resonating in L:

$$k_n = \frac{2\pi}{L} n \quad n = 1, 2, ...\infty$$

Therefore, the unstable wavenumber band determined by the linear stability analysis in Section 3.5 turns into a finite set of allowed wavenumbers, represented by the discrete k_n that fall into the instability interval:

$$[k_-, k_+] \qquad \rightarrow \qquad k^*_{n_i} \in [k_-, k_+] \quad \forall\, n_i = n_1, ...n_M$$

In particular, we expect that the dominating mode will be the one whose k_n is closer to the continuous wavenumber at which λ_+ is maximum. Recalling the notation adopted in Chapter 2, $Re[\lambda_+(k)]$ is maximum at $k = k_c$: then, the dominating discrete mode will be the $k^*_{n_i}$ closest to k_c, which we label simply as k^*_n.

The fact that the domain has finite length L has also the consequence that, clearly, the smallest visible wavenumber is $k_{min} = 2\pi/L$.
In the numerical implementation there is, however, another aspect that must be taken into account, due to the discretization of space. If the resolution in space is determined by dx, then there is an upper limit on the visible wavenumber too, given by $k_{max} = \frac{2\pi}{dx}$. Therefore, when numerically integrating a system with a given set of parameters determining the instability range, one must be particularly careful to set N_x and dx in such a way that the unstable wavevectors $k^*_{n_1}$, $k^*_{n_2}$, ...$k^*_{n_M}$ fall well within the visibility interval of the discretized domain:

$$k_{min} \ll k^*_{n_1},\, k^*_{n_2},\, ...k^*_{n_M} \ll k_{max}$$

otherwise the emerging pattern would not be discernible.

In order for the outcoming pattern to be comparable with the analytical predictions, one must set the system parameters in such a way that the system is only weakly unstable to the spatially-dependent perturbations: this step is performed by plotting the shape of the real part of the eigenvalues and by checking that the maximum of the larger eigenvalues does not exceed values of $\sim, 1e-6, 1e-5$.
Moreover, we place ourselves in the case in which there is only one allowed unstable wavenumber falling into the instability interval $[k_-, k_+]$, in such a way that we remove any ambiguity in the expected periodicity of the pattern, and the dynamics of the system is predictably simpler.

The time evolution of the system is obtained by means of a simple integration scheme. Given the initial condition, which must respect the boundary condition, the values of each population at each site in the lattice are recorded into an array, which is evolved according to the forward-time centered-space Euler method. N_t steps of integration of size dt are performed, leading to a total integration time of:

$$T = N_t \cdot dt$$

which is chosen in such a way that $T > \tau$, where $\tau = 1/Re[\lambda(k_n^*)]$ is the typical timescale of the instability.
To check the evolution of the system through time in a way that is not too computationally demanding, another variable N_{out} is introduced, representing the number of integration steps after which the state of the system is saved and is made available for later plotting.
At each integration cycle, the periodic boundary conditions are enforced by attaching virtual copies of the boundary sites to the population arrays. The spatial derivatives are then evaluated according to the central finite difference method, and the time evolution of the system is predicted. If the integrated model requires it[1], a further check on the positivity of the populations is performed at each cycle: in case a population becomes negative at some point in space, the negative value is set to zero to prevent from potential numerical problems that could arise if a population accidentally becomes negative at some point in space.

Indicating with $u(x,t)$ the population field[2], the integration has been tested by starting from the following initial conditions:

a) homogeneous equilibrium solution $u(x, t = 0) = u^*$; in this case the system is expected to remain in the initial state.

b) generic homogeneous state $u(x, t = 0) = \bar{u}$, different from the equilibrium solution u^*; in this case the system is expected to uniformly reach the homogeneous equilibrium configuration u^*.

c) random fluctuations around the equilibrium solution: $u(x, t = 0) = u^* + \eta(x)$ with $\eta(x)$ Gaussian noise and $\eta(x) \ll u^* \, \forall \, x$; in this situation the system is expected to evolve towards a regular pattern configuration if $Re[\lambda(k_n^*)] > 0$ or to go back to the equilibrium solution if $Re[\lambda(k_n^*)] < 0$.

d) spatially periodic oscillations around the equilibrium solution: $u(x, t = 0) = u^* + A\, cos(kx)$ with A small compared to u^*; in this situation the system is expected to evolve towards a regular pattern configuration if $Re[\lambda(k_n^*)] > 0$ and $k = k_n^*$, while it should return to the equilibrium solution if $Re[\lambda(k_n^*)] < 0$ or $k \neq k_n^*$.

e) a superposition of cosine oscillations around the equilibrium value: $u(x, t = 0) = u^* + A \sum_k cos(kx)$ with A small compared to u^*; in this situation the system is expected to select the unstable modes, if they are present, and to evolve towards the homogeneous equilibrium solution otherwise.

[1] This step was always included in the integration of the spatial extension of the MacArthur's model, which requires positive populations, but not in the integration of the Swift-Hohenberg's, which allows negative values of the field.

[2] For brevity of description, I have considered a single population field, but in the case of the MacArthur's model all above the considerations must be trivially extended to include the resource population field as well.

4.2 Swift-Hohenberg equation

The integration of the Swift-Hohenberg equation is performed by testing several combinations of the model parameters, spatial parameters and integration parameters, and starting from all the previously mentioned initial conditions. All the results are consistent with the theoretical expectations, and the system behavior is very robust with respect to the variation in the integration and spatial discretization parameters.

To present the results, we fix the spatial parameters $dx = 1$ and $N_x = 250$, the integration timestep $dt = 0.1$, as well as the parameter $k_c = 0.2$ of the SH model, which coincides with the wavenumber at which the growth rate[3] of the spatially-dependent perturbation is maximum. We underline that k_c falls well inside the visibility interval determined by the numerical implementation:

$$k_{min} \sim 0.01 < k_c < k_{max} \sim 1.57 \qquad (\text{indeed } dx = 1 < 2\pi/k_c < L)$$

We report below three cases, relative to three different instability scenarios obtained by varying the control parameter r of the model (see (2.4)). The selected initial condition consists of random deviations around the homogeneous state, which represents the most general spatially heterogeneous initial condition, since it essentially contains all the possible perturbation modes.

Case 1: $r < r_c$, no unstable modes

In this case, being the eigenvalue $\lambda(k) < 0 \, \forall \, k$, the system rapidly recovers from the perturbation by settling down to the homogeneous equilibrium state.

Case 2: $r > r_c$, one unstable mode

In this scenario, the eigenvalue is positive in a very small interval, and only one discrete allowed mode, $k^*_{n=8} \approx 0.201 \equiv k^*$, falls into the instability band. Such wavenumber is very close to the one corresponding to the maximum of $\lambda(k)$, $\max(\lambda) = 5e-05$. The expected timescale of the instability amounts to $\tau \sim 1/\lambda(k^*) \sim 2e4$, therefore the system is integrated up to a final time of $T = 5e5$, which is well beyond τ.

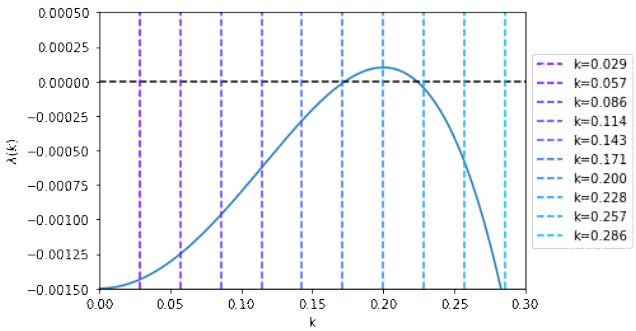

FIG. 4.1. Plot of the eigenvalue λ derived in the linear analysis of the SH model as a function of the perturbation wavenumber k. The vertical lines correspond to the discrete wavenumbers allowed into the finite domain of length $L = 250$. The only unstable mode is the one with wavenumber $k^* = 0.201$.

By examining the spatial distributions collected along the temporal evolution of the system for a total of 100 sample points, it can be deduced that the system reaches a stationary state around $t \sim 1e5$: after a short transient in which the random fluctuations are reshaped into an ordered sinusoidal pattern, the amplitude of the distribution starts to grow, until it eventually reaches a steady state which remains unchanged for all the rest of the integration time (Fig. 4.2).

[3] It is the $\lambda(k)$ derived in the linear stability analysis of the model, in Section 2.3.2.

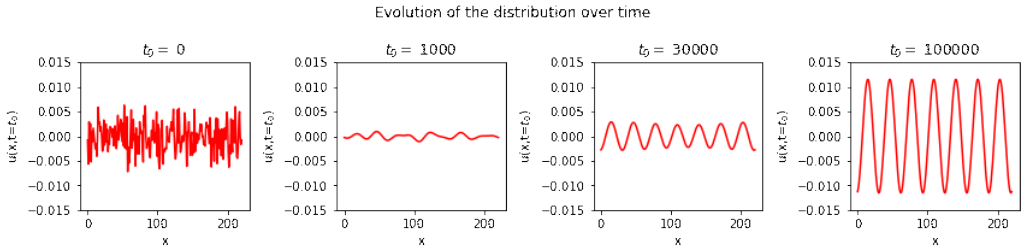

FIG. 4.2. Plot outlining the process of pattern formation in the SH model.

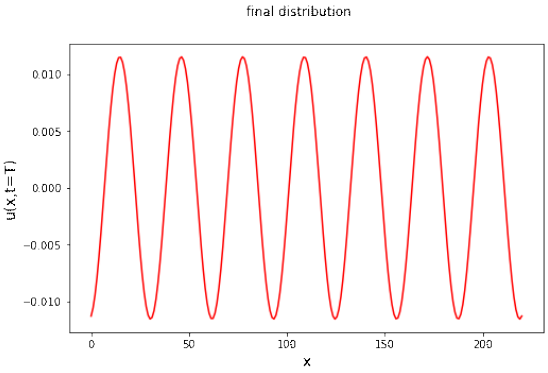

FIG. 4.3. Plot displaying the final, stationary distribution of the field $u(x,t)$: it clearly consists of a spatially periodic pattern with definite wavelength. The picture is taken at the integration time $t = 1e5$.

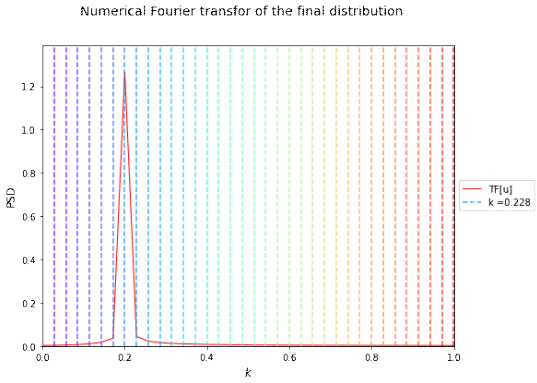

FIG. 4.4. Numerical Fourier transform of the final distribution. Only one peak appears, that coincides with the unstable wavenumber $k^* = 0.201$. The vertical colored lines represent the discrete set of allowed wavenumbers.

Case 3: $r > r_c$, multiple unstable modes

In this case the control parameter value is $r = 0.001$ and there exists a finite set of unstable modes falling into the instability interval:

$$k^*_{n_i} \text{ for } n_i \in \{4, 5, 6, 7, 8, 9, 10\}$$

The one closest to the maximum is obviously again $k^*_{n=8} \approx 0.201 \equiv k^*$.
The timescale is set by $\lambda(k^*) \sim 1e-3 \rightarrow \tau \sim 1e3$ and the system is integrated up to times $T \sim 1e5$.

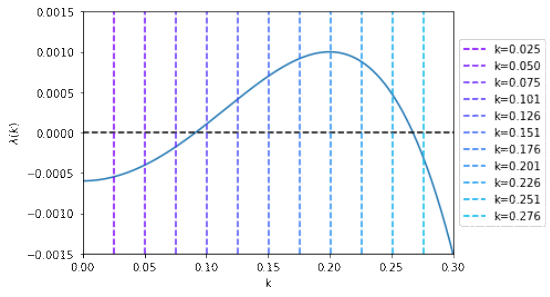

FIG. 4.5. Plot of the eigenvalue λ derived in the linear analysis of the SH model as a function of the perturbation wavenumber k. The vertical lines correspond to the discrete wavenumbers allowed into the finite domain of length $L = 250$. There exist seven discrete modes falling in the instability interval.

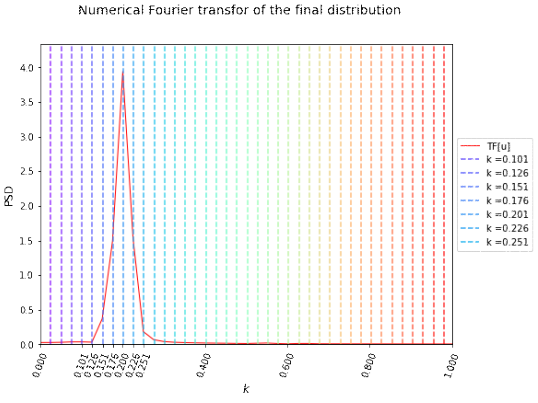

FIG. 4.6. Numerical Fourier transform of the final distribution. There appears a broad peak, with maximum at $k^* = 0.201$ and essentially containing all the unstable modes visible in Fig. 4.5 with the only slight modifications at the boundary wavenumbers.

The stationary state is attained around $t \sim 1.5e4$.

The final distribution is a regular pattern which does not differ by eye from Fig. 4.3, a part from its reasonably larger amplitude. A comparison of the PSD spectra Fig. 4.4 and Fig. 4.6 actually shows that the pattern obtained in this case is not truly monochromatic, since it essentially contains all the unstable components visible in Fig. 4.5, However, the less unstable modes are suppressed with respect to the dominating mode $k^* = 0.201$, consistently with the theoretical expectations.

4.3 Spatial MacArthur's model

The integration of the spatially extended MacArthur's model (Section 3.5) proves to be a more complicated task. Indeed, the numerical evolution does not yield in this case the desired results, since the increase in the unstable mode pattern's amplitude, which is expected in the linear regime, never actually ceases, and the growing abundances eventually produce a numerical overflow.

This behavior seems to be very robust, being completely unaffected by the modifications that will be listed in the following, and occurring despite setting the spatial parameters, the integration parameters and the model's parameters in such a way that all the approximations assumed in the theoretical analysis are safely met. In particular, a very large spatial domain is adopted, and an extremely low value for the $\max(Re[\lambda_+])$ (3.34) is imposed, with the disadvantage of the integration time becoming very long and the task very computationally demanding, but with the aim of setting the system very close to the bifurcation point, where it is expected to be less unstable.

To test the system, the parameters of the model are set according to the conditions obtained in Section 3.5: since the diffusion of the resources and the term related to pathogens are not necessary for pattern initiation, the parameters $\bar{D}$ and ϵ are initially set to zero for simplicity. Indeed, in such case we have a clearer analytical picture on the allowed values for the other parameters[4]. In the chosen configuration, the homogeneous equilibrium state is:

$$n_{eq} = 5.00, \quad c_{eq} = 0.17$$

The system domain length is $L = dx \cdot N_x \sim 3142$. The diffusion coefficients D_0, D_1 and β are set in such a way that a single wavenumber mode falls into the region where $Re[\lambda_+(k)] > 0$:

$$k^*_{n=127} \approx 0.254 \equiv k^*$$

that is very close to the value at which $Re[\lambda_+(k^*)]$ reaches its maximum value, which amounts to

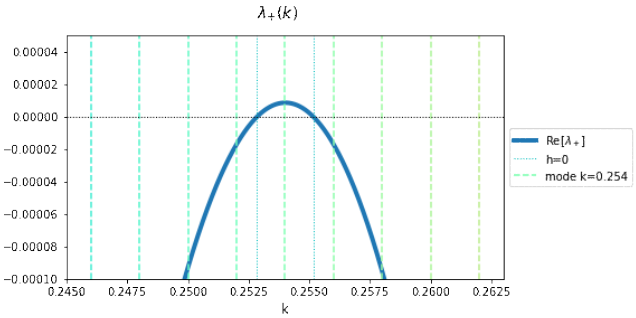

FIG. 4.7. Plot of the real part of the eigenvalue λ_+ (derived in the linear analysis of the spatially extended MacArthur's model, Section 3.5) as a function of the perturbation wavenumber k. The vertical lines correspond to the discrete wavenumbers allowed into the finite domain of length L. The only unstable mode is the one with wavenumber $k^* = 0.254$. The eigenvalue λ_- has negative real part $\forall\, k$ with the chosen set of parameters.

[4]The precise values set for the parameters of the model in the above considered case are: $\alpha = 0.6$, $\epsilon = 0$, $d = 0.1$, $s = 0.5$, $\beta = 24.023$, $\bar{D} = 0$, $D_0 = 0.4$, $D_1 = 0.7$ ($\Rightarrow D \approx -3$).

$Re[\lambda_+(k^*)] \sim 9e-6$, yielding a typical time of $\tau \sim 1e5$. Lastly, we underline that the numerical implementation allows to observe patterns with wavenumbers included in the range:

$$k_{min} = 0.001 < k < 1.500 = k_{max}$$

therefore the unstable mode is expected to be well visible.
The integration timestep is set to $dt = 1e-3$, and the system is integrated up to times $T = 5e5 > \tau$. The integration always yields the theoretically wanted results in the cases in which the system is expected to return to the homogeneous equilibrium state. However, it does not display the desired behavior when starting in a configuration which should lead to pattern formation.
Indeed, despite providing the emergence of a spatially periodic pattern consisting in an oscillation with wavenumber remarkably coincident with the one predicted by the theory, the amplitude of the sinusoidal pattern in the species and resource abundances never ceases to grow, and the system has a tendency to produce a divergence which leads to a numerical overflow.
Several tests have been carried out to clarify this behavior, and the simplest initial condition **d)** (i.e. oscillations with wavenumber k^* around the homogeneous equilibrium values) has been usually adopted for a better readability. Therefore, we report here the results relative to the evolution of the model by starting from such an initial state. By setting the previously specified parameters, the system is observed to diverge between $t \sim 3.5e5$ and $t \sim 3.6e5$.
The plot relative to the distribution of abundances attained at $t \sim 3.5e5$, before overflow occurs, is reported in Fig. 4.8.

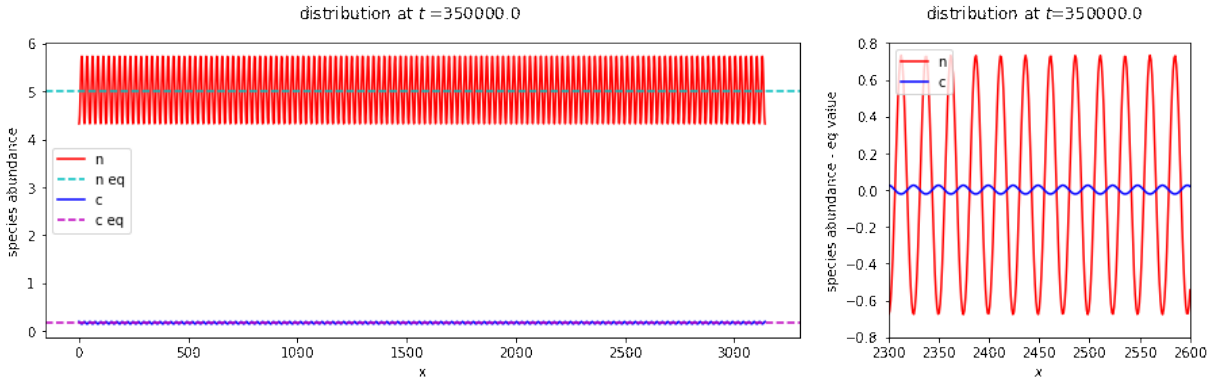

FIG. 4.8. Left: plot of the distributions of consumer and resource abundances around their uniform equilibrium values, at integration time $t = 3.5e5$. Divergence occurs soon after, at times $t > \tau = 1/Re[\lambda_+(k^*)]$. **Right:** detail between $x = 2300$ and $x = 2600$, where the equilibrium values around which the abundances oscillate have been rescaled to zero, for better visualization.

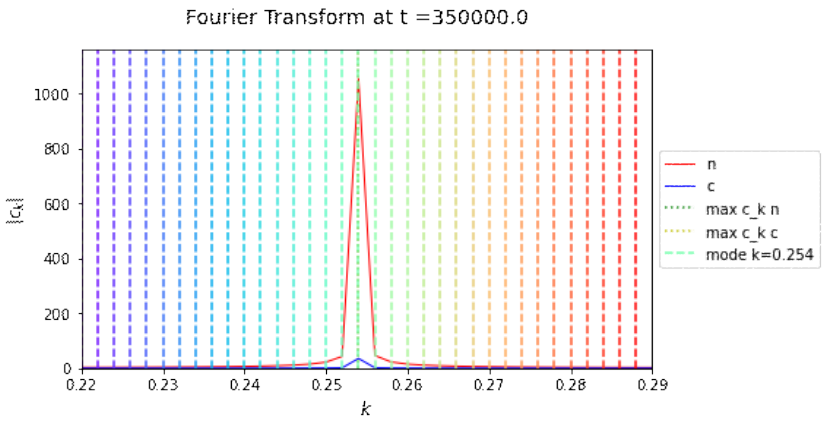

FIG. 4.9. PSD of the spatial oscillations of abundances around their uniform equilibrium values, at integration time $t = 3.5e5$. The unstable modes are again highlighted by the colored vertical lines.

The PSD extracted from such distribution clearly shows that the mode with $k = k^*$ is conserved in the evolution of the system, and no other mode relevantly appears, a part from very low tails around the dominant mode's peak.

The system's amplitude grows in a spatially-homogeneous way as the integration progresses. When starting in a random initial condition **c)**, instead, the amplitude initially assumes an uneven smooth profile, which varies a little depending on the random initial state, and is progressively evened out while the system evolves in time, as visible from Fig. 4.10. The PSD of the obtained distribution, for large enough t, essentially contains only the leading mode k^*, similarly to that obtained by starting in the initial condition **d)**. Likewise, the system diverges at integration times $t \gtrsim \tau$.

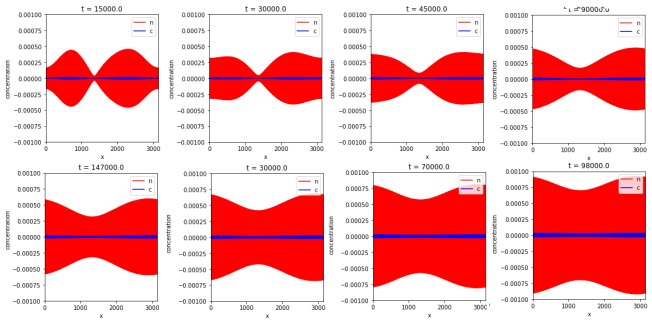

FIG. 4.10. Evolution of the amplitude of the emerging pattern starting from an initial condition consisting of random Gaussian fluctuations around the homogeneous equilibrium values. The amplitude tends to flatten out and grow in magnitude as the integration progresses, until it eventually leads to a numerical overflow at times $t > \tau = 1/Re[\lambda_+(k^*)]$.

4.3.1 Tests and trials

To solve the above presented issue, relative to the numerical divergence occurring at t slightly larger than the typical time τ, many strategies have been attempted. The main approaches are briefly outlined below.

Changing the set of the model parameters

- More parameters of the model are switched on. In particular, the diffusion of the resources is introduced by setting $\bar{D} > 0$, hoping to smooth out the distribution. The same attempt is tried with the parameter related to pathogens ϵ. However, in none of the cases the behavior of the system seems to change at all.
- The set of parameters is also varied in order to modify the position of the maximum of $Re[\lambda_+]$, i.e. the value of k_c and consequently of k^*, but this attempt does not lead to any solution.
- Another hypothesis that is explored is that such behavior has to do with the equilibrium value c_{eq} being too close to zero with respect to n_{eq}, and that the pattern might be affected by the constraint on the positivity of population abundances. However, even with equilibrium values such as $(n_{eq}, c_{eq}) = (1.11, 0.75)$, the divergences do not disappear.
- The spatial domain length is modified, but this does not affect the behavior of the system (a part from obviously introducing a higher number of unstable modes, with fixed model parameters).

Changing the integration scheme and parameters

- The integration timestep is diminished; however, the time at which overflow occurs is not affected by such modification at all, as long as dt remains smaller than $1e-3$.
- Other explicit integration schemes are implemented, such as the midpoint scheme and the 4-th order Runge-Kutta method but, again, this does not influence the performance at all, and the

time at which overflow occurs remains unchanged.

- Some implicit integration schemes are shortly tested, by exploiting two pre-defined integration schemes: the implicit solver implemented in `py-pde` [26] and the BDF method of the `solve_ivp` function of `scipy.integrate` [27]. The latter is especially used for the solution of stiff systems of differential equations. Even adopting these integration schemes, however, seems to leave the problem unaffected, even though more accurate and rigorous attempts should be made before totally excluding the possibility of solving the issue by applying the appropriate implicit integration scheme.

Further checks

- A test is performed on the numerical integration of the linearised differential equations: indeed, although the behavior of the system in the nonlinear regime is less certain, the linearised system must necessarily follow the analytical predictions. The linearised system's equations (3.33) are numerically integrated using the same scheme applied to the full nonlinear system, and the numerical outcomes are compared to the ones predicted by the theoretical linear analysis.
  In particular, a projection of the amplitudes of the resource and consumer fields on the $\vec{v_+}$ and $\vec{v_-}$ eigenvectors relative to the eigenvalues λ_+, λ_- is exploited.
  In general, indeed, a state of the linearised system can be decomposed into the basis of the eigenvectors as follows:

$$\begin{pmatrix} n(x,t) \\ c(x,t) \end{pmatrix} = \begin{pmatrix} n_{eq} \\ c_{eq} \end{pmatrix} + \begin{pmatrix} A_n(t) \\ A_c(t) \end{pmatrix} \cos(k^* x) \quad \text{with} \quad \begin{pmatrix} A_n(t) \\ A_c(t) \end{pmatrix} = A_+(t)\,\vec{v}_+ + A_-(t)\,\vec{v}_- \tag{4.1}$$

  and analytically:

$$A_+(t) = A_{+,0}\,\exp(Re[\lambda_+(k^*)]\,t)$$
$$A_-(t) = A_{-,0}\,\exp(Re[\lambda_-(k^*)]\,t)$$

  The linearised system is then numerically evolved by starting in one of the following two initial conditions:

$$\begin{pmatrix} n_0(x) \\ c_0(x) \end{pmatrix}_{\pm} = \begin{pmatrix} n_{eq} \\ c_{eq} \end{pmatrix} + \vec{\delta}_\pm(x) \quad \text{with:} \quad \vec{\delta}_\pm(x) \propto \vec{v}_\pm \cos(k^* x)$$

  and the numerical evolution of the projections A_+, A_-, A_n, A_c is compared with the theoretical one. When the real part of both eigenvalues λ_+, λ_- is negative, the amplitudes vanish for $t \to \infty$ by starting in any of the above initial conditions. On the contrary, if $Re[\lambda_-(k)] < 0 < Re[\lambda_+(k)]$ for some k, the amplitudes vanish when starting from the initial condition $(n_0,\, c_0)_-$ and diverge when starting from the initial condition $(n_0,\, c_0)_+$. The timescales and amplitude values are in good agreement with the theoretical expectations, even though the effects of the finite numerical precision can be noticed when the order of magnitude of the amplitudes becomes particularly small: this happens when starting from the initial condition in the direction of $\vec{v}_-$ (Fig. 4.11,

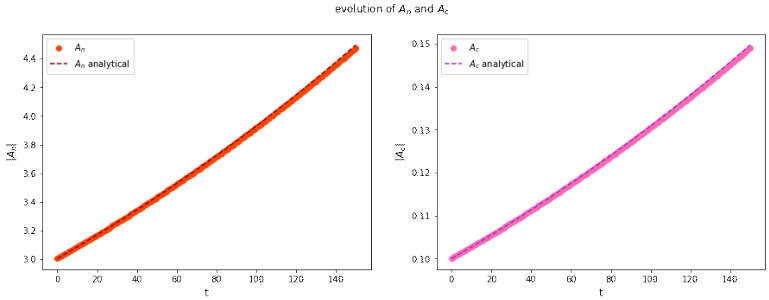

FIG. 4.11. Evolution of the amplitudes A_n and A_c starting from an initial condition in the direction of $\vec{v}_+$, in the case in which $Re[\lambda_+(k)]$ is positive in a limited interval of k.

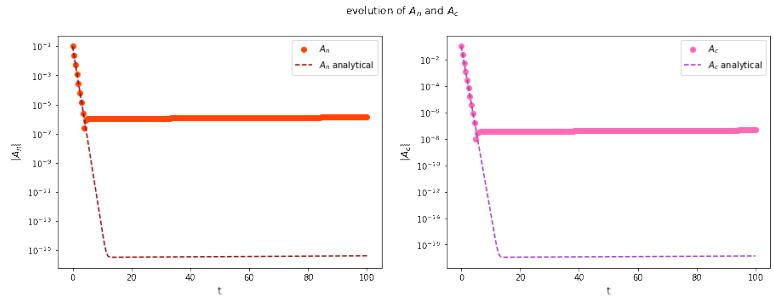

FIG. 4.12. Evolution of the amplitudes A_n and A_c starting from an initial condition in the direction of $\vec{v}_-$, in the case in which $Re[\lambda_+(k)]$ is positive in a limited interval of k.

Fig. 4.12). Overall, however, this test proves that the numerical solution of the linearised system behaves as expected, and no striking criticalities are detected.

- Further checks are performed in order to exclude that the behavior of the system might be related to more subtle problems, such as issues arising from discretization. Indeed, one can analytically derive the expressions for the eigenvectors by starting from a discretized spatial domain and by substituting the finite difference expressions for the spatial derivatives used in the numerical integration into the model equations. The expressions obtained for the eigenvalues[5] are functions of the cosines of k and $2k$, rather than being functions of k^2 as in the continuous case (3.34): this could produce sensible differences in the form of the eigenvalues and in the resulting qualitative behavior of the system. As visible from the plot below, however, this is not the case, as the discrete eigenvalues reproduce closely the continuous ones. Only one difference can be spotted, consisting in the fact that the smallest discrete wavenumber falling into the instability band is actually not unstable in the corresponding discrete case. This observation is not relevant to our purposes, since it does not change the overall behavior of the system. It may be however useful to explain a peculiarity of some of the PSD spectra obtained from the analysis of the emerging patterns in the case of few multiple unstable modes: it was noticed that the smallest unstable wavenumber $k^*_{n_1}$ is sometimes suppressed, while a further mode with wavenumber $k^*_{n_{M+1}}$ often appears to the right of the highest allowed wavenumber k_{n_M}. This could be explained by observing that the discretization produces a slight shift in the eigenvector towards higher wavenumber values, that could contribute to the observed effect. It is not, however, the only reason, since the nonlinear terms do also produce a modification in the observed pattern's modes.

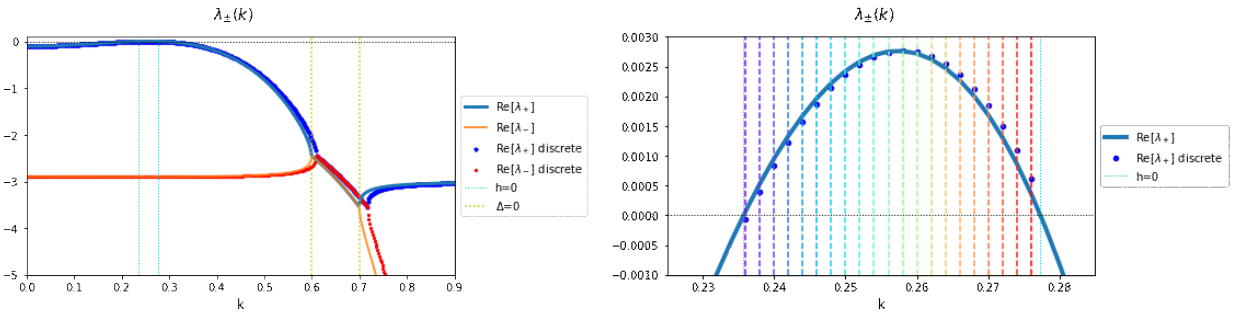

FIG. 4.13. Plot showing the comparison between the discrete eigenvalues, obtained by imposing the spatial discretization of the system into the linear analysis, and the continuous eigenvalues obtained by performing the usual continuous analysis. **Left:** the real parts of λ_+ and λ_- are reported both in their continuous and in their discrete versions. **Right:** zoom on the area of interest, where $Re[\lambda_+(k)]$ is positive in some interval of k, yielding instability. The vertical colored lines represent the discrete modes falling into the unstable wavenumbers band.

[5]The explicit expressions and their derivation are reported in Appendix C.

Modifying the model

- An exponentially decreasing supply rate is introduced:

  $$s(t) = s_0\, e^{-t\, r}$$

  and tested by varying the decay rate parameter r. However, this attempt is not successful because the system rapidly enters the parameter region in which it becomes stable to spatially-dependent perturbations and no pattern is produced, unless the temporal decay of the supply rate is so slow that no difference can be detected with respect to the case in which s is constant. Similarly, a Monod function (1.2) is substituted to the linear growth rate $\alpha\, c$, with no substantial results.

- By observing the structure of the reaction dynamics of equations (3.31), one immediately realises that this behavior is counterintuitive: indeed, if the species population becomes very large, it will lead to a decay of the resource abundance, which should lead to a decrease in the species population in turn. However, by examining the diffusion-like terms, it can be noticed that the negative diffusion coefficient required by the instability conditions (3.37) tends to produce a concentration of the densities, and could therefore responsible contribute to the formation of divergences. Therefore, I checked the behavior of the terms resulting from $\partial_x[(D_0 - D_1 n)\partial_x n]$ as a function of the integration time t, in order to understand if there is any term in particular producing the divergences. To do so, I imposed an initial condition of the kind:

  $$\begin{aligned} n(x, t=0) &= n_{eq} + A\, cos(k^* x) \\ c(x, t=0) &= c_{eq} + B\, cos(k^*\, x) \end{aligned} \qquad \text{with} \quad k^* = 0.254,\ A \sim 8e-3,\ B \sim 2e-4$$

  and saved the mean values of the terms $D_0\partial_x^2 n$, $-D_1 n\partial_x^2 n$, $-D_1(\partial_x n)^2$, at an x value multiple of $2\pi/k^*$, where the cosine distribution of the emerging pattern is maximum.

  As visible from Fig. 4.14, the terms $D_0\partial_x^2 n$ and $\beta\partial_x^4 n$ seem to have a stabilising effect, as expected. Conversely, the overflow occurring around $t \sim 35000$ seems to be led by the term $-D_1 n\partial_x^2 n$, plotted in orange.

  To solve this issue, one could think of modifying the diffusion term $\partial_x[(D_0 - D_1 n)\partial_x n]$ in Eq. (3.30) in such a way that it does not grow indefinitely with n. The simplest way to do so is to replace the $D_1 n$ with a sort of Monod function:

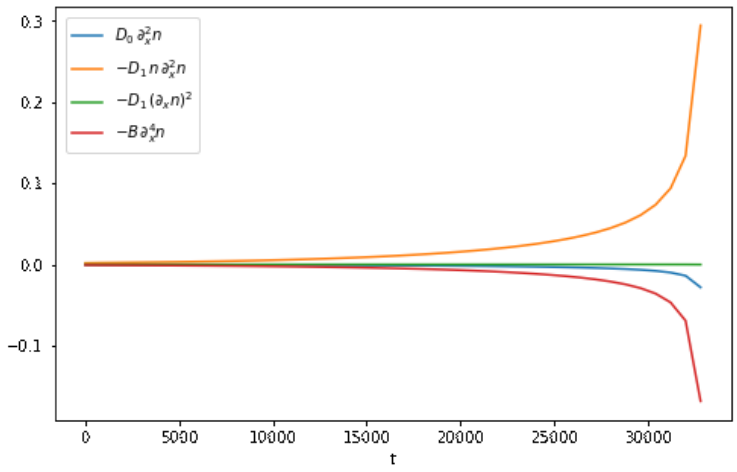

FIG. 4.14. Temporal evolution of the spatial mean value of the terms $D_0\partial_x^2 n$, $-D_1 n\partial_x^2 n$, $-D_1(\partial_x n)^2$, $-\beta\,\partial_x^4 n$ computed at x multiple of $2\pi/k^*$, where the cosine distribution of the emerging pattern is maximum.

$$\partial_x \left[(D_0 - D_1 n)\, \partial_x n \right] \quad \rightarrow \quad \partial_x \left[\left(D_0 - D_1 \frac{n}{1+\frac{n}{n_0}} \right) \partial_x n \right]$$

which is bounded by the saturation value $n_0 > 0$. Indeed, for $n \ll n_0$ the term $\frac{n}{1+\frac{n}{n_0}}$ grows like $\sim n$, but for $n \gg n_0$ it tends to the saturation value $\frac{n}{1+\frac{n}{n_0}} \sim n_0$.
Let us analyse this modified term in the linear approximation, by applying as usual a small perturbation δn around the equilibrium value n^*:

$$\begin{aligned}
\partial_x \left[\left(D_0 - D_1 \frac{n}{1+\frac{n}{n_0}} \right) \partial_x n \right] &= D_0\, \partial_x^2 n - D_1 \frac{n}{1+\frac{n}{n_0}}\, \partial_x^2 n - D_1 \frac{1}{\left(1+\frac{n}{n_0}\right)^2} (\partial_x n)^2 = \\
&= D_0\, \partial_x^2 \delta n - D_1 \frac{n^* + \delta n}{1+\frac{n^*+\delta n}{n_0}}\, \partial_x^2 \delta n - D_1 \frac{1}{\left(1+\frac{n^*+\delta n}{n_0}\right)^2} (\partial_x \delta n)^2 = \\
&\approx D_0\, \partial_x^2 \delta n - D_1 \frac{n^*}{1+\frac{n^*+\delta n}{n_0}}\, \partial_x^2 \delta n \approx \\
&\approx D_0\, \partial_x^2 \delta n - D_1 \frac{n^*}{\frac{n_0+n^*}{n_0}} \left(1 - \frac{\delta n}{\frac{1}{n_0}+n^*} + O(\delta n^2) \right) \partial_x^2 \delta n \approx \\
&\approx \left(D_0 - D_1 \frac{n^*}{1+\frac{n^*}{n_0}} \right) \partial_x^2 \delta n
\end{aligned}$$

Therefore, the results of the linear stability analysis remain the same, except exchanging:

$$D = D_0 - D_1 n^* \quad \rightarrow \quad D' = D_0 - D_1 \frac{n^*}{1+\frac{n^*}{n_0}} > D \;\forall\, n_0 \qquad \left(\text{i.e. } |D'| < |D|\right)$$

Thus the linear effect of this term is to make the diffusion coefficient less negative, i.e. the system less unstable. The smaller n_0 is, the less unstable the system will be. For this reason, we will consider very large values for n_0, in such a way that the linear behavior of the system remains almost unaffected, but this modification will hopefully cure the nonlinear saturation of the unstable modes.
Without changing the values of the system parameters, one finds that for $n_0 \lesssim 5e5$ the real part of λ_+ is always negative; therefore, the integration is tested by setting the new parameter n_0 to values of $\sim 1e6$ and larger, for instance $\sim 1e9$, $1e12$.
The numerical solution diverges nonetheless, at integration times $t \gtrsim 1/\max(Re[\lambda_+(k)])$.

In coclusion, none of these attempts managed to solve the problem, the behavior of the system seeming very robust with respect to the above proposed modifications.

4.3.2 Multiple unstable modes

For the sake of completeness, I report in the following an exemplary numerical result relative to a case in which the system displays multiple unstable modes. An analogue behavior is observed.

The system parameters are left unchanged with respect to the previous case, with the only exception of β, which is lowered to $\beta = 23.83$. A a result, 12 unstable modes appear:

$$\{k^*_{n_i}\}_{i=1,..12} \quad \text{with} \quad n_i = 122, ... 133$$

The dominant mode is again $k^*_{n=127} \approx 0.254$.

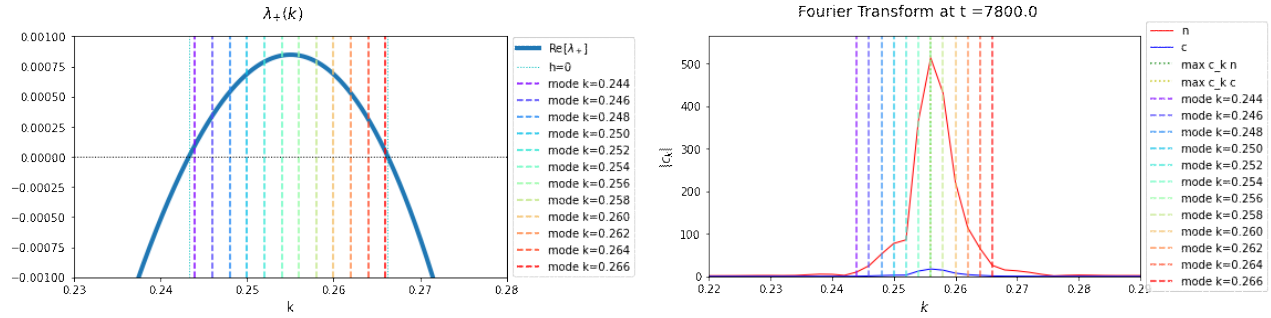

FIG. 4.15. Left: Plot of the eigenvalue $\lambda_+(k)$. Multiple modes fall into the instability region, and are highlighted by the colored vertical lines. **Right:** PSD of the spatial oscillations of abundances around their uniform equilibrium values, at integration time $t = 7800$. Divergence occurs soon after, at a time $t > \tau = 1/Re[\lambda_+(k^*)] \sim 1e3$. The unstable modes are again highlighted by the colored vertical lines.

The maximum value of $\lambda_+(k)$ increases to $\sim 1e-3$, yielding a typical time of $\tau \sim 1e3$. The system is evolved up to an integration time of $T = 1e4$: the behavior of the amplitude of the pattern is plotted Fig. 4.16. Divergence occurs between $t \sim 7.8e-3$ and $8e-3$, and the last distribution obtained before the overflow is reported in Fig. 4.17.

By examining the PSD spectra obtained at various integration times, a correspondence with the set of unstable modes is observed, with a small tail appearing at higher wavenumber values as the integration progresses (Fig. 4.15). This is most likely due to the influence of the nonlinear terms in the dynamical equation (3.31). The PSD is visibly peaked at the dominant mode $k^* = 0.254$.

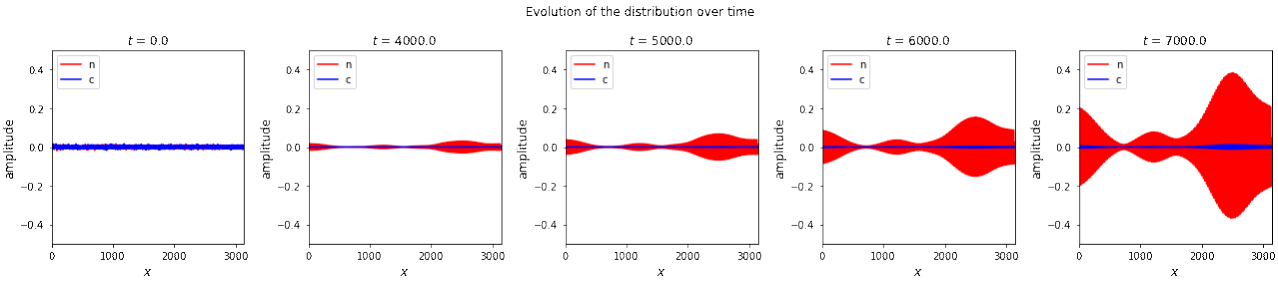

FIG. 4.16. Evolution of the amplitude of the emerging pattern at different integration times.

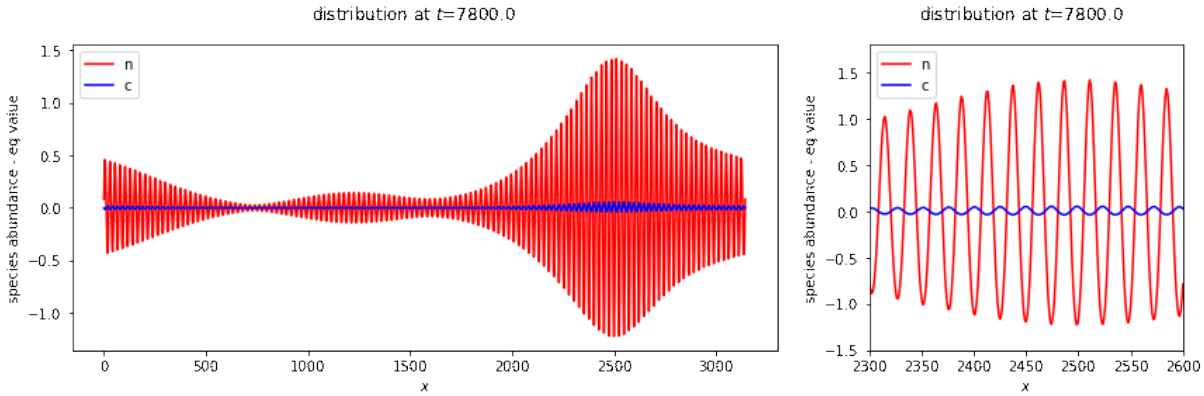

FIG. 4.17. Left: plot of the spatial oscillations of consumer and resource abundances around their uniform equilibrium values (which are rescaled to zero for better visualization), at integration time $t = 7800$. Divergence occurs soon after, at a time $t > \tau = 1/Re[\lambda_+(k^*)] \sim 1e3$. **Right:** detail between $x = 2300$ and $x = 2600$.

Conclusions and future prospects

This work has shown that the one-dimensional spatial extension of the MacArthur's consumer-resource model, discussed in Section 3.5 in the case of one species and one resource, successfully provides a mechanism for pattern initiation: indeed, the analysed model exhibits a linear instability of type I_s or I_o for specific sets of parameter values (see Fig. 3.11, Fig. 3.13, Fig. 3.14).
In particular, the minimally required spatial extension of the model consists in the addition of a density-dependent diffusion term to the consumer's equation, accounting for an overcrowding dispersal behavior of the species, as well as a stabilising squared laplacian term in the consumer's population. Specifically, the overcrowding term is needed to provide a negative sign to the effective diffusion term, which has proven to be necessary for spatial instability to be allowed, while the squared laplacian term ensures that such instability occurs in a limited interval of wavenumbers.
Proper conditions have been derived in terms of the the model's parameters (Tab. 3.1), yielding instability under spatially-heterogeneous perturbations: the expected lengthscale of the emerging pattern can be, therefore, easily predicted.

However, despite accounting for the emergence of a pattern with wavelength corresponding precisely to the one indicated by the theory, the numerical integration of the model does not produce a steady state final configuration in the abundances of consumer and resource populations. Indeed, the growth of the amplitude of the unstable spatial perturbation's mode, which is expected to take place in the linear regime, never actually ceases after the system enters the nonlinear regime, and leads to a divergence in the population abundances.
After attempting several methods to cure this issue, we must conclude that the numerical integration of the spatially extended MacArthur's model, exploiting an explicit finite-difference Euler scheme, cannot lead to the formation of a stationary spatially heterogeneous state, in the case of one species and one resource and in a one-dimensional spatial domain.

Being the dynamics MacArthur's equations intrinsically self-balancing for what concerns the abundances of consumer and resource, however, a solution to this issue is likely to exist. The observed undesired behavior might indeed be due to an extremely high requirement on the numerical precision, or to some effect related to the destabilizing influence of the negative density-dependent diffusion coefficient. Further in-depth studies could be performed to explore these possibilities, both theoretically and computationally.
Moreover, this same analysis could be generalized by extending it to more complex systems, containing multiple species and resource populations, as well as to higher spatial dimensions, which might influence the outcome of instability.

Lastly, an alternative perspective was also proposed, by exploring the possibility of obtaining a linear spatial instability by means of a non-local version of MacArthur's model (Section 3.6). This approach has proved to support the possibility of pattern initiation if an appropriate kernel function is chosen, by constraining the properties of its Fourier transform. More research in this direction is desirable, as it may open the way for the development of a further consumer-resource based pattern formation mechanism.

In conclusion, this thesis shows that additional work is needed on the spatial extension of this model to account for the spontaneous formation of stable spatially periodic patterns, and that such system seems nonetheless worth further study.

Appendix A

MacArthur 3s 1r

Merely to gain more confidence into the generalisation of the results obtained in Section 3.3, I report here the linear analysis of the MacArthur extended model for three species and one resource. We will see that the pathological nature of the instability cannot reasonably solved by adding populations to the systems, but it needs to be dealt with in a different manner.

Consider the following equations:

$$\begin{cases} \dot{n_1} = (\alpha_1 \mu(c) - d_1)\, n_1 + \partial_x J_1 \\ \dot{n_2} = (\alpha_2 \mu(c) - d_2)\, n_2 + \partial_x J_2 \\ \dot{n_3} = (\alpha_3 \mu(c) - d_3)\, n_3 + \partial_x J_3 \\ \dot{c} = s - (\alpha_1\, n_1 + \alpha_2\, n_2 + \alpha_3\, n_3)\mu(c) \end{cases} \quad \text{with} \quad \partial_x J_\sigma = \partial_x \left[(\, D_\sigma - \sum_\rho D_{\sigma\rho} n_\rho \,)\, \partial_x n_\sigma \right] \text{ for } \sigma = 1, 2, 3$$

with α_1, α_2, $\alpha_3, 1, d_1$, d_2, $d_3 > 0$ population parameters, $\mu(c) > 0$ growth function with $\frac{d\mu}{dc} > 0 \, \forall c$, and D_σ, $D_{\sigma\rho} > 0$ diffusion coefficients.

Uniform equilibrium

The uniform equilibria of the system are:

$$\begin{cases} \mu(c^*) = d_1/\alpha_1, \\ n_1^* = s/d_1, \\ n_2^* = 0 \\ n_3^* = 0 \end{cases} \vee \begin{cases} \mu(c^*) = d_2/\alpha_2, \\ n_2^* = s/d_2, \\ n_1^* = 0 \\ n_3^* = 0 \end{cases} \vee \begin{cases} \mu(c^*) = d_3/\alpha_3, \\ n_3^* = s/d_3, \\ n_1^* = 0 \\ n_2^* = 0 \end{cases}$$

Stability under uniform perturbation

Let us choose the first equilibrium:

$$\begin{pmatrix} n_1^* \\ n_2^* \\ n_3^* \\ c^* \end{pmatrix} = \begin{pmatrix} s/d_1 \\ 0 \\ 0 \\ \mu^{-1}(d_1/\alpha_1) \end{pmatrix} \tag{A.1}$$

We uniformly perturb the system around this equilibrium:

$$\begin{pmatrix} n_1(t) \\ n_2(t) \\ n_3(t) \\ c(t) \end{pmatrix} = \begin{pmatrix} n_1^* \\ n_2^* \\ n_3^* \\ c^* \end{pmatrix} + \begin{pmatrix} \delta n_1(t) \\ \delta n_2(t) \\ \delta n_3(t) \\ \delta c(t) \end{pmatrix} \quad \text{with} \quad \begin{pmatrix} \delta n_1(t) \\ \delta n_2(t) \\ \delta n_3(t) \\ \delta c(t) \end{pmatrix} = \vec{\delta}\, e^{\lambda t}$$

$$\mathbb{J} = \begin{pmatrix} 0 & 0 & 0 & \frac{\alpha_1 s}{d_1}\frac{d\mu}{dc}\big|_{c^*} \\ 0 & \frac{\alpha_2}{\alpha_1}d_1 - d_2 & 0 & 0 \\ 0 & 0 & \frac{\alpha_3}{\alpha_1}d_1 - d_3 & 0 \\ -d_1 & -\frac{\alpha_2}{\alpha_1}d_1 & -\frac{\alpha_3}{\alpha_1}d_1 & -\frac{\alpha_1 s}{d_1}\frac{d\mu}{dc}\big|_{c^*} \end{pmatrix} = \begin{pmatrix} 0 & 0 & 0 & \mathcal{A} \\ 0 & \frac{\alpha_2}{\alpha_1}d_1 - d_2 & 0 & 0 \\ 0 & 0 & \frac{\alpha_3}{\alpha_1}d_1 - d_3 & 0 \\ -d_1 & -\frac{\alpha_2}{\alpha_1}d_1 & -\frac{\alpha_3}{\alpha_1}d_1 & -\mathcal{A} \end{pmatrix} \quad \text{(A.2)}$$

$$\det\left(\mathbb{J} - \lambda\mathbb{I}\right) = \left(\frac{\alpha_2}{\alpha_1}d_1 - d_2 - \lambda\right)\left(\frac{\alpha_3}{\alpha_1}d_1 - d_3 - \lambda\right)\left(\lambda^2 + \mathcal{A}\lambda + \mathcal{A}d_1\right) = 0$$

$$\Rightarrow \quad \begin{cases} \lambda_2 = \dfrac{\alpha_2}{\alpha_1}d_1 - d_2 \quad \text{stable if} \quad \dfrac{\alpha_2}{\alpha_1}d_1 - d_2 < 0 \\ \lambda_3 = \dfrac{\alpha_3}{\alpha_1}d_1 - d_3 \quad \text{stable if} \quad \dfrac{\alpha_3}{\alpha_1}d_1 - d_3 < 0 \\ \lambda_\pm = \dfrac{-\mathcal{A} \pm \sqrt{\mathcal{A}^2 - 4\mathcal{A}d_1}}{2} \quad \text{always stable} \end{cases}$$

having defined $\mathcal{A} \coloneqq \frac{\alpha_1 s}{d_1}\frac{d\mu}{dc}\big|_{c^*} > 0$.

Non-uniform perturbation

I consider the following perturbation around the equilibrium values $(n_1^*, n_2^*, n_3^*, c^*)$ reported in (A.1).

$$\begin{pmatrix} n_1(x,t) \\ n_2(x,t) \\ n_3(x,t) \\ c(x,t) \end{pmatrix} = \begin{pmatrix} n_1^* \\ n_2^* \\ n_3^* \\ c^* \end{pmatrix} + \begin{pmatrix} \delta n_1(x,t) \\ \delta n_2(x,t) \\ \delta n_3(x,t) \\ \delta c(x,t) \end{pmatrix} \qquad \text{with} \qquad \begin{pmatrix} \delta n_1(x,t) \\ \delta n_2(x,t) \\ \delta n_3(x,t) \\ \delta c(x,t) \end{pmatrix} = \vec{\delta}\, e^{\lambda t + ikx}$$

The corresponding eigenvalue problem reads:

$$\lambda\,\vec{\delta} = (\mathbb{J} - k^2\mathbb{D})\,\vec{\delta} \qquad \text{with} \quad \mathbb{D} = \begin{pmatrix} D_1 - D_{11}\frac{s}{d_1} & 0 & 0 & 0 \\ 0 & D_2 - D_{21}\frac{s}{d_1} & 0 & 0 \\ 0 & 0 & D_3 - D_{31}\frac{s}{d_1} & 0 \\ 0 & 0 & 0 & 0 \end{pmatrix}, \quad \mathbb{J} \text{ defined in (A.2).}$$

$$\det\left(\mathbb{J} - k^2\mathbb{D} - \lambda\mathbb{I}\right) = \left[\frac{\alpha_2}{\alpha_1}d_1 - d_2 - k^2\left(D_2 - D_{21}\frac{s}{d_1}\right) - \lambda\right]\left[\frac{\alpha_3}{\alpha_1}d_1 - d_3 - k^2\left(D_3 - D_{31}\frac{s}{d_1}\right) - \lambda\right] \times \\ \times \left[\lambda^2 + \lambda\left(\mathcal{A} + k^2\mathcal{D}\right) + \mathcal{A}\left(d_1 + k^2\mathcal{D}\right)\right]$$

where I defined $\mathcal{D} \coloneqq D_1 - D_{11}\frac{s}{d_1}$.

$$\det\left(\mathbb{J} - k^2\mathbb{D} - \lambda\mathbb{I}\right) = 0 \quad \Leftrightarrow \quad \begin{cases} \lambda_2 = \dfrac{\alpha_2}{\alpha_1}d_1 - d_2 - k^2\left(D_2 - D_{21}\dfrac{s}{d_1}\right) \\ \lambda_3 = \dfrac{\alpha_3}{\alpha_1}d_1 - d_3 - k^2\left(D_3 - D_{31}\dfrac{s}{d_1}\right) \\ \lambda_\pm = \dfrac{1}{2}\left(-\mathcal{A} - k^2\mathcal{D} \pm \sqrt{\left[-\mathcal{A} - k^2\mathcal{D}\right]^2 - 4\mathcal{A}\left[d_1 + k^2\mathcal{D}\right]}\right) \end{cases}$$

Spatial instability

Again, a correspondence with previous results can be easily noticed:

$\lambda_2 \to$ SM2 with instability conditions (3.7)
$\lambda_3 \to$ SM2
$\lambda_\pm \to$ MA1s1r with instability conditions (3.16)

From these calculations, we can better observe that the real eigenvalue λ_2, λ_3 refer to the species that go extinct in the uniform equilibrium conditions (A.1): in correspondence of such species, the Jacobian matrix (A.2) has diagonal entries, and as a result the form of such eigenvalues reflects the one found for the single-species model described in Section 3.1.1.
The fact that these eigenvalues are unstable for all large enough wavevectors is due to the conditions that must be imposed to guarantee the stability of the uniform equilibrium under spatially-independent perturbations. A modification of their undesired behavior is therefore hardly feasible.
The remaining eigenvalues $\lambda_\pm$, which can take complex values, correspond to the non-extinct species and the resource. Indeed, they have exactly the same form as the eigenvalues of the MacArthur model for one species and one resource studied in Section 3.2. The reason for their positivity for large k values is not really dependent on the choice of parameters, but derives rather from their form as a function of k, as can be seen in (3.17).

Appendix B

Linear stability analysis for the non-local MacArthur's model

I report here the calculations relative to the non-local extension of MacArthur's model in terms of a generic function $\widetilde{\phi}(k)$. As usual, we need to study the sign of $\mathrm{Re}[\lambda_{\pm}]$, and we start by analysing the functions $g(k)$ and $h(k)$ in the simplest cases, by putting to zero some parameters.

Case ϵ=0, $\bar{D}$=0, $D = 0$

$$g(k^2) = n_0\,\widetilde{\phi}(k)$$
$$h(k^2) = s\,\widetilde{\phi}(k)$$

$$Re[\lambda_+] > 0 \quad \Leftrightarrow \quad g(k) < 0 \vee \begin{cases} g(k) > 0 \\ h(k) < 0 \end{cases} \quad \Leftrightarrow \quad \widetilde{\phi}(k) < 0$$

Even in this extremely simple case, if $\widetilde{\phi}$ is negative in a limited interval $[k_1, k_2]$, we expect to find the desired instability behavior.

Case ϵ=0, $D = 0$

$$g(k^2) = \bar{D}\,k^2 + n_0\,\widetilde{\phi}(k)$$
$$h(k^2) = s\,\widetilde{\phi}(k)$$

$$\begin{aligned} Re[\lambda_+] > 0 \qquad &\Leftrightarrow \qquad g(k) < 0 \quad \vee \quad \begin{cases} g(k) > 0 \\ h(k) < 0 \end{cases} \\ &\Leftrightarrow \qquad \widetilde{\phi}(k) < -\frac{\bar{D}}{n_0}k^2 \quad \vee \quad \begin{cases} \widetilde{\phi}(k) > -\frac{\bar{D}}{n_0}k^2 \\ \widetilde{\phi}(k) < 0 \end{cases} \\ &\Leftrightarrow \qquad \widetilde{\phi}(k) < -\frac{\bar{D}}{n_0}k^2 \quad \vee \quad -\frac{\bar{D}}{n_0}k^2 < \widetilde{\phi}(k) < 0 \\ &\Leftrightarrow \qquad \widetilde{\phi}(k) < 0 \end{aligned}$$

Case ϵ=0, $\bar{D} = 0$

$$g(k^2) = D\,k^2 + n_0\,\widetilde{\phi}(k)$$
$$h(k^2) = \widetilde{\phi}(k)\left(n_0\,D\,k^2 + s\right)$$

Sign of g(k)

$$g(k) > 0 \quad \Leftrightarrow \quad \widetilde{\phi}(k) > -\frac{D}{n_0}k^2$$
$$g(k) < 0 \quad \Leftrightarrow \quad \widetilde{\phi}(k) < -\frac{D}{n_0}k^2$$

Sign of h(k)

$$\mathrm{sgn}\big(h(k)\big) = \mathrm{sgn}\big(\widetilde{\phi}(k)\big) \cdot \mathrm{sgn}\big(n_0\,D\,k^2 + s\big)$$

If $D > 0$:

$$\mathrm{sgn}\big(h(k)\big) = \mathrm{sgn}\big(\widetilde{\phi}(k)\big)$$

If $D < 0$:

$$h(k) > 0 \Leftrightarrow \begin{cases} \widetilde{\phi}(k) > 0 \\ k^2 < -\dfrac{sD}{n_0} \end{cases} \vee \begin{cases} \widetilde{\phi}(k) < 0 \\ k^2 > -\dfrac{sD}{n_0} \end{cases}$$
$$h(k) < 0 \Leftrightarrow \begin{cases} \widetilde{\phi}(k) < 0 \\ k^2 < -\dfrac{sD}{n_0} \end{cases} \vee \begin{cases} \widetilde{\phi}(k) > 0 \\ k^2 > -\dfrac{sD}{n_0} \end{cases}$$

Spatial instability

$$Re[\lambda_+] > 0 \quad \Leftrightarrow \quad g < 0 \vee \begin{cases} g > 0 \\ h < 0 \end{cases}$$

If $D > 0$:

$$\begin{aligned} Re[\lambda_+] > 0 \quad &\Leftrightarrow \quad \widetilde{\phi}(k) < -\frac{D}{n_0}k^2 \quad \vee \quad \begin{cases} \widetilde{\phi}(k) > -\dfrac{D}{n_0}k^2 \\ \widetilde{\phi}(k) < 0 \end{cases} \\ &\Leftrightarrow \quad \widetilde{\phi}(k) < -\frac{D}{n_0}k^2 \quad \vee \quad -\frac{D}{n_0}k^2 < \widetilde{\phi}(k) < 0 \\ &\Leftrightarrow \quad \widetilde{\phi}(k) < 0 \end{aligned}$$

If $D < 0$:

$$\begin{aligned} Re[\lambda_+] > 0 \quad &\Leftrightarrow \quad \widetilde{\phi}(k) < -\frac{D}{n_0}k^2 \quad \vee \quad \begin{cases} \widetilde{\phi}(k) > -\dfrac{D}{n_0}k^2 \quad (> 0) \\ \begin{cases} \widetilde{\phi}(k) < 0 \\ k^2 < -\dfrac{sD}{n_0} \end{cases} \vee \begin{cases} \widetilde{\phi}(k) > 0 \\ k^2 > -\dfrac{sD}{n_0} \end{cases} \end{cases} \\ &\Leftrightarrow \quad \widetilde{\phi}(k) < -\frac{D}{n_0}k^2 \quad \vee \quad \begin{cases} \widetilde{\phi}(k) > -\dfrac{D}{n_0}k^2 \\ k > \sqrt{-\dfrac{sD}{n_0}} \end{cases} \end{aligned} \tag{B.1}$$

This corresponds to a $\widetilde{\phi}(k)$ belonging to the area highlighted in green in Fig. B.2.

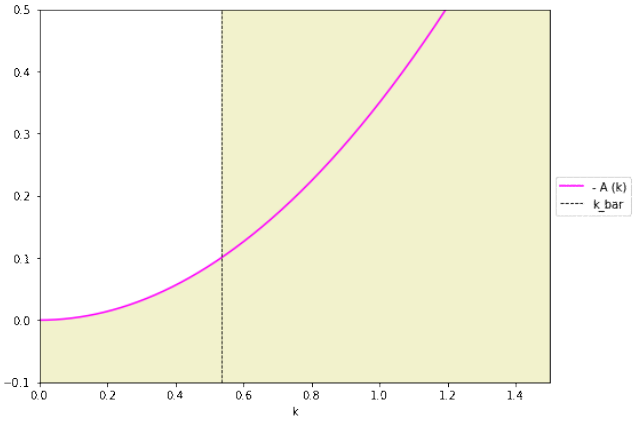

FIG. B.1. The region highlighted in green corresponds to the conditions (B.7), with $\bar{k} = \sqrt{-\frac{sD}{n_0}}$, $A(k) = \frac{D}{n_0}k^2$

General case

Recalling the most general form of g and h :

$$g(k) = \left(D + \bar{D}\right)\, k^2 + n_0\,\epsilon + n_0\,\widetilde{\phi}(k) = n_0\left(A(k) + \widetilde{\phi}(k)\right)$$
$$h(k) = D\bar{D}\,k^4 + n_0\epsilon\bar{D}\,k^2 + \widetilde{\phi}(k)\left(n_0 D\,k^2 + s + \epsilon\,n_0^2\right) = B(k) + C(k)\,\widetilde{\phi}(k)$$

Where:

$$\begin{aligned} A(k) &:= \frac{D+\bar{D}}{n_0}\,k^2 + \epsilon \\ B(k) &:= D\bar{D}\,k^4 + n_0\epsilon\bar{D}\,k^2 \\ C(k) &:= n_0 D\,k^2 + s + \epsilon\,n_0^2 \end{aligned} \tag{B.2}$$

And we also calculate, for later use:

$$n_0\,(AC - B)(k) = n_0\,D^2\,k^4 + \left[(2\epsilon n_0^2 + s)\,D + s\,\bar{D}\right]k^2 + \epsilon n_0\,(\epsilon n_0^2 + s) \equiv c_2 k^4 + c_1 k^2 + c_0 \tag{B.3}$$

Study of g(k) and h(k)

$$\begin{aligned} g(k) > 0 \quad &\Leftrightarrow \quad \widetilde{\phi}(k) > -A(k) \\ g(k) > 0 \quad &\Leftrightarrow \quad \widetilde{\phi}(k) < -A(k) \end{aligned}$$

$$\begin{aligned} h(k) > 0 \quad &\Leftrightarrow \quad \begin{cases} C(k) > 0 \\ \widetilde{\phi}(k) > -\dfrac{B(k)}{C(k)} \end{cases} \vee \begin{cases} C(k) < 0 \\ \widetilde{\phi}(k) < -\dfrac{B(k)}{C(k)} \end{cases} \\ h(k) < 0 \quad &\Leftrightarrow \quad \begin{cases} C(k) > 0 \\ \widetilde{\phi}(k) < -\dfrac{B(k)}{C(k)} \end{cases} \vee \begin{cases} C(k) < 0 \\ \widetilde{\phi}(k) > -\dfrac{B(k)}{C(k)} \end{cases} \end{aligned}$$

Therefore $Re[\lambda_+] > 0 \quad \Leftrightarrow$

$$
\begin{aligned}
&\Leftrightarrow \quad g(k) < 0 \vee \begin{cases} g(k) > 0 \\ h(k) < 0 \end{cases} \\
&\Leftrightarrow \quad \widetilde{\phi}(k) < -A(k) \vee \begin{cases} \widetilde{\phi}(k) > -A(k) \\ \begin{cases} C(k) > 0 \\ \widetilde{\phi}(k) < -\dfrac{B(k)}{C(k)} \end{cases} \vee \begin{cases} C(k) < 0 \\ \widetilde{\phi}(k) > -\dfrac{B(k)}{C(k)} \end{cases} \end{cases} \\
&\Leftrightarrow \quad \widetilde{\phi}(k) < -A(k) \vee \begin{cases} C(k) > 0 \\ -A(k) < -\dfrac{B(k)}{C(k)} \\ -A(k) < \widetilde{\phi}(k) < -\dfrac{B(k)}{C(k)} \end{cases} \vee \begin{cases} C(k) < 0 \\ -A(k) > -\dfrac{B(k)}{C(k)} \\ \widetilde{\phi}(k) > -A(k) \end{cases} \vee \begin{cases} C(k) < 0 \\ -A(k) < -\dfrac{B(k)}{C(k)} \\ \widetilde{\phi}(k) > -\dfrac{B(k)}{C(k)} \end{cases} \\
&\Leftrightarrow \quad \widetilde{\phi}(k) < -A(k) \vee \begin{cases} C(k) > 0 \\ (AC-B)(k) > 0 \\ -A(k) < \widetilde{\phi}(k) < -\dfrac{B(k)}{C(k)} \end{cases} \vee \begin{cases} C(k) < 0 \\ (AC-B)(k) > 0 \\ \widetilde{\phi}(k) > -A(k) \end{cases} \vee \begin{cases} C(k) < 0 \\ (AC-B)(k) < 0 \\ \widetilde{\phi}(k) > -\dfrac{B(k)}{C(k)} \end{cases}
\end{aligned}
\tag{B.4}
$$

If $D > 0$, from (B.2), (B.3) :

- $C(k) > 0 \quad \forall\, k$
- $n_0(AC-B)(k) > 0 \quad \forall\, k$

$$
\Rightarrow \quad Re[\lambda_+] > 0 \quad \Leftrightarrow \quad \widetilde{\phi}(k) < -A(k) \vee -A(k) < \widetilde{\phi}(k) < -\frac{B(k)}{C(k)} \quad \Leftrightarrow \quad \widetilde{\phi}(k) < -\frac{B(k)}{C(k)} \tag{B.5}
$$

If $D < 0$, from (B.2), (B.3) :

- $C(k) > 0 \quad \Leftrightarrow \quad k < \bar{k}$
  $C(k) < 0 \quad \Leftrightarrow \quad k > \bar{k}$
- $n_0(AC-B)(k) > 0 \quad \Leftrightarrow \quad c_1 > 0 \vee \begin{cases} c_1 < 0 \\ c_1^2 - 4C - 2c_0 < 0 \end{cases} \vee \begin{cases} c_1^2 - 4C - 2c_0 < 0 \\ k < k_- \vee k > k_+ \end{cases}$

  $n_0(AC-B)(k) < 0 \quad \Leftrightarrow \quad \begin{cases} c_1 < 0 \\ c_1^2 - 4C - 2c_0 > 0 \\ k- < k < k_+ \end{cases}$

And such further requirements must be substituted in (B.4).

B.1 Gaussian kernel

In this section, I consider a simple Gaussian kernel function:

$$\phi(x) = \alpha \exp\left(-\frac{x^2}{2\sigma^2}\right) \quad \rightarrow \quad \widetilde{\phi}(k) = \alpha\,\sigma \exp\left(-\frac{\sigma^2 k^2}{2}\right) \equiv \phi_0 \exp\left(-\frac{\sigma^2 k^2}{2}\right) > 0 \,\forall\, k \tag{B.6}$$

We will study the sign of $\mathrm{Re}[\lambda_\pm]$ in terms of the function $\widetilde{\phi}(k)$. As usual, we start by analysing the functions $g(k)$ and $h(k)$ in the simplest cases, by putting to zero some parameters.
First of all, we notice that, since $\widetilde{\phi}(k) > 0 \,\forall\, k$, $D > 0 \Rightarrow h(k), g(k) > 0 \,\forall\, k$ therefore we will not find instability in the case of positive D.

Case ϵ=0, $\bar{D} = 0$, D< 0

$$g(k^2) = D\,k^2 + n_0\,\widetilde{\phi}(k)$$
$$h(k^2) = \widetilde{\phi}(k)\left(n_0\,D\,k^2 + s\right)$$

Then:

$$g(k) > 0 \quad \Leftrightarrow \quad \widetilde{\phi}(k) > -\frac{D}{n_0}k^2 \qquad\qquad h(k) > 0 \Leftrightarrow k < \sqrt{-\frac{sD}{n_0}}$$
$$g(k) < 0 \quad \Leftrightarrow \quad \widetilde{\phi}(k) < -\frac{D}{n_0}k^2 \qquad\qquad h(k) < 0 \Leftrightarrow k > \sqrt{-\frac{sD}{n_0}}$$

$$\Rightarrow \quad Re[\lambda_+] > 0 \quad \Leftrightarrow \quad g < 0 \vee \begin{cases} g > 0 \\ h < 0 \end{cases} \quad \Leftrightarrow \quad \widetilde{\phi}(k) < -\frac{D}{n_0}k^2 \vee \begin{cases} \widetilde{\phi}(k) > -\frac{D}{n_0}k^2 \\ k > \sqrt{-\frac{sD}{n_0}} \end{cases} \tag{B.7}$$

This means that instability occurs when $\widetilde{\phi}(k)$ belongs to the area highlighted in green in Fig. B.2. As we can see, this corresponds to an instability for all $k > \bar{k}$.

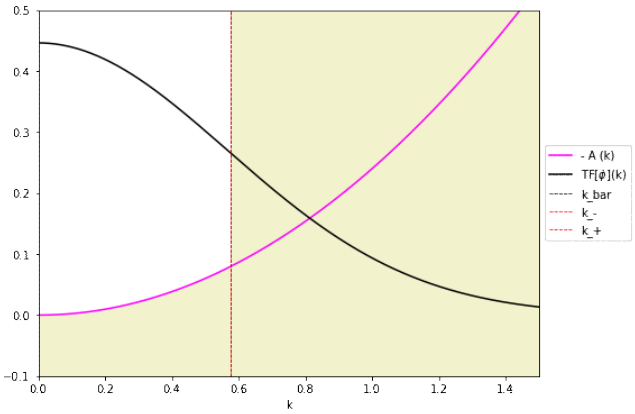

FIG. B.2. Case $\epsilon = 0$, $\bar{D} = 0$, $D < 0$. The region highlighted in green corresponds to the conditions (B.7) for $\widetilde{\phi}(k)$, with $\bar{k} = \sqrt{-\frac{sD}{n_0}}$, $A(k) = \frac{D}{n_0}k^2$

Case ϵ=0, D<0

$$g(k) = \left(D + \bar{D}\right)\, k^2 + n_0\, \widetilde{\phi}(k)$$
$$h(k) = D\bar{D}\, k^4 + \widetilde{\phi}(k)\left(n_0 D\, k^2 + s\right)$$

We study the signs:

$$g(k) > 0 \quad \Leftrightarrow \quad \widetilde{\phi}(k) > -\frac{D+\bar{D}}{n_0}k^2 \qquad h(k) > 0 \Leftrightarrow \begin{cases} Dn_0k^2 + s > 0 \\ \widetilde{\phi}(k) > -\dfrac{D\bar{D}k^4}{Dn_0k^2+s} \end{cases}$$
$$g(k) < 0 \quad \Leftrightarrow \quad \widetilde{\phi}(k) < -\frac{D+\bar{D}}{n_0}k^2 \qquad h(k) < 0 \Leftrightarrow \begin{cases} Dn_0k^2 + s < 0 \\ \widetilde{\phi}(k) < -\dfrac{D\bar{D}k^4}{Dn_0k^2+s} \end{cases} \vee\ Dn_0k^2 + s < 0$$

where, for $h > 0$, we have neglected the case:

$$\begin{cases} Dn_0k^2 + s < 0 \\ \widetilde{\phi}(k) < -\dfrac{D\bar{D}k^4}{Dn_0k^2+s} < 0 \end{cases}$$

because $\widetilde{\phi}(k)$ is positive for definition. For the same reason, $\widetilde{\phi}(k) < -\frac{D\bar{D}k^4}{Dn_0k^2+s} > 0$ is always satisfied when $Dn_0k^2 + s < 0$.

If $D + \bar{D} > 0$, then $g(k) > 0 \,\forall\, k$:

$$Re[\lambda_+] > 0 \quad \Leftrightarrow \quad h(k) < 0 \quad \Leftrightarrow \quad \begin{cases} k < \sqrt{-\dfrac{s}{n_0 D}} \\ \widetilde{\phi}(k) < -\dfrac{D\bar{D}k^4}{Dn_0k^2+s} \end{cases} \vee\ k > \sqrt{-\frac{s}{n_0 D}} \tag{B.8}$$

If $D + \bar{D} < 0$:

$$Re[\lambda_+] > 0 \quad \Leftrightarrow \quad g < 0 \vee \begin{cases} g > 0 \\ h < 0 \end{cases}$$
$$\Leftrightarrow \quad \widetilde{\phi}(k) < -\frac{D+\bar{D}}{n_0}k^2 \vee \begin{cases} k < \sqrt{-\dfrac{s}{n_0 D}} \\ -\dfrac{D+\bar{D}}{n_0}k^2 < \widetilde{\phi}(k) < -\dfrac{D\bar{D}k^4}{Dn_0k^2+s} \end{cases} \vee \begin{cases} k > \sqrt{-\dfrac{s}{n_0 D}} \\ \widetilde{\phi}(k) > -\dfrac{D+\bar{D}}{n_0}k^2 \end{cases} \tag{B.9}$$

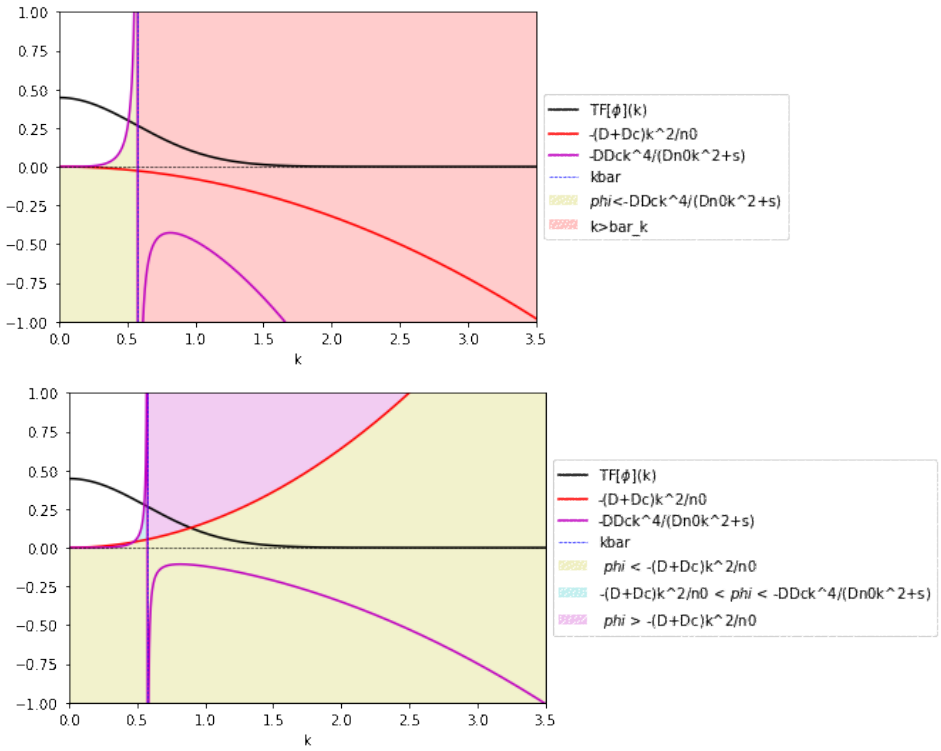

FIG. B.3. Top: case $\epsilon = 0$, $D + \bar{D} > 0$. **Bottom:** case $\epsilon = 0$, $D + \bar{D} < 0$. The highlighted regions correspond to the instability conditions for $\widetilde{\phi}(k)$, i.e. (B.8) and (B.9), respectively.

The two cases are pictured in Fig. B.3. We notice that the situation is very similar to the one studied in the previous section: in both cases instability is allowed for all $k > k_0$, however now $k_0 < \bar{k}$.

General case, $D < 0$

Referring to the complete expressions for $g(k)$ and $h(k)$ (3.44), if $D + \bar{D} > 0$, then $g(k) > 0 \,\forall\, k$:

$$
\begin{aligned}
Re[\lambda_+] > 0 \quad \Leftrightarrow \quad h(k) < 0 \quad \Leftrightarrow \quad & \begin{cases} Dn_0k^2 + \epsilon n_0^2 + s > 0 \\ \widetilde{\phi}(k) < -\dfrac{D\bar{D}k^4 + \bar{D}\epsilon n_0 k^2}{Dn_0k^2 + \epsilon n_0^2 + s} \end{cases} \vee \begin{cases} Dn_0k^2 + \epsilon n_0^2 + s < 0 \\ \widetilde{\phi}(k) > -\dfrac{D\bar{D}k^4 + \bar{D}\epsilon n_0 k^2}{Dn_0k^2 + \epsilon n_0^2 + s} \end{cases} \\
\Leftrightarrow \quad & \begin{cases} Dn_0k^2 + \epsilon n_0^2 + s > 0 \\ D\bar{D}k^4 + \bar{D}\epsilon n_0 k^2 < 0 \\ \widetilde{\phi}(k) < -\dfrac{D\bar{D}k^4 + \bar{D}\epsilon n_0 k^2}{Dn_0k^2 + \epsilon n_0^2 + s} \end{cases} \vee \begin{cases} Dn_0k^2 + \epsilon n_0^2 + s < 0 \\ \widetilde{\phi}(k) > -\dfrac{D\bar{D}k^4 + \bar{D}\epsilon n_0 k^2}{Dn_0k^2 + \epsilon n_0^2 + s} \end{cases} \\
\Leftrightarrow \quad & \begin{cases} \widetilde{k} < k < \bar{k} \\ \widetilde{\phi}(k) < -\dfrac{D\bar{D}k^4 + \bar{D}\epsilon n_0 k^2}{Dn_0k^2 + \epsilon n_0^2 + s} \end{cases} \vee \begin{cases} k > \bar{k} \\ \widetilde{\phi}(k) > -\dfrac{D\bar{D}k^4 + \bar{D}\epsilon n_0 k^2}{Dn_0k^2 + \epsilon n_0^2 + s} \end{cases}
\end{aligned}
\tag{B.10}
$$

where $\quad \bar{k} := \sqrt{-\dfrac{s + \epsilon n_0^2}{n_0 D}} > \widetilde{k} := \sqrt{-\dfrac{\epsilon n_0}{D}}$

and $\quad \dfrac{D\bar{D}k^4 + \bar{D}\epsilon n_0 k^2}{Dn_0k^2 + \epsilon n_0 k^2 + s}$ is negative for $k < \widetilde{k} \vee k > \bar{k}$ and positive for $\widetilde{k} < k < \bar{k}$

If $D+\bar{D}<0$:

$$Re[\lambda_+]>0 \quad \Leftrightarrow \quad g(k)<0 \vee \begin{cases} g>0 \\ h<0 \end{cases}$$

$$\Leftrightarrow \quad \widetilde{\phi}(k)<-\frac{D+\bar{D}}{n_0}-\epsilon \vee \begin{cases} \widetilde{k}<k<\bar{k} \\ -\frac{D+\bar{D}}{n_0}-\epsilon<\widetilde{\phi}(k)<-\frac{D\bar{D}k^4+\bar{D}\epsilon n_0 k^2}{Dn_0k^2+\epsilon n_0^2+s} \end{cases} \vee \begin{cases} k>\bar{k} \\ \widetilde{\phi}(k)>-\frac{D+\bar{D}}{n_0}k^2-\epsilon \\ \widetilde{\phi}(k)>-\frac{D\bar{D}k^4+\bar{D}\epsilon n_0}{Dn_0k^2+\epsilon n_0^2+s} \end{cases}$$

$$\Leftrightarrow \quad \widetilde{\phi}(k)<-\frac{D+\bar{D}}{n_0}-\epsilon \vee \begin{cases} \widetilde{k}<k<\bar{k} \\ -\frac{D+\bar{D}}{n_0}-\epsilon<\widetilde{\phi}(k)<-\frac{D\bar{D}k^4+\bar{D}\epsilon n_0 k^2}{Dn_0k^2+\epsilon n_0^2+s} \end{cases} \vee \begin{cases} k>\bar{k} \\ \widetilde{\phi}(k)>-\frac{D\bar{D}k^4+\bar{D}\epsilon n_0}{Dn_0k^2+\epsilon n_0^2+s} \end{cases} \tag{B.11}$$

being $-\frac{D+\bar{D}}{n_0}k^2-\epsilon<-\frac{D\bar{D}k^4+\bar{D}\epsilon n_0}{Dn_0k^2+\epsilon n_0^2+s} \quad \forall\, k>\bar{k}$

The instability conditions are plotted below. In this case, instability is allowed for all $k>k_1$ with $\widetilde{k}<k_1<\bar{k}$.

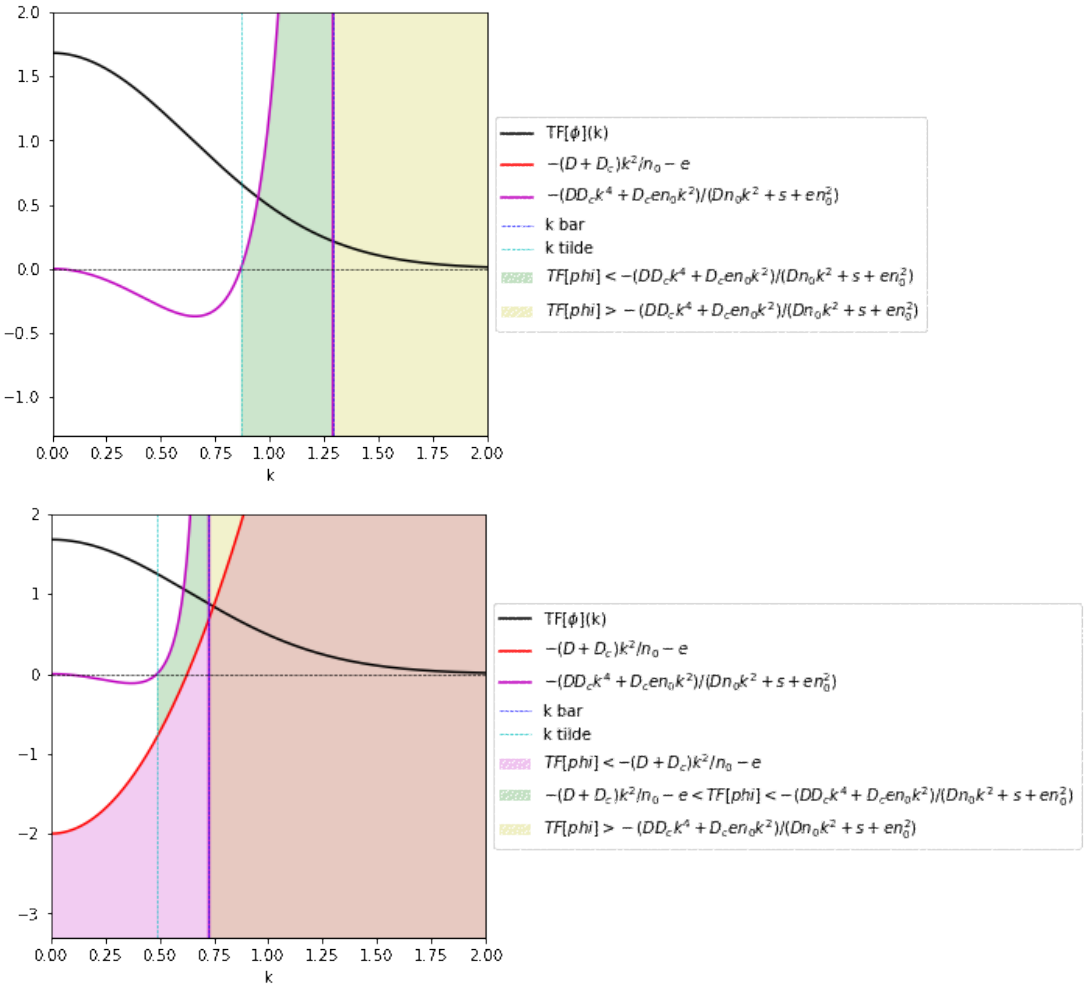

FIG. B.4. Top: case $D+\bar{D}>0$. **Bottom:** case $D+\bar{D}<0$. The highlighted regions correspond to the instability conditions for $\widetilde{\phi}(k)$, reported in (B.10) and (B.11), respectively.

B.1.1 Expansion for $k \gg 1$

We can try to get insight into the problem by performing an expansion of the eigenvalues for large k in the general case $\epsilon \neq 0$, $D \neq 0$, $\bar{D} \neq 0$. Remembering our hypothesis on $\widetilde{\phi}$ (B.6) and substituting the expressions for g and h, calling $\Delta = g^2 - 4h$:

$$\begin{aligned}\Delta &= (D-\bar{D})^2 k^4 + 2n_0\epsilon(D-\bar{D})\,k^2 + n_0^2\epsilon^2 - 2n_0(D-\bar{D})k^2\widetilde{\phi} - 2(n_0^2\epsilon + 2s)\widetilde{\phi} + n_0^2\widetilde{\phi}^2 = \\ &= k^4\,(D-\bar{D})^2\left[1 + \frac{2}{k^2}\frac{n_0\epsilon}{D-\bar{D}} + \frac{1}{k^4}\frac{n_0^2\epsilon^2}{(D-\bar{D})^2} - \frac{2}{k^2}\frac{n_0}{D-\bar{D}}\widetilde{\phi} - \frac{2}{k^4}\frac{n_0^2\epsilon + 2s}{(D-\bar{D})^2}\widetilde{\phi} + \frac{1}{k^4}\frac{n_0^2}{(D-\bar{D})^2}\widetilde{\phi}^2\right]\end{aligned}$$

Expanding for $k \to +\infty$:

$$\begin{aligned}\sqrt{\Delta} &\approx k^2\,|D-\bar{D}|\left[1 + \frac{1}{k^2}\frac{n_0\epsilon}{D-\bar{D}} - \frac{1}{k^2}\frac{n_0}{D-\bar{D}}\widetilde{\phi} + O\left(\frac{1}{k^4}\right)\right] = \\ &= k^2\,|D-\bar{D}| + n_0\epsilon\,\mathrm{sgn}(D-\bar{D}) - n_0\,\widetilde{\phi}(k)\,\mathrm{sgn}(D-\bar{D}) + O\left(\frac{1}{k^2}\right) \\ \Rightarrow \quad \lambda_\pm &\approx \frac{k^2[-(D+\bar{D}) \pm (|D-\bar{D}|)] + n_0\epsilon[-1 \pm \mathrm{sgn}(D-\bar{D})] - n_0\widetilde{\phi}(k)[1 \pm \mathrm{sgn}(D-\bar{D})]}{2}\end{aligned}$$

Then we find that:

$$\begin{aligned}&\text{if } D-\bar{D} < 0: \quad \lambda_+ \approx -D\,k^2 - n_0\,\epsilon \\ &\qquad\qquad\quad\;\; \lambda_- \approx -\bar{D}\,k^2 - n_0\,\widetilde{\phi}(k) \\ &\text{if } D-\bar{D} > 0: \quad \lambda_+ \approx -\bar{D}\,k^2 - n_0\,\widetilde{\phi}(k) \\ &\qquad\qquad\quad\;\; \lambda_- \approx -D\,k^2 - n_0\,\epsilon\end{aligned} \tag{B.12}$$

Therefore, λ_+ is always positive for large k if $D < 0$: no desired instability behavior is found under these hypotheses.
For visualisation, we report in Fig. B.5 the behavior of the eigenvalues relative to the case $D < 0$ reported in the right panel of Fig. B.4, where the same parameters were used. Two examples for the case $D > 0$ are plotted as well.

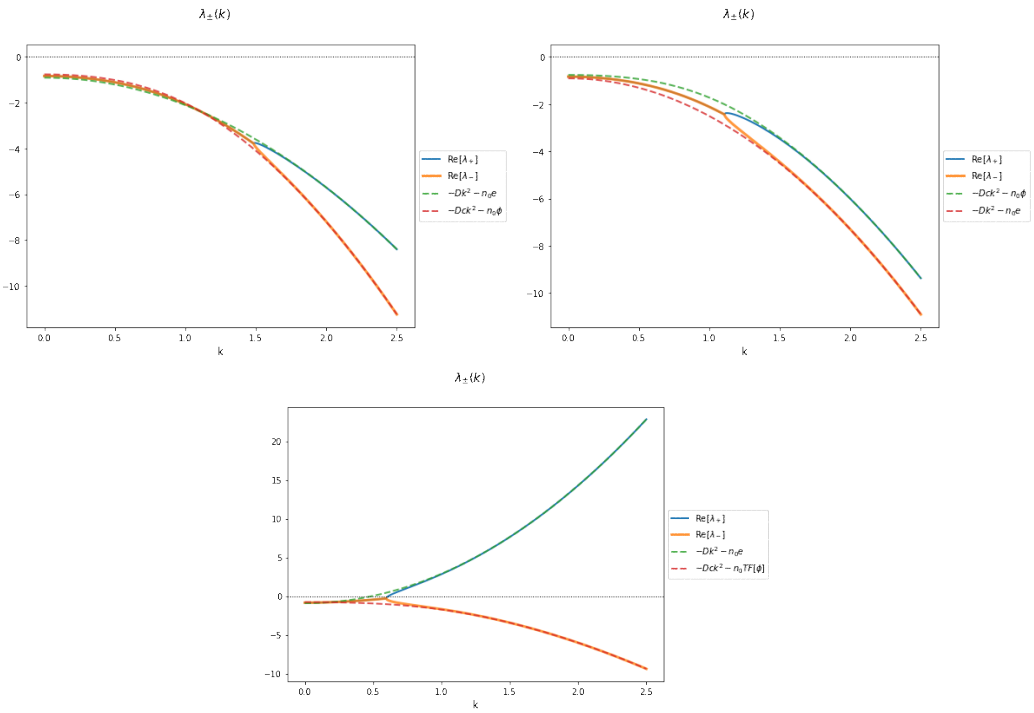

FIG. B.5. Top left: case D>0, D< $\bar{D}$. **Top right:** case D>0, D> $\bar{D}$. **Bottom:** case D<0.

Appendix C

Spatially discrete model

I report here the calculations relative to the spatially discrete version of the extension of MacArthur's model presented in Section 3.5.
Assuming that the spatial domain is a discrete lattice of N_x sites, separated by a distance dx, the spatial variable becomes:

$$x \quad \rightarrow \quad x_j = j\,dx \quad j \in [0, N_x]$$

and the length of the spatial domain is $L = N_x\,dx$.
Then, the consumer and resource population fields read:

$$\begin{aligned} n(x,t) \quad &\rightarrow \quad n(x_i,t) =: n_i(t) \\ c(x,t) \quad &\rightarrow \quad c(x_i,t) =: c_i(t) \end{aligned}$$

Being the domain finite, a discrete set of wavenumbers is allowed, labeled by the index n:

$$k_n = \frac{2\pi}{L}\,n$$

To perform the linear stability analysis, we consider the uniform equilibrium[1]:

$$\begin{pmatrix} n_j \\ c_j \end{pmatrix} \equiv \begin{pmatrix} n_{eq} \\ c_{eq} \end{pmatrix} \quad \forall\, j$$

and apply a perturbation of the kind:

$$\begin{pmatrix} n_j(t) \\ c_j(t) \end{pmatrix} = \begin{pmatrix} n_{eq} \\ c_{eq} \end{pmatrix} + \begin{pmatrix} \delta n_j(t) \\ \delta c_j(t) \end{pmatrix} \qquad \text{with} \quad \begin{pmatrix} \delta n_j(t) \\ \delta c_j(t) \end{pmatrix} = \vec{\delta}\, e^{\lambda t + i k_n x_j}$$

where $k_n\,x_j = \frac{2\pi}{N_x\,dx}\,n\,dx\,j = \frac{2\pi}{N_x}\,n\,j$.
The discretized model's equations thus read, at linear order:

$$\begin{cases} \delta\dot{n}_j = \alpha\,n_{eq}\,\delta c_j - \epsilon\,n_{eq}\,\delta n_j + (D_0 - D_1\,n_{eq})\;\partial_x^2\,\delta n_j - \beta\,\partial_x^4\,\delta n_j \\ \delta\dot{c}_j = -\alpha\,c_{eq}\,\delta n_j - \alpha\,n_{eq}\,\delta c_j + \bar{D}\,\partial_x^2\,\delta c_j \end{cases}$$

where the derivatives are calculated with the central finite difference method:

$$\begin{aligned} \partial_x^2\,\delta n_j &= \frac{1}{dx^2}\,(\delta n_{j+1} + -2\,\delta n_j + \delta n_{j-1}) \\ \partial_x^2\,\delta c_j &= \frac{1}{dx^2}\,(\delta c_{j+1} + -2\,\delta c_j + \delta c_{j-1}) \\ \partial_x^4\,\delta n_j &= \frac{1}{dx^4}\,(\delta n_{j+2} - 4\,\delta n_{j+1} + 6\,\delta n_j - 4\,\delta n_{j-1} + \delta n_{j-2}) \end{aligned}$$

[1] The explicit equilibrium values as a function of the system parameters are the ones reported in (3.31)

Substituting the explicit expression for the perturbations, one obtains the following eigenvalue problem:

$$\lambda\,\vec{\delta} = (\mathbb{J} + \mathbb{D})\,\vec{\delta}$$

with:

$$\mathbb{D} = \begin{pmatrix} \gamma(n) & 0 \\ 0 & \eta(n) \end{pmatrix} \qquad \mathbb{J} = \begin{pmatrix} f_n & f_c \\ g_n & g_c \end{pmatrix} = \begin{pmatrix} -n_{eq}\,\epsilon & n_{eq}\,\alpha \\ -s/n_{eq} & -n_{eq}\,\alpha \end{pmatrix}$$

$$\gamma(n) = 2\left\{\frac{D}{dx^2}\left[\cos(n) - 1\right] - \frac{\beta}{dx^4}\left[\cos(2\,n) - 4\,\cos(n) + 3\right]\right\}$$

$$\eta(n) = 2\,\frac{\bar{D}}{dx^2}\left[\cos(n) - 1\right]$$

Therefore, the discrete eigenvalues expressions follow from:

$$\det\left(\mathbb{J} - \lambda\,\mathbb{I}\right) = 0 \quad \Leftrightarrow \quad \lambda_{\pm}(n) = \frac{-g(n) \pm \sqrt{g^2(n) - 4h(n)}}{2}$$

with:

$$g(n) = -(g_c + f_n)$$
$$h(n) = f_n\,g_c - g_n\,f_c$$

Bibliography

[1] M. Rietkerk and J. van de Koppel, "Regular pattern formation in real ecosystems," *Trends in Ecology & Evolution*, vol. 23, no. 3, pp. 169–175, 2008.

[2] M. C. M. Rietkerk et al. R. HilleRisLambers, J. v. de Koppel, L. Kumar, H. H. T. Prins, and A. M. de Roos, "Self-organization of vegetation in arid ecosystems," *The American Naturalist*, vol. 160, p. 524, 10 2002.

[3] M. Molles and A. Sher, *Ecology: Concepts & Applications*. McGraw-Hill Education, 2018.

[4] A. Turing, "The chemical basis of morphogenesis," *Philosophical Transactions of the Royal Society B*, vol. 237, pp. 37–72, 1952.

[5] M. C. Cross and P. C. Hohenberg, "Pattern formation outside of equilibrium," *Rev. Mod. Phys.*, vol. 65, pp. 851–1112, Jul 1993.

[6] J. P. Grover, *Resource Competition*. Population and Community Biology Series, New York: Springer.

[7] R. MacArthur, "Species packing and competitive equilibrium for many species," *Theoretical Population Biology*, vol. 1, no. 1, pp. 1–11, 1970.

[8] G. J. Hardin, "The competitive exclusion principle," *Science*, vol. 131 3409, pp. 1292–7, 1960.

[9] G. E. Hutchinson, "The paradox of the plankton," *The American Naturalist*, vol. 95, no. 882, pp. 137–145, 1961.

[10] C. de Vargas et al., "Eukaryotic plankton diversity in the sunlit ocean," *Science*, vol. 348, no. 6237, p. 1261605, 2015.

[11] P. Cermeño et al., "Sampling the limits of species richness in marine phytoplankton communities," *Journal of Plankton Research*, vol. 36, pp. 1135–1139, 05 2014.

[12] G. F. Gause, *The Struggle for Existence*. Baltimore: William & Wilkins, 1934.

[13] M. Scheffer et al., "Why plankton communities have no equilibrium: solutions to the paradox: Recent developments in fundamental and applied plankton research," *Hydrobiologia*, vol. 491, 01 2003.

[14] S. Roy and J. Chattopadhyay, "Towards a resolution of 'the paradox of the plankton': A brief overview of the proposed mechanisms," *Ecological Complexity*, vol. 4, pp. 26–33, 03 2007.

[15] C. Suttle, A. Chan, and M. Cottrell, "Infection of phytoplankton by viruses and reduction of primary productivity," *Nature*, vol. 347, pp. 467–469, 10 1990.

[16] E. Seth and M. Taga, "Nutrient cross-feeding in the microbial world," *Frontiers in microbiology*, vol. 5, p. 350, 07 2014.

[17] F. Peruzzo, M. Mobilia, and S. Azaele, "Spatial patterns emerging from a stochastic process near criticality," *Phys. Rev. X*, vol. 10, p. 011032, Feb 2020.

[18] D. Gupta, S. Garlaschi, S. Suweis, S. Azaele, and A. Maritan, "Effective resource competition model for species coexistence," *Phys. Rev. Lett.*, vol. 127, p. 208101, Nov 2021.

[19] D. Tilman and J. A. Downing, "Biodiversity and stability in grasslands," *Nature*, vol. 367, pp. 363–365, 1994.

[20] D. Tilman, "Competition and biodiversity in spatially structured habitats," *Ecology*, vol. 75, pp. 2–16, 1994.

[21] D. Tilman, R. M. May, C. L. Lehman, and M. A. Nowak, "Habitat destruction and the extinction debt," *Nature*, vol. 371, pp. 65–66, 1994.

[22] R. Durrett and S. Levin, "The importance of being discrete (and spatial)," *Theoretical Population Biology*, vol. 46, no. 3, pp. 363–394, 1994.

[23] H. Comins, M. Hassell, and R. May, "The spatial dynamics of host-parasitoid systems," *Journal of Animal Ecology*, vol. 61, no. 3, pp. 735–748, 1992.

[24] M. P. Hassell et al., "Competition, succession and pattern in fungal communities: Towards a cellular automaton model," *Oikos*, vol. 70, no. 3, pp. 435–442, 1994.

[25] J. G. Skellam, "Random dispersal in theoretical populations," *Biometrika*, vol. 38, no. 1/2, pp. 196–218, 1951.

[26] "Py-pde reference manual - pde.solvers package." https://py-pde.readthedocs.io/en/latest/packages/pde.solvers.implicit.html.

[27] "Scipy user guide - scipy.integrate." https://docs.scipy.org/doc/scipy/reference/generated/scipy.integrate.solve_ivp.html#scipy-integrate-solve-ivp.

[28] B. G. Weiner, A. Posfai, and N. S. Wingreen, "Spatial ecology of territorial populations," *Proceedings of the National Academy of Sciences*, vol. 116, no. 36, pp. 17874–17879, 2019.

[29] P. Chesson, "Macarthur's consumer-resource model," *Theoretical Population Biology*, vol. 37, no. 1, pp. 26–38, 1990.

[30] J. D. Murray, *Mathematical Biology I. An Introduction*, vol. 17 of *Interdisciplinary Applied Mathematics*. New York: Springer, 3 ed., 2002.

[31] J. D. Murray, *Mathematical Biology II: Spatial Models and Biomedical Applications*, vol. 18 of *Interdisciplinary Applied Mathematics*. New York: Springer, 2003.

[32] P. Chesson, "Mechanisms of maintenance of species diversity," *Annual Review of Ecology and Systematics*, vol. 31, pp. 343–366, 2000.

[33] R. Hoyle, *Pattern Formation: An Introduction to Methods*. Cambridge University Press, 2006.

[34] C. C. Robert Stephen Cantrell, *Spatial Ecology via Reaction-Diffusion Equations*. John Wiley & Sons, Ltd, 2004.